

72-1029



July 2, 2004
ANUH-01-04-05

Ms. Mary Jane Ross-Lee
Spent Fuel Project Office, NMSS
U. S. Nuclear Regulatory Commission
11555 Rockville Pike M/S 0-6-F-18
Rockville, MD 20852

Subject: Response to the Request for Additional Information (RAI) for Chapter A.4 and Submittal of Revision 2 of Application for Amendment No.1 of Advanced NUHOMS® Certificate of Compliance (CoC) No. 1029 for Dry Spent Fuel Storage Casks (TAC No. L23606)

References:

1. Request for Additional Information Regarding the Transnuclear Advanced NUHOMS® Amendment No. 1 Application (TAC No. L23606), Dated October 14, 2003.
2. Revision 1 of Application for Amendment No. 1 of the Advanced NUHOMS® Certificate of Compliance (CoC) No. 1029, Submitted March 12, 2004.

Dear Ms. Ross-Lee:

Transnuclear Inc. (TN) herewith submits our response to the thermal RAI questions (Reference 1) and Revision 2 of our Application for Amendment No. 1 of the Advanced NUHOMS® System CoC No. 1029. This submittal closes the open item identified in our Revision 1 submittal (Reference 2).

Revision 2 of this application updates the SAR and the Technical Specifications as a result of the responses to the thermal RAIs. This submittal is organized in the following format to facilitate your staff's review:

- Affidavit for withholding proprietary information (Enclosure 1),
- Response to the RAI (Enclosure 2),
- Ten (10) copies of Application for Amendment No. 1 to Advanced NUHOMS® COC 1029, Proprietary Version (Replacement Pages Only, Enclosure 3),
- Three (3) copies of Application for Amendment No. 1 to Advanced NUHOMS® COC 1029, Non-Proprietary Version (Replacement Pages Only, Enclosure 4),
- Two (2) Proprietary Calculations with Input files (2 CDs, Enclosure 5), and
- Two (2) Non Proprietary Calculations (Enclosure 6).

AMSS01

Please note that the CFD based thermal analysis results in higher temperatures for the DSC support rods and guide sleeve. TN plans to resolve this item within the next 2-4 weeks.

This submittal includes proprietary information which may not be used for any purpose other than to support your staff's review of the application. In accordance with 10 CFR 2.390, I am providing an affidavit (Enclosure 1) specifically requesting that you withhold this proprietary information from public disclosure.

Should you or your staff require additional information to support review of this application, please do not hesitate to contact me at 510-744-6053 or Mr. Jayant Bondre at 510-744-6043.

Sincerely,

U. B. Chopra
Licensing Manager

Docket 72-1029

- Enclosures:
1. Affidavit for withholding proprietary information.
 2. RAI Response.
 3. Ten (10) copies of Application for Amendment No. 1 to Advanced NUHOMS® COC 1029 (Replacement Pages Only, Proprietary Version).
 4. Three (3) copies of Application for Amendment No. 1 to Advanced NUHOMS® COC 1029 (Replacement Pages Only, Non-Proprietary Version).
 5. Proprietary Calculations SCE-23-0410 Revision 2 and SCE-23-0411, Revision 0 (2 CDs, Proprietary version).
 6. Non-Proprietary Calculations SCE-23-0410 Revision 2 and SCE-23-0411, Revision 0.

**AFFIDAVIT PURSUANT
TO 10 CFR 2.390**

Transnuclear, Inc.)
State of Washington) SS.
County of Pierce)

I, William D. Gallo, depose and say that I am Senior Vice President of Transnuclear, Inc., duly authorized to make this affidavit, and have reviewed or caused to have reviewed the information which is identified as proprietary and referenced in the paragraph immediately below. I am submitting this affidavit in conformance with the provisions of 10 CFR 2.390 of the Commission's regulations for withholding this information.

The information for which proprietary treatment is sought is contained in the Calculation package and Input files included in Enclosure 5 of this submittal and as listed below:

1. Calculation SCE-23.0410, Revision 2 (Proprietary)
2. Calculation SCE-23.0411, Revision 0 (Proprietary)

This document has been appropriately designated as proprietary.

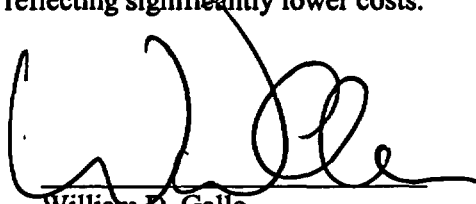
I have personal knowledge of the criteria and procedures utilized by Transnuclear, Inc. in designating information as a trade secret, privileged or as confidential commercial or financial information.

Pursuant to the provisions of paragraph (b) (4) of Section 2.390 of the Commission's regulations, the following is furnished for consideration by the Commission in determining whether the information sought to be withheld from public disclosure, included in the above referenced document, should be withheld.

- 1) The information sought to be withheld from public disclosure are calculation packages and Input files relating to the analysis of the Advanced NUHOMS[®] Cask, which is owned and has been held in confidence by Transnuclear, Inc.
- 2) The information is of a type customarily held in confidence by Transnuclear, Inc. and not customarily disclosed to the public. Transnuclear, Inc. has a rational basis for determining the types of information customarily held in confidence by it.
- 3) The information is being transmitted to the Commission in confidence under the provisions of 10 CFR 2.390 with the understanding that it is to be received in confidence by the Commission.
- 4) The information, to the best of my knowledge and belief, is not available in public sources, and any disclosure to third parties has been made pursuant to regulatory provisions or proprietary agreements which provide for maintenance of the information in confidence.
- 5) Public disclosure of the information is likely to cause substantial harm to the competitive position of Transnuclear, Inc. because:
 - a) A similar product is manufactured and sold by competitors of Transnuclear, Inc.

- b) Development of this information by Transnuclear, Inc. required expenditure of considerable resources. To the best of my knowledge and belief, a competitor would have to undergo similar expense in generating equivalent information.
- c) In order to acquire such information, a competitor would also require considerable time and inconvenience related to the development of a design and analysis of a dry spent fuel storage system.
- d) The information required significant effort and expense to obtain the licensing approvals necessary for application of the information. Avoidance of this expense would decrease a competitor's cost in applying the information and marketing the product to which the information is applicable.
- e) The information consists of description of the design and analysis of a dry spent fuel storage and transportation system, the application of which provides a competitive economic advantage. The availability of such information to competitors would enable them to modify their product to better compete with Transnuclear, Inc., take marketing or other actions to improve their product's position or impair the position of Transnuclear, Inc.'s product, and avoid developing similar data and analyses in support of their processes, methods or apparatus.
- f) In pricing Transnuclear, Inc.'s products and services, significant research, development, engineering, analytical, licensing, quality assurance and other costs and expenses must be included. The ability of Transnuclear, Inc.'s competitors to utilize such information without similar expenditure of resources may enable them to sell at prices reflecting significantly lower costs.

Further the deponent sayeth not.



William D. Gallo
Senior Vice President, Transnuclear, Inc.

Subscribed and sworn to me before this 1st day of July, 2004, by William D. Gallo.

Bonnie M Hargis
Notary Public



DOCKET NO. 72-1029
TAC NO. L23606

TN INC. RESPONSES TO NRC REQUEST FOR ADDITIONAL INFORMATION

Chapter A.4 Thermal Evaluation

Question 4-1

Justify the fill gas pressure and density values used for the canister backfill analysis, or forward details of the modified calculations for staff review.

On page 7 of TN calculation package SCE-23.0406, the helium fill gas is assumed to come to equilibrium at a temperature of 230° F. This temperature is then used to calculate the number of moles of helium in the canister. As stated in the package, the number of moles is conservative for pressure calculations for structural analysis (because the very low temperature ensures a [large] bounding number of moles). However, when this number of moles is used in density calculations for thermal analysis, it appears to be non-conservative as the gas will actually be at a much higher temperature (fewer moles, lower density).

NUREG-1536, "Standard Review Plan for Dry Cask Storage Systems" (SRP), Section 4.V states that the staff, "should assess models used by the applicant for thermal analysis." SRP Section 4.V.4.a requires staff to verify that the model used in the thermal evaluation is clearly described.

Response to 4-1

The number of helium gas moles used for the design basis DSC cavity internal pressure calculation is based on a conservatively low average helium temperature of 230°F to maximize the initial gas moles, and a maximum fill pressure of 7 psig (based on a revision to Tech Spec 3.1.3) which results in maximum internal pressures of 17.5, 22.3 and 80.7 psig for the normal, off-normal and accident conditions respectively. To be conservative, as documented in SAR Table A.4.4-10, the pressures used in the structural analysis of the DSC are 20, 26, and 90 psig for normal, off-normal and accident conditions, respectively.

In response to RAI Question 4-5, a new DSC thermal analysis, Calculation SCE-23-0411, was performed. This calculation uses a computational fluid dynamics (CFD) model. The program selected for this analysis is Icepak™/FLUENT™.

In this calculation, the number of helium gas moles used for this DSC CFD thermal analyses, 1) the number of gas moles used to calculate average gas density in the DSC cavity was corrected to the minimum 6 psig fill pressure (per revised Tech Spec 3.1.3) which is the lower bound gas fill pressure. Also, the average helium gas temperature during helium backfill of 375°F, based on the maximum steady state helium temperature

was used. This results in a lower number of moles, than that used in the internal pressure analysis, therefore, the convection modeled in the CFD analyses is conservative.

SAR Sections A.4.4.8 and Table A.4.4-10 have been revised to reflect the new pressure analysis results. A copy of Calculation SCE-23-0411 is included with this submittal.

Question 4-2

Provide details of the backfill pressure and density analyses (both the basis and the actual calculations) to the staff for review.

During the phone call between TN and NRC staff on September 10, 2003, there was much conversation regarding the effect of the canister pressure on the gas density (and hence the convection efficiency). Based on the conversation and the application materials, the staff could not discern how the calculations were performed and the basis of the results.

SRP Section 4.V.4.a requires staff to verify that the model used in the thermal evaluation is clearly described.

Response to 4-2

This question was based on Calculation SCE-23-0404, which is no longer required to support this submittal.

The DSC thermal analysis is performed using Icepak™/FLUENT™ code as documented in response to RAI 4-5. In this CFD analysis, the density of the backfill gas used in the DSC is computed within the model at each discrete location where a convection coefficient or mass flow is required. Since temperature and density are local variables, while pressure is a global variable and since the calculation model covers only a section of the DSC and fuel basket, the approach used to compute the local density value was to use the global pressure value as an input. Then, using the ideal gas law and the local temperature, the value of the local density is computed. It should be noted that the alternative of assuming a constant number of gram-moles per unit volume would be non-conservative in that it would over-predict the system performance in the areas of high temperature (i.e., low density).

SAR Section A.4.4.8 has been revised to address the changes.

Question 4-3

There appears to be contradictions in the application and supporting documents regarding how convection is treated in the canister. Clarify these apparent contradictions and submit the resolution for review. In addition, details of the convection model should also be submitted.

On page 10 of TN calculation package SCE-23.0402, it is stated that "convection within the 24PT4-DSC basket free spaces is conservatively neglected in this calculation." On page 45 of TN calculation package SCE-23.0404 ("SCE-404"), footnote 1 of Table 5-1

states that "SAR [Safety Analysis Report] analysis w/ ANSYS code is insensitive to canister pressure since no convection heat transfer is directly modeled." On page 18 of the SCE-404 (as shown on Figure 3-1), it is stated that the fuel region effective thermal conductivity (k_{eff}) used in the ANSYS model includes the effects of convection outside of the guide sleeve within the thermal conductivity for the fuel region. This results in the ANSYS k_{eff} values being 3 to 6 times higher than the more detailed SINDA/FLUINT analysis values. On page 68 of SCE-404, it is stated that the ANSYS thermal model does not account for the internal convection.

As stated in SAP Section 4.V.4.a, "[The staff should] verify that the model used in the thermal evaluation is clearly described. . . Convection by natural circulation should be limited to that between the external surface of the cask and the ambient environment. The staff has not previously approved specific thermal models for natural circulation internal to the cask because of the difficulty in modeling and the lack of test data. Applicants seeking NRC approval of specific internal convection models should propose, in the SAR, a comprehensive test program to demonstrate the adequacy of the cask design and validation of the convection models. Actual spent fuel properties and uncertainties (e.g., friction factors, crud and oxide buildup, eccentricities, non-uniform axial and radial decay heat profiles) should also be addressed."

Response to 4-3

SAR Chapter A.4 has been revised to eliminate the use of the EMAD test data for determining the fuel effective thermal conductivity.

In response to RAI Question 4-5, a new DSC analysis using Icepak™/FLUENT™ code has been generated for the bounding thermal cases. SAR Section A.4.4.4 has been revised to include the details of the CFD model.

Calculation SCE-23.0404 is no longer required to support this submittal.

Question 4-4

Submit details of the specific steps used in the k_{eff} formulation. Address concerns regarding the use of E-MAD data for k_{eff} of fuel with helium backfill.

On page 18 of the SCE-404 (as shown on Figure 3-1), it is stated that the fuel region effective thermal conductivity (k_{eff}) used in the ANSYS model includes the effects of convection outside of the guide sleeve within the thermal conductivity for the fuel region. This results in the ANSYS k_{eff} values being 3 to 6 times higher than the more detailed SINDA/FLUINT analysis values.

It appears that the SAR Section A.4.2.m table of k_{eff} values for PWR fuel with helium backfill is taken directly from Figure 4.5-2 of the Westinghouse E-MAD test report (24PT1 SAR Reference 4.15). These values could be non-conservative as they are for a vertical fuel assembly where natural convection could significantly increase the k_{eff} when compared to a horizontal canister. In addition, the k_{eff} value listed in the SAR table for 400° F appears to be higher than the value presented in the E-MAD figure.

As stated in SAP Section 4.V.4.a, "Applicants using an effective thermal conductivity for the cover gas (e.g., helium) in lieu of a specific convection model should also justify values used in the analysis. . . . Use of effective thermal conductivity coefficients for regions within the confinement cask other than the fuel ... may overestimate heat transfer. If the effective thermal conductivity is used in this manner, [staff should] verify that the same values have been determined from test data that are representative of similar geometry, materials, temperatures, and heat fluxes used in the current application." As stated in SRP Section 4.V.4.b, "If the transverse effective thermal conductivity of the fuel is greater than 0.5 BTU/hr-ft-°F ... under the conditions described in Effective Thermal Conductivity and Edge Configuration Model for Spent Fuel Assembly, the method in which it was determined shall be thoroughly described and supported."

Response to 4-4

SAR Chapter A.4 has been revised to eliminate the use of the E-MAD test data for determining the fuel effective thermal conductivity. Instead, a new methodology has been developed for determining the transverse and axial fuel effective thermal conductivity. A new SAR Section A.4.9 presents the specific details of the methodology used.

Calculation SCE-23.0404 is no longer required to support this submittal.

Question 4-5

Justify the use of the ANSYS model of the thermal performance of the canister and its contents by validating the model against data provided by the INEEL and PNNL studies (or equivalent) of the thermal performance of storage casks. The details of the validation should be submitted for staff review together with details of any new ANSYS models and analyses.

The TN SCE-404 confirmatory analyses shown in Figures 5-2 and 5-4 using SINDA/FLUINT predict a shape of the temperature distribution along a vertical axis of the canister which is consistent with the thermodynamics of the canister. It appears that the ANSYS thermal calculation results (also shown in the two figures) are not consistent with the temperature profiles from the more detailed SINDA/FLUINT model.

As stated in SRP Section 4.V.4.a, [The staff should] "examine the heat transfer processes used in the analysis." In addition, the staff stated in the safety evaluation report for the 24PT1 that "In future reviews, the applicant will be asked to validate the thermal code used for the thermal analysis against data provided by the INEEL and PNNL studies of fuel temperatures in storage casks."

Response to 4-5

A new CFD based DSC analysis using Icepak™/FLUENT™ code has been generated for the bounding thermal cases. This CFD analysis of the DSC is documented in SAR Section A.4.4.4. The methodology for determining the fuel effective conductivity values is provided in a new SAR Section A.4.9.

Plots of the DSC basket temperatures through cross-sections of the DSC from the CFD model is provided in Figures A.4.4-27 and A.4.4-28.

Calculation SCE-23.0404 is no longer required to support this submittal.

Question 4-6

A new (or revised) analysis of the thermal performance of the AHSM should be submitted for staff review.

The staff previously reviewed the thermal design features of the AHSM and 24PT1 canister and the associated HEATING 7 thermal analyses. Approval was granted for a maximum heat load of 13.706 kW when loaded with MOX fuel and 14 kW when loaded with SS304 fuel. The staff concluded that the information provided in the SAR was not sufficient to make a finding of reasonable assurance that the predicted temperatures of the module and canister shell (for higher heat loads) are conservative estimates of the thermal performance of these components.

The module is a complex three dimensional structure. A model of the thermal performance of the module should address the flow patterns throughout the module (for normal, off-normal, and accident conditions), should be sensitive enough to identify "hot spots" in the module, and to predict the three dimensional canister surface temperature distribution. Satisfying these requirements would help to ensure that the module components (particularly the concrete), canister components and fuel cladding temperature limits would not be exceeded.

The staff's expectations are that the model would be discussed in detail, including validation from experimental data from tests of similar systems (that is, geometric complexity and heat loading) or from analyses from previously validated codes. In addition, uncertainties would be quantified (including material properties and calculation accuracy), input and output files would be provided on CDs, and diagrams of the temperature and flow patterns throughout the module and on the surface of the canister would be provided, together with tables of pertinent data.

SRP Section 4.V.4.a states "[The staff should] verify that the model used in the thermal evaluation is clearly described." In addition, SRP Section 4.V.5.a states "The SAR documentation should include input and output file listings for the thermal evaluations. The applicant should also describe, in the SAR, the code and justification for use in the thermal evaluation. ... [The staff should] verify that the information from the thermal model is properly input into the code. [The staff should] verify that the output has been properly interpreted and applied in the thermal and structural analyses."

Response to 4-6

A new CFD based AHSM analysis has been performed for the bounding storage condition case. This analysis uses Icepak™/FLUENT™ code and is documented in SAR Section A.4.4.2. This 3-D AHSM model accurately captures the geometry and layout of the AHSM and its subcomponents as described in SAR section A.4.4.2. The 3-D model

is developed in sufficient detail to address accurate modeling of the expected fluid flow patterns in the AHSM. Hence, the model results pinpoint expected hot-spots in the module.

The methodology for the Icepak™/FLUENT™ model of the AHSM was validated against the NUHOMS®-7P test data and is documented in a new SAR Section A.4.10.

Question 4-7

Evaluate the initial conditions for the canister heatup analysis presented in SAR Section A.4.7.3 and revise them as necessary. Update all related analyses for air and helium as appropriate (accounting for new initial conditions and the issues presented in Question 4-1) and submit the model details and results for staff review. Provide a graph of maximum fuel cladding temperature versus time for helium (similar to Figure A.4.7-2 for air) in addition to an updated graph for air.

In SAR Section A.4.7.3, it is stated that "All temperatures in the 24PT4-DSC are initially assumed to be at the maximum spent fuel pool temperature." In addition, it is stated that the analyses are performed for a fuel pool temperature of 140°F. It appears that this initial condition is non-conservative. During loading operations, the canister and transfer cask are placed in a dedicated section of the spent fuel pool. Since no forced convection is used to maintain the canister water at the pool bulk temperature, the water will heat up as fuel bundles are loaded. Though the fuel cladding for each fuel element may be close to the bulk pool temperature during movement into the canister, the interior of the individual elements will be warmer, and will continue to heat up until an equilibrium is reached between the canister, transfer cask and the pool water.

SAP Section 4.V states that the staff "should assess models used by the applicant for thermal analysis." SAP Section 4.V.4.a states "[The staff should] verify that the model used in the thermal evaluation is clearly described."

Response to 4-7

Since small temperature differences in water will generate relatively large buoyancy forces, the temperature inside a cask/canister submerged in water will be very near that of the water above the cask/canister. There may be some localized boiling at the fuel rod surface but boiling will result in very high heat transfer coefficients at the clad/water interface keeping the temperature of the cladding very close to the water temperature. However, to be conservative, the time to boil has been redefined as the time from the initiation of fuel loading (time-to-boil clock starts when first fuel assembly is loaded in the DSC). The only potential concern associated with steam generation is shielding. A significant loss of water within the DSC cavity during loading operations could result in increased occupational exposure. Additional guidance is provided in Chapter A.8 in the event of boiling in the DSC.

The wording in SAR Section A.4.7.3 has been clarified to reflect this change in the definition of the time to boil.

In order to assure that known conditions exist at the start of blowdown and also the initial fuel clad temperature assumed is conservative for the vacuum drying transient, the DSC cavity will be filled with water, if needed, to assure that the initial cladding temperature is bounded by the 230°F annulus temperature used in the vacuum drying transient. Section A.8 of the SAR is revised accordingly to include this step in the operating procedure.

Figure A.4.7-8 has been updated to reflect the conservative starting temperature of 230°F. The predicted helium steady state temperature demonstrates that no time limit is required for the helium blowdown configuration. This analysis has been generated using the DSC CFD analyses. The model details are included in SAR Section A.4.4.4.

Question 4-8

Revise all proposed TS, bases and SAR contents as necessary to account for any new pressure, density and temperature calculations for normal, off-normal and accident conditions.

The issues presented in Questions 4-1 through 4-7 could lead to significant changes in the predicted behavior of the module/canister system and should be appropriately documented.

SAP Section 4.V.1 states "[The staff should] verify that the applicant includes technical specifications which ensure that the maximum allowed initial cladding temperatures will not be exceeded during normal operations. Technical Specifications should also identify the maximum time permitted for fuel to be submerged in a cask which has been removed from the pool (i.e., when the cask has not been evacuated and sealed)."

Response to 4-8

The vacuum drying time in Technical Specification 3.1.1.b was revised to reflect the change in initial vacuum drying temperature and use of a CFD analysis to determine the steady state helium backfill temperature.

The helium backfill pressure tech spec is revised to reflect a 6 psig +/-0 pressure (Tech Spec 3.1.2.b) to address concerns identified in Question 4-1.

The AHSM thermal monitoring requirements were revised in Tech Spec Section 5.2.5 to increase the frequency as a result of a shorter blocked vent transient timeframe.

No changes to Technical Specification bases are required.

Revision to the contents of the SAR as needed are discussed as part of the responses to RAI Questions 4-1 through 4-7 above.

3.1.1.b 24PT4-DSC Vacuum Drying Time (Duration) and Pressure

LCO 3.1.1.b

Duration: Vacuum Drying of the 24PT4-DSC shall be achieved within the following durations (depending upon the 24PT4-DSC specific heat load configuration) following completion of blowdown using air. No time limits apply for vacuum drying of 24PT4-DSC if helium is used for blowdown. Transfer between air and helium blowdown within the time limits specified below is acceptable. Blowdown with helium with a volume equal to the DSC free volume is required within the air time limit.

Heat Load Configuration	Time Limit Using Air	Time Limit Using Helium
1	35 Hours	No Limit
2	35 Hours	No Limit
3	26 Hours	No Limit

Pressure: The 24PT4-DSC vacuum drying pressure shall be sustained at or below 3 Torr (3 mm Hg) absolute for a period of at least 30 minutes following stepped evacuation.

APPLICABILITY: During **LOADING OPERATIONS**.

ACTIONS

----- **NOTE** -----

This specification is applicable to all 24PT4-DSCs.

CONDITION	REQUIRED ACTION	COMPLETION TIME
A. 24PT4-DSC vacuum drying pressure limit not met when using air for blowdown within 33 hours (Configurations #1 or 2) or 24 hours (Configuration #3).	A.1 Establish helium pressure of at least 1 atm and no greater than 20 psig in the 24PT4-DSC. Vacuum drying can proceed with no time limit.	2 hours
	<u>OR</u> A.2 Flood the 24PT4-DSC with water submerging all FUEL ASSEMBLIES.	2 hours

- d. *TC surface dose rates with 24PT4-DSC payload as specified below shall be confirmed prior to 24PT4-DSC closure to assure proper loading and consistency with the offsite dose analysis.*
- a. *≤ 260 mrem/hr (gamma) at 3 feet from the centerline of the top of the welder neutron shield prior to wet welding operations, with the shield plug in place and approximately 4" of water drained and the welder with its neutron shield in place.*
- b. *≤ 95 mrem/hr (gamma) at 3 feet from the surface of the TC neutron shield at the centerline (mid-height) of the TC prior to wet welding operations.*

5.2.5 AHSM Thermal Monitoring Program

This program provides guidance for temperature measurements that are used to monitor the thermal performance of each AHSM. The intent of the program is to prevent conditions that could lead to exceeding the concrete and fuel clad temperature criteria.

a) AHSM Concrete Temperature

The temperature measurement will be a direct measurement of the AHSM concrete temperature, or other means that would identify and allow for the correction of off-normal thermal conditions that could lead to exceeding the concrete and fuel clad temperature criteria. A temperature measurement of the thermal performance for each AHSM will be taken *on a daily basis for the 24PT1-DSC with a 40 hour blocked vent time limit and twice a day for the 24PT4-DSC with a 25 hour blocked vent time limit.*

If the temperature of the AHSM at the monitored location rises by more than 80°F for the 24PT1-DSC and 30°F for the 24PT4-DSC, based on *this* surveillance, then it is possible that some type of an inlet and or outlet vent blockage has occurred. *Visual inspection of the vents will be initiated and appropriate corrective actions will be taken to avoid exceeding the concrete and cladding temperature limits. The 80°F/30°F values are obtained from a review of a transient thermal analysis of the AHSM with a 24 kW heat load to ensure that the rapid heatup is detected in time to initiate corrective action prior to exceeding concrete or DSC basket material temperature limits for the respective AHSM DSC payloads.*

In addition, if the temperature of the AHSM at the monitored location is greater than 225°F, then it is possible that some type of an inlet and or outlet vent blockage has occurred. *Visual inspection of the vents will be initiated and appropriate corrective actions need to be taken to avoid exceeding the concrete and cladding temperature limits. The 225°F temperature limits are chosen based on the expected concrete temperature for the 24 kW blocked vent scenarios to ensure that the associated fuel clad temperature is not exceeded.*

The AHSM Thermal Monitoring Program provides a positive means to identify conditions that could approach the temperature criteria for proper AHSM operation and

allow for the correction of off-normal thermal conditions that could lead to exceeding the concrete and fuel clad temperature criteria.

b) **AHSM Air Temperature Difference**

Following initial *DSC* transfer to the AHSM, the air temperature difference between ambient temperature and the roof vent temperature will be measured 24 hours (*plus or minus 8 hours*) after *DSC* insertion into the AHSM and again 5 to 7 days after insertion into the AHSM and prior to removing the AHSM door to perform the *DSC* retainer adjustment. If the air temperature differential is greater than 100°F, the air inlets and exits should be checked for blockage. If after removing any blockage found, the temperature differential is still greater than 100°F, corrective actions and analysis of existing conditions will be performed in accordance with the site corrective action program to confirm that conditions adversely affecting the concrete or fuel cladding do not exist.

The specified air temperature rise ensures the fuel clad and concrete temperatures are maintained at or below acceptable long-term storage limits. If the temperature rise is within the $\leq 100^\circ\text{F}$, then the AHSM and *DSC* are performing as designed and no further temperature measurements are required.

c) **AHSM Air Vents**

Since the AHSMs are located outdoors, there is a possibility that the AHSM air inlet and outlet openings could become blocked by debris. Although the ISFSI security fence and AHSM bird screens reduce the probability of AHSM air vent blockage, the ISFSI FSAR postulates and analyzes the effects of air vent blockage.

The AHSM design and accident analyses demonstrate the ability of the ISFSI to function safely if obstructions in the air inlets or outlets impair airflow through the AHSM for extended periods. This specification ensures that blockage will not exist for periods longer than assumed in the analyses.

Site personnel will conduct a daily visual inspection of the air vents to ensure that AHSM air vents are not blocked for more than 40 hours (*with 24PT1-DSC*). For the 24PT4-DSC credit will be taken for the temperature measurement taken in Section 5.2.5.a. Visual inspection of the AHSM air vents with the 24PT4-DSC will be performed only if the temperature monitoring system data is unavailable or if the temperature limits specified in Section 5.2.5.a are exceeded to ensure that AHSM air vents are not blocked for more than 25 hours.

5.3 **Lifting Controls**

5.3.1 **Cask Lifting Heights**

The lifting height of a loaded TC/DSC, is limited as a function of location and temperature as follows:

- a) The maximum lift height of the TC/DSC inside the Fuel Handling Building shall be 80 inches if the ambient temperature is below 0°F but higher than -80°F.
- b) No lift height restriction other than 10CFR50 administrative controls is imposed on the TC/DSC during **LOADING OPERATIONS** *provided that a single-failure-proof crane is used and* if the ambient temperature is higher than 0°F.
- c) The maximum lift height and handling height for all **TRANSFER OPERATIONS** shall be 80 inches if the ambient temperature is greater than 0°F.

These restrictions ensure that any DSC drop as a function of location or low temperature is within the bounds of the accident analysis. If the ambient temperature is outside of the specification limits, **LOADING** and **TRANSFER OPERATIONS** will be terminated.

List of Effective Pages

- Replace entire Chapter A4, revision 0 with attached Chapter A4, revision 2.
- Replace page A.8.1-6, revision 1 with attached page A.8.1-6, revision 2.

A.4 THERMAL EVALUATION

The 24PT1-DSC results presented in Chapter 4 were developed for a maximum heat load of 14 kW. The 24PT4-DSC is designed for 24 kW and the analyses and results are presented herein.

This chapter presents the evaluations that demonstrate that the Advanced NUHOMS® System with the 24PT4-DSC meets the thermal requirements of 10CFR72 [A4.18]. Thermal analysis methodology for fuel cladding temperature limit criteria is consistent with the guidelines given in ISG-11, Revision 3 [A4.21].

A.4.1 Discussion

A.4.1.1 Overview and Purpose of Thermal Analysis

The Advanced NUHOMS[®] System is designed to passively reject decay heat under normal and off-normal conditions of storage, and for accident and loading/unloading conditions while maintaining canister temperatures and pressures within specified limits.

To establish the heat removal capability, several thermal design criteria are established for the Advanced NUHOMS[®] System. These are:

- Pressures within the 24PT4-DSC cavity are within design values considered for structural and confinement analyses.
- Maximum and minimum temperatures of the confinement structural components must not adversely affect the confinement function.
- Maximum fuel cladding temperature limit of 400°C (752°F) is applicable to normal conditions of storage, transfer operations from spent fuel pool to ISFSI pad, and all short term operations including vacuum drying and helium backfilling of the 24PT4-DSC per Interim Staff Guidance (ISG) No. 11 [A4.21]. In addition, ISG-11 does not permit thermal cycling of the fuel cladding with temperature differences greater than 65°C (117°F) during drying and backfilling operations.
- Maximum fuel cladding temperature limit of 570°C (1058°F) is applicable to accidents or off-normal thermal transients [A4.21].
- Thermal stresses for the 24PT4-DSC when appropriately combined with other loads, will be maintained at acceptable levels to ensure the confinement integrity of the Advanced NUHOMS[®] System (see Chapters A.3 and A.11). Chapter A.2 presents the principal design bases for the Advanced NUHOMS[®] System.

A.4.1.2 Thermal Load Specification/Ambient Temperature

The ambient temperature ranges and the hourly temperature variation for the extreme summer ambient conditions that are considered in the thermal analyses of the 24PT4-DSC are the same as those given in Table 4.1-1 and Table 4.1-2. See Section 4.1.2 for a discussion on the basis for these design temperatures.

The maximum total heat load per DSC is 24 kW (Figures A.2.1-1 and Figure A.2.1-2) or 23.76 kW (Figure A.2.1-3) depending on the specific heat load zoning configurations (*HLZCs*) shown in Chapter A.2. To be conservative, the 24PT4-DSC thermal analysis is based on a maximum heat load of 24 kW from 20 to 24 assemblies. Figure A.4.4-11, Figure A.4.4-12, and Figure A.4.4-13 show the three *HLZCs* used in the thermal analysis of the 24PT4-DSC. The maximum heat load per assembly in *HLZC* #3 of 1.3 kW is higher than the 1.26 kW allowed in Chapter A.2 and 0.8 kW is lower than the 0.9 kW allowed in Chapter A.2. However, use of 1.3 kW and 0.8

kW analyzed here for HLZC #3, results in higher temperatures and differential temperatures, and therefore, is considered as bounding for HLZC #3.

A review of these loading configurations confirms that HLZC #1 and HLZC #3 bound HLZC #2. HLZC #1 results in the highest fuel assembly, spacer disc, guidesleeve, oversleeve and BORAL temperatures due to the high heat load in the center of the DSC. HLZC #3 results in the highest support rod temperatures due to proximity of higher heat load assemblies. The 104°F ambient normal storage condition was evaluated with both HLZC #1 and HLZC #3. The results confirm that HLZC #1 has the highest temperature for all DSC basket components except the support rods. The support rod temperature in HLZC #3 exceeds that in HLZC #1 by only 5°F. Therefore, all thermal analyses provided in this chapter will be based on HLZC #1 and the resulting support rod temperatures will be increased by 10°F to conservatively account for the higher support rod temperature for the HLZC #3 DSC heat load configuration.

An axial burnup peaking factor for a typical PWR fuel assembly of 1.08 based on Reference [A4.1] is conservatively applied in the analyses. The parameters of the CE 16x16 fuel assembly type are given in Chapter A.2. Analyses results for normal and off-normal conditions are provided in Section A.4.4, accident conditions in Section A.4.6, and loading/unloading conditions in Section A.4.7. A summary of the results from the analyses performed for normal, off-normal, and accident conditions, as well as maximum and minimum allowable temperatures, is provided in Table A.4.1-1, Table A.4.1-2, and Table A.4.1-3, respectively. The thermal evaluation concludes that with these heat loads, all design criteria for 24PT4-DSC are satisfied for normal, off-normal, and accident conditions.

The transfer cask (TC) was previously licensed for 24 kW [A4.12], which is equal to the maximum heat load of 24 kW for the 24PT4-DSC being licensed in this application. Results are, therefore, not repeated here for the TC.

**Table A.4.1-1
Component Minimum and Maximum Temperatures in the Advanced NUHOMS® System
(Storage or Transfer Mode) for Normal Conditions**

Component	Maximum Storage Mode (°F)	Maximum Transfer ⁽³⁾ Mode (°F)	Minimum ⁽¹⁾ (°F)	Allowable Range (°F) Reference
AHSM Concrete	232	N/A	0	300
AHSM Heat Shield	314	N/A	0	800
AHSM Support Steel	281	N/A	0	800
DSC Shell	459	439	0	0 to 800 [A4.4]
DSC Spacer Disc	653	663	0	0 to 1000 [A4.4]
DSC Guidesleeve or FF Cans	662	670	0	0 to 800 [A4.4]
DSC Oversleeve	662	670	0	0 to 800 [A4.4]
DSC Support Rod/Spacer Sleeve	560	574	0	0 to 650 [A4.4]
DSC Boral® Sheet	662	670	0	0 to 850 [A4.5]
CE 16x16 Zircaloy Cladding	697	707	0	0 to 752 ⁽²⁾ [A4.21]

- (1) For the minimum daily averaged temperature condition of 0°F ambient, the resulting component temperatures will approach 0°F if no credit is taken for the decay heat load.
- (2) These fuel cladding limits apply to the normal conditions of storage and all short term operations, including vacuum drying, helium backfilling and transfer operations from spent fuel pool to ISFSI pad [A4.21].
- (3) Interpolated based on shell temperature between 117°F and -40°F transfer conditions.

**Table A.4.1-2
Component Minimum and Maximum Temperatures in the Advanced NUHOMS® System
(Storage or Transfer Mode) for Off-Normal Conditions**

Component	Maximum Storage Mode (°F)	Maximum Transfer Mode (°F)	Minimum ⁽¹⁾ (°F)	Allowable Range (°F) Ref
AHSM Concrete	242 ⁽²⁾	N/A	-40	300
AHSM Heat Shield	324 ⁽²⁾	N/A	-40	800
AHSM Support Steel	291 ⁽²⁾	N/A	-40	800
DSC Shell	469 ⁽²⁾	443	-40	-40 to 800 [A4.4]
DSC Spacer Disc	663 ⁽²⁾	668	-40	-40 to 1000 [A4.4]
DSC Guidesleeve or FF Can	672 ⁽²⁾	675	-40	-40 to 800 [A4.4]
DSC Oversleeve	672 ⁽²⁾	675	-40	-40 to 800 [A4.4]
DSC Support Rod/Spacer Sleeve	570 ⁽²⁾	580	-40	-40 to 650 [A4.4]
DSC Boral® Sheet	672 ⁽²⁾	675	-40	-40 to 1000 [A4.5]
CE 16x16 Zircaloy Cladding	707 ⁽²⁾	712	-40	Storage: 1058 [A4.21] Transfer: 752 [A4.21]

- (1) For the minimum daily averaged temperature condition of -40°F ambient, the resulting component temperatures will approach -40°F if no credit is taken for the decay heat load.
- (2) Conservatively estimated from Table A.4.1-1 plus 10°F (difference between maximum off-normal daily average ambient temperature, 107°F, and maximum normal daily average ambient temperature, 97°F).

**Table A.4.1-3
Component Minimum and Maximum Temperatures in the Advanced NUHOMS® System
(Storage and Transfer) for Accident Conditions**

Component	Maximum ⁽²⁾ (°F)	Minimum ⁽¹⁾ (°F)	Allowable Range (°F) Ref
AHSM Concrete	392 ⁽³⁾⁽⁴⁾	-40	300
AHSM Heat Shield	542 ⁽³⁾	-40	800
AHSM Support Steel	615 ⁽³⁾	-40	800
DSC Shell	642 ⁽⁶⁾	-40	-40 to 800 [A4.4]
DSC Spacer Disc	836 ⁽⁵⁾	-40	-40 to 1000 [A4.4]
DSC Guidesleeve or FF Can	845 ⁽⁵⁾	-40	-40 to 900 [A4.4] ⁽⁷⁾
DSC Oversleeve	845 ⁽⁵⁾	-40	-40 to 900 [A4.4] ⁽⁷⁾
DSC Support Rod/Spacer Sleeve	738 ⁽⁵⁾	-40	-40 to 800 [A4.4] ⁽⁷⁾
DSC Boral® Sheet	845 ⁽⁵⁾	-40	-40 to 1000 [A4.5]
CE 16x16 Zircaloy Cladding	880 ⁽⁵⁾	-40	-40 to 1058 [A4.21]

- (1) For the minimum daily averaged temperature condition of -40°F ambient, the resulting component temperatures will approach -40°F if no credit is taken for the decay heat load.
- (2) The maximum accident temperature is during a storage mode blocked vent condition.
- (3) Maximum temperature for 40 hour blocked vent from Table 4.4-2 provides conservative estimate for 24PT4-DSC blocked vent condition.
- (4) 392°F is above the 300°F limit given in NUREG-1536. Testing will be performed to document that concrete compressive strength will be greater than that assumed in structural analyses and that the concrete did not degrade (does not show signs of spalling, cracks and/or loss of cement bond to aggregate) due to the elevated temperature.
- (5) Conservatively extrapolated based on blocked vent shell temperature from 117°F storage condition.
- (6) Shell temperature after 25-hour blocked vent for an initial condition of 117°F off-normal storage condition
- (7) See Table A.3.1-6 for code exception with respect to maximum allowable temperature.

A.4.2 Summary of Thermal Properties of Materials

The thermal properties of materials used in the thermal analyses are reported below. The values are listed as given in the corresponding references.

a. Helium

Used for: Blowdown during canister drying operations and for gaps in canister during storage mode. The thermal properties for helium are presented in Section 4.2.a.

b. SA-240, Type 304, ASTM A240, Type 304, 18Cr-8Ni

Used for: Guidesleeves, failed fuel cans and oversleeves. The thermal properties for SA-240, Type 304 stainless steel are presented in Section 4.2.b.

c. SA-240, Type 316, 16Cr-12Ni-2Mo

Used for: 24PT4-DSC shell, outer top cover, outer bottom cover and top shield plug forging. The thermal properties for SA-240, Type 316 stainless steel are presented in Section 4.2.c.

d. SA-533, Gr B, Class 1, Mn-1/2Mo-1/2Ni

Used for: Spacer discs

Temp. °F	Conductivity [A4.4] Btu/hr-ft-°F	Specific Heat, [A4.4] Btu/lbm-°F	Density ⁽¹⁾ [A4.26] lbm/in ³
70	22.3	0.1059	0.284
100	22.6	0.1078	
150	23.1	0.1110	
200	23.4	0.1135	
250	23.7	0.1164	
300	23.8	0.1189	
350	23.8	0.1215	
400	23.8	0.1247	
450	23.7	0.1278	
500	23.5	0.1308	
550	23.2	0.1335	
600	23.0	0.1370	
650	22.7	0.1402	
700	22.3	0.1424	

(1) Density is assumed to be independent of temperature.

e. SA-564, Type 630, 17Cr-4Ni-4Cu

Used for: Support rods, spacer sleeves.

Temp. °F	Conductivity [A4.4] Btu/hr-ft-°F	Specific Heat [A4.4] Btu/lbm-°F	Density ⁽¹⁾ [A4.6] Lbm/in ³
70	9.9	0.107	0.285
100	10.1	0.109	
150	10.4	0.112	
200	10.6	0.114	
300	11.2	0.120	
400	11.7	0.124	
500	12.2	0.130	
600	12.7	0.136	
650	13.0	0.140	

(1) Density is assumed to be independent of temperature.

f. SA-182, Type F316, 16Cr-12Ni-2Mo

Used for: 24PT4 bottom and top shield plug assembly forgings

Temp. °F	Conductivity [A4.4] Btu/hr-ft-°F	Specific Heat, [A4.4] Btu/lbm-°F	Density ⁽¹⁾ [A4.6] lbm/in ³
70	7.7	0.117	0.285
100	7.9	0.118	
150	8.2	0.121	
200	8.4	0.121	
250	8.7	0.124	
300	9.0	0.126	
350	9.2	0.126	
400	9.5	0.128	
450	9.8	0.130	
500	10.0	0.130	
550	10.3	0.132	
600	10.5	0.132	
650	10.7	0.132	
700	11.0	0.134	

(1) Density is assumed to be independent of temperature.

g. ASTM B29 Lead

Used for: Top and Bottom Shield Plugs

Temp °F	Conductivity [A4.14] Btu/hr-ft-°F	Specific Heat ⁽¹⁾ [A4.14] Btu/lbm-°F	Density ⁽¹⁾ [A4.3] lbm/in ³
32	20.1	0.03	0.410
212	19.0		
572	18.0		

(1) Density and specific heat are assumed to be independent of temperature.

h. Boral®

Used for: Poison sheets. The thermal properties for Boral® are the same as those presented in Section 4.2.e.

i. Water

Used for: Water in 24PT4-DSC cavity during loading operations. The thermal properties for water are the same as those presented in Section 4.2.f.

j. Air

Used for: Cover gas for 24PT4-DSC during vacuum drying (see Section A.4.7.1.2 for justification). The thermal properties for air are the same as those presented in Section 4.2.g.

k. Concrete/Soil

Used for: AHSM walls and basemat. Soil is under the basemat. The thermal properties are the same as Sections 4.2.h and 4.2.i.

l. Emissivities

Used for: Modeling thermal radiation

Material Emissivities

Material	Nominal ϵ	References
Stainless steel	0.40	[A4.16]
Rolled steel surfaces ⁽¹⁾	0.587	[A4.9]
Carbon steel	0.35	[A4.7]
Electroless nickel coating	0.15	[A4.17]
Boral plate	0.1	[A4.5]
Zircaloy cladding	0.8	[A4.11]

(1) The rolled steel surfaces (DSC shell), will have higher emissivity than the nominal for a smooth steel surface. Reference [A4.10] gives a ϵ of 0.66 for rolled steel, but a value of 0.587 is conservatively used.

m. PWR Fuel in Helium or Vacuum Environment

The effective thermal conductivity of PWR fuel for the DSC basket analysis are derived in Section A.4.9.

A.4.3 Specifications for Components

Allowable temperature ranges for the structural materials used in the design are given in Table A.4.1-1, Table A.4.1-2, and Table A.4.1-3 for normal, off-normal and accident conditions, respectively. Because of the passive design of the Advanced NUHOMS[®] System, there is no need for rupture discs or pressure relief in the safety related components of the 24PT4-DSC.

A.4.4 Thermal Evaluation for Normal and Off-Normal Conditions of Storage and Transfer

This section describes the thermal analyses of the 24PT4-DSC for normal *and off-normal* conditions of storage and transfer. The analytical models of the 24PT4-DSC *and basket* within the AHSM and the TC are described and the analysis results are provided in this section. The thermophysical properties of the Advanced NUHOMS[®] System components used in the thermal analysis are listed in Section A.4.2.

For normal and off-normal conditions of storage, the 24PT4-DSC components are evaluated for a range of design ambient temperatures listed in Table 4.1-1. For summer ambient conditions, an insolation of 123 BTU/hr-ft², is conservatively applied to the AHSM roof surface. The enveloping solar heat flux of 123 Btu/hr-ft² [A4.13] for the extreme off-normal case is based on a flat horizontal surface averaged over a 24 hour day [A4.2]. Solar heat loads are conservatively neglected for the AHSM thermal analysis for off-normal winter ambient conditions.

The off-normal thermal analysis is performed using the same models as those used for the 24PT4-DSC inside the AHSM, the TC, and the 24PT4-DSC basket for normal conditions as described in this Section. A sunshade is required to be placed over the TC for ambient temperatures above 100°F. This requirement is in Reference [A4.12].

A.4.4.1 Overview of Thermal Analysis for Normal and Off-Normal Conditions of Storage and Transfer

The thermal analysis of the 24PT4-DSC is carried out for the following cases during normal *and off-normal* conditions of storage and transfer.

1. Thermal Analysis of the 24PT4-DSC in the AHSM (Section A.4.4.2),
2. Thermal Analysis of the 24PT4-DSC in the TC (Section A.4.4.3), and
3. Thermal Analysis of the 24PT4-DSC basket (Section A.4.4.4).

A.4.4.2 Thermal Analysis of 24PT4-DSC in the AHSM

A computational fluid dynamics (CFD) model has been developed for analysis of the AHSM. This model has been used to analyze the bounding storage case at an ambient temperature of 104°F. This case is considered bounding for the storage condition since it is associated with the fuel clad temperature limit of 752°F, as compared to a higher fuel clad temperature limit of 1058°F for the off-normal and accident storage cases.

A.4.4.2.1 AHSM Thermal Model Description

Based on the AHSM geometry summarized in Chapter A.1 and detailed in Chapter 1 and the AHSM drawings provided in Section 1.5.2, the thermal-hydraulic environment within the AHSM storage module is evaluated for the bounding hot day condition and a DSC decay heat loading of 24 kW. The program selected for this evaluation is the FLUENT[™] code [A4.31] with the Icepak[™] module [A4.32]. The FLUENT[™] code is a general purpose computational fluid

dynamics (CFD) code that is recognized internationally as one of the premier codes in its class. The general modeling capabilities of the code as they relate to this application include:

- Meshing flexibility using structured and unstructured mesh generation with hexahedra, non-hexahedra, and tetrahedral mesh types
- Capability to model low speed, buoyancy driven flow regimes
- Steady-state and transient flows
- Inviscid, laminar, and turbulent flows
- Heat transfer including forced, natural, and mixed convection, conjugate heat transfer, and radiation
- Custom materials property database
- Integrated problem set-up and post-processing

The Icepak™ module is a fully interactive, object-based graphical interface that allows complex geometries to be modeled and meshed using a combination of shapes in a 'building block' approach. The Icepak™ module does not perform any CFD related numerical calculations itself, but only serves as a pre- and post-processor to the FLUENT™ code. While the Icepak™ module is specifically designed for the analysis of electronic enclosures, its operational features are fully capable of handling the geometry for this application.

Validation of the CFD code for handling the convection and radiation heat transfer includes modeling of the full scale test results for a NUHOMS®-7P DSC in a horizontal storage module [A4.20]. That testing evaluated the thermal performance of the NUHOMS®-7P DSC using a combination of electrical heaters and actual spent fuel assemblies. A summary of this validation is provided in Section A.4.10.

Figure A.4.4-1 illustrates an isometric wire frame view of the AHSM thermal-hydraulic model developed for this evaluation. The +x axis of the model's coordinate system extends across the 101" width of the module from left to right when facing the front of the module. The +y axis is aligned with the elevation of the module with the 0 dimension at the top of the base mat and the maximum 222" dimension at the top of the module's roof. The +z axis extends 235" from the back of the module to the front face of the module.

The model accurately captures the geometry of the curved vault structure of the AHSM along the two vertical air ducts leading from the vault to the horizontal exhaust duct in the roof of the AHSM. While a symmetry plane can be assumed along a y-z plane through the center of the module, a full 3-D model is used since radiative exchange is a major heat transfer mode within the AHSM module and a symmetry model would not permit the correct calculation of the view or shape factors.

The concrete walls and roof of the module are modeled using a combination of block shapes. The program automatically handles the thermal connections between the various model blocks to

create a unified thermal model of the concrete sections. The geometry of the support rails and concrete support blocks are also modeled.

The geometry of the inlet duct within the base unit is modeled to match the actual flow path within the AHSM. A screened opening with a loss coefficient of 0.58 is assumed at the front of the module.

Figure A.4.4-2 shows a 24-sided polygon used to model the DSC within the AHSM. Each side of the polygon spans 15° of the DSC circumference within the AHSM module. This representation is used since the surface-to-surface radiation methodology implemented within the Icepak™ module applies the computed view factors across the entire surface instead of over a sub-set of the surface mesh. Since the number of segments used closely approximates the circular cross section of the DSC, the modeling approach has a minor impact on the flow regime around the DSC and provides a conservative representation of the DSC's surface area.

A 6.88-inch long solid block is used to represent the bottom shield plug and a 8.75-inch long solid block is used to represent the top shield plug. The 180.67-inch long, 0.5-inch thick shell of the DSC is simulated by breaking the DSC into 5 axial segments with lengths of 4", 50", 50", 50", and 26.67" from bottom to top, respectively. At each axial segment, twenty-four (24) 0.5-inch thick polygon blocks, each spanning 15° of the circumference of the DSC, are used to approximate the cylindrical shape of the DSC shell. Based on the support structure design and assuming the DSC is pushed all the way back until it mates with the canister stops, the top of the DSC begins 7.25-inches from the back wall of the module.

The fuel basket is not specifically modeled. Instead, the decay heat loading is simulated as a uniform heat flux applied over the 150", corresponding to the active fuel length of the CE 16x16 FAs. Allowing for the bottom nozzle height of the FA, the active fuel region is assumed to begin 4" above the bottom shield plug.

Figure A.4.4-3 illustrates the model geometry for the heat shields within the AHSM. As seen, the curved shape of the upper heat shields is captured, as is the placement of the inner heat shield at the top of the AHSM's vault. The heat shields are modeled using thin conducting plate elements.

The final flow turn before the outlet opening and the wire mesh at the screened opening are not specifically modeled in order to simplify the modeling and since the flow losses associated with these flow path items have been well defined by experimental testing [A4.30]. Instead, a combined flow loss factor, based on the approach velocity, is applied as a flow resistance element at the outlet. The loss factors are 0.58 for the screened opening, plus 1.0 for the diverging tee turn, or a total flow loss coefficient of approximately 1.6.

The ability of the FLUENT™ program to create non-conformal computational meshes is utilized to concentrate the mesh density in those areas requiring greater fluid flow and/or thermal resolution and decrease the mesh density in those areas (i.e., within the concrete walls, etc.) that do not experience large thermal gradients. The use of non-conformal meshes greatly reduces the size of the problem to be solved, while not negatively impacting the accuracy of the solution. A total of approximately 1,260,300 mesh elements are used for the analysis.

Figure A.4.4-4 illustrates an elevation view of the mesh profile along the y-z plane through the center of the module. The non-conformal nature of the mesh is evident from the figure with the mesh density being significantly higher in the region of the inlet duct, the DSC shell and heat shields, and the outlet duct and much lower elsewhere.

The CFD analysis is conducted with radiation and turbulent flow enabled. The radiation view factors were calculated using the 'hemicube' methodology, with the mesh coarsening option disabled to avoid lessening the resolution for the curved and angled surface shapes. The effects of flow turbulence are calculated using the 'mixing-length zero-equation' turbulence model, while the temperature-dependent fluid density is computed using the Boussinesq model. Both of these computational options represent the FLUENT™ recommendations for natural convection, buoyancy driven problems. The appropriateness of assuming a turbulent flow regime was validated via a sensitivity run wherein only a laminar flow regime was permitted and another sensitivity run using the 2-equation turbulence model with wall enhancements. Both sensitivity runs produced results that were similar to those obtained with 'mixing-length zero-equation' turbulence model. The use of the Boussinesq model was also validated via a sensitivity run wherein the use of the ideal gas option to compute density produced similar peak temperatures.

Direct simulation of insolation on the outside vertical and horizontal surfaces of the AHSM could not be included in the selected modeling approach due to program limitations on the number of boundary conditions that can be applied at each surface. Therefore, the simulation of the insolation was addressed by increasing the reference temperature used to compute the convective and radiation heat transfer exchange from the affected surfaces to account for the insolation heating of the surface.

Adiabatic conditions are assumed for the side and back walls of the module.

A.4.4.2.2 Description of Cases Evaluated for the AHSM

As stated in Section A.4.4.2, AHSM analysis at 104°F represents the bounding case. In addition, a -40°F case was evaluated as a bounding off-normal case, since this case results in maximum thermal gradients for the structural analysis of the AHSM components.

The evaluation of the AHSM for 117°F off-normal condition is extrapolated from the results obtained from the 104°F condition. A review of the results presented in Table 4.4-3 and Table 4.4-5 from the HEATING7 analysis demonstrates that the relationship between the ambient temperatures and the individual component temperatures is approximately linear. Hence, the extrapolations of results from the 104°F case by adding the difference in the average daily ambient temperatures between the normal and off-normal ambient temperature (107°F -97°F) to the calculated component temperatures is appropriate.

A.4.4.2.3 AHSM Thermal Analysis Results

Figure A.4.4-5 presents the predicted temperature profile of the DSC surface temperature distribution for the analyzed decay heat loading of 24 kW within the DSC and the bounding normal hot day condition with a peak daily temperature of 104°F and a 24-hour average of 97°F.

Figure A.4.4-6 illustrates the temperature profile of the heat shields within the AHSM. The variation in temperature from back to front on the heat shield reflects the computed distribution of airflow over the DSC.

Figure A.4.4-7 illustrates the flow profile along a y-z plane through the center of the module. The figure depicts the expected regions of flow recirculation within the inlet duct and in the plenum below the DSC. The figure also shows that, despite interior obstructions, the airflow is relatively evenly distributed along the length of the DSC. A maximum flow velocity of approximately 5.6 feet per second is seen to occur in the vertical exhaust duct at the rear of the module.

Table A.4.4-1 and Table A.4.4-2 summarize the results of the AHSM thermal analysis performed. Table A.4.4-3 summarizes the peak temperatures for the AHSM components based on this model. Table A.4.4-4 summarizes the peak DSC shell surface temperatures as a function of its geometry (from bottom to top) for the normal and off-normal conditions.

A.4.4.3 Thermal Analysis of 24PT4-DSC in the TC

The thermal analysis of the 24PT4-DSC in the TC is also split into separate models for the 24PT4-DSC and TC. This allows for independent calculation of 24PT4-DSC internal temperatures, using the 24PT4-DSC shell temperatures calculated in the TC model as input.

The purpose of the TC analysis is to determine the 24PT4-DSC shell temperatures to be used as boundary conditions in a subsequent 24PT4-DSC basket thermal analysis described in Section A.4.4.4. The thermal analysis of the TC with total heat load of 24 kW is presented in Section 4.4.3. The shell temperatures were provided for the 24PT1-DSC for the required range of ambient conditions with a 24 kW heat load. These shell temperatures are directly applicable for 24PT4-DSC since the shell outside diameter, wall thickness, and materials are the same for both designs. Since the thermal analysis of the TC is based on a homogenized DSC model, a small difference in basket dimensions between 24PT1-DSC and 24PT4-DSC will have a negligible affect on the results.

A.4.4.3.1 TC Model Description

See Section 4.4.3.1.

A.4.4.3.2 Description of Cases Evaluated for the 24PT4-DSC inside the TC

The TC thermal analyses are performed for the range of design basis ambient air temperatures defined in Section 4.1 for normal and off-normal conditions. The TC thermal analysis was not performed for the design life average temperature since this case is enveloped by the other normal cases.

The thermal stress analysis of the 24PT4-DSC shell assembly is based on the temperature results of 24PT1-DSC shell assembly with 24 kW heat load presented in Section 4.4.3.3. The cases which are used to determine the thermal stresses for normal and off-normal conditions are listed in Table A.4.4-8.

A.4.4.3.3 TC Thermal Model Results

The calculated temperature for the 24PT4-DSC shell with a 24 kW heat load during *normal and off-normal* transfer operations is presented in Table A.4.4-4. These results are used in the structural analysis described in Chapter A.3 and are used as boundary conditions in the 24PT4-DSC basket thermal analysis presented in Section A.4.4.4.

A.4.4.4 24PT4-DSC Basket Thermal Analysis

A CFD model has also been developed for the thermal analysis of the DSC basket and fuel assemblies. This CFD model has been used to analyze the bounding cases for storage and transfer conditions. The bounding storage configuration is the maximum normal storage case (104°F ambient) while the bounding transfer configuration is the maximum off-normal condition (117°F ambient). These cases are considered bounding since they represent the minimum margin with respect to the fuel clad temperature limit.

A.4.4.4.1 24PT4-DSC Basket Model Description

Based on the 24PT4-DSC geometry summarized in Section Chapter A.1 and the drawings provided in Section A.1.5, the thermal-hydraulic environment within the DSC is evaluated for the bounding storage and transfer conditions and a decay heat loading of 24 kW. The program selected for this evaluation is the FLUENT™ code [A4.31] with the Icepak™ module [A4.32]. A discussion of the FLUENT™ code and the Icepak™ module is provided in Section A.4.4.2.1.

Figure A.4.4-8 illustrates an isometric wire frame view of the thermal-hydraulic model of the DSC basket developed to simulate a representative segment of the fuel basket along its axial length. The modeled segment spans from the mid-plane on one spacer disc to the mid-plane on an adjacent spacer disc (a 6.8" length) and is centered on the section of the active fuel length exhibiting the peak heat flux. The thermal model encompasses a 360° segment of the basket cross-section with symmetry conditions assumed to exist at the axial boundaries of the model. The x-axis of the model's coordinate system is aligned with the horizontal axis and the y-axis is aligned with the vertical axis of the horizontally oriented DSC. The z-axis is aligned along the length of the DSC. The origin of the coordinate system is at the center of the modeled canister segment.

Twenty-four (24) individual plate segments are used to approximate the curved geometry of the DSC shell in order to facilitate the imposition of a variable boundary temperature condition at the shell of the DSC as a function of the circumferential position. Table A.4.4-4 lists the shell temperatures calculated in Section A.4.4.2 and A.4.4.3, which are imposed as a boundary condition in this calculation.

The fuel assemblies are modeled as solids with anisotropic effective thermal properties. Section A.4.9 determines the axial and radial thermal conductivity values used for the fuel assemblies as a function of temperature. The radial or 'through' direction of the fuel is across the width of the fuel assembly (i.e., in the x-axis and y-axis directions), while the 'axial' direction is in the z-axis direction.

The poison sheets are modeled as a composite material consisting of the BORAL™, the stainless steel wrapper, and the assumed air gaps in the interfaces between these materials.

Figure A.4.4-9 illustrates the model geometry for the spacer discs. Both the placement and the size of the disc cutouts are accurately reflected in the model geometry. A total of approximately 1,050,000 mesh elements are used for the analysis to represent the various components of the DSC shell, the fuel basket, and the fuel assemblies. Figure A.4.4-10 illustrates a plan view of the mesh for the spacer discs.

The CFD analysis is conducted with radiation and turbulent flow enabled. The radiation view factors were calculated using the 'hemicube' methodology, with the mesh coarsening option disabled to avoid lessening the resolution for the curved and angled surface shapes. The effects of flow turbulence are calculated using the 'mixing-length zero-equation' turbulence model, while the temperature-dependent fluid density is computed using the Boussinesq model. Both of these computational options represent the FLUENT™ recommendations for natural convection, buoyancy driven problems. The use of the Boussinesq model was validated via a sensitivity run wherein the use of the ideal gas option to compute density produced similar peak temperatures.

The steady state shell surface temperatures for the 24PT4-DSC resting inside the AHSM are calculated in the AHSM CFD thermal analysis, described in Section A.4.4.2 above. The shell surface temperatures for the 24PT4-DSC resting inside the TC are calculated in the TC thermal analysis as described in Section A.4.4.3. The temperatures for the 24PT4-DSC shell presented in Table A.4.4-4 are used as the temperature boundary conditions for the 24PT4-DSC basket model.

The decay heat is applied as a volumetric heat generation uniformly distributed over the homogenous fuel regions inside the guidesleeve assemblies. The resulting volumetric heat density, including a peaking factor of 1.08, which was applied over the active fuel length of 150 inches, are computed.

The resulting calculated temperature profiles for the 24PT4-DSC show guidesleeve, failed fuel can, poison plate, and oversleeve temperatures, and other 24PT4-DSC internal component temperatures. These component temperature profiles are used for the evaluation of fuel cladding maximum temperatures and helium temperatures (for use in the 24PT4-DSC internal pressure evaluation). These temperatures are also used to evaluate the thermal stresses in the 24PT4-DSC shell and the spacer discs as described in Chapters A.3 and A.11.

A.4.4.4.2 Description of Cases Evaluated for the 24PT4-DSC Basket

The 24PT4-DSC basket and fuel assembly heat transfer analyses with the 24PT4-DSC inside the AHSM, is performed for the bounding 104°F ambient case. The basket analyses with the 24PT4-DSC inside the TC are performed for the bounding 117°F and -40°F ambient cases.

Temperature profiles for the spacer disc are used to determine thermal stresses shown in Chapter A.3. The normal and off-normal storage and transfer cases which are considered are listed in Table A.4.4-8.

A.4.4.4.3 24PT4-DSC Thermal Model Results

The results obtained from the *CFD* analytical model for each of the three *HLZCs* are in the form of temperature profiles. From these analytical results, the 24PT4-DSC component temperatures are extracted and summarized in Table A.4.4-6. The bounding fuel cladding temperature results are summarized in Table A.4.4-7. The basket components and fuel cladding maximum temperatures are compared against their limits in Table A.4.1-1 and Table A.4.1-2. The results demonstrate that all the material temperature limits are satisfied and there is a very low probability of cladding failure during *normal* or *off-normal* storage or transfer conditions.

A.4.4.4.3.1 24PT4-DSC Basket Thermal Analysis Results Inside AHSM

The design basis analysis of the thermal performance in the *AHSM* is conducted for the normal condition of storage with a peak daily temperature of 104°F, a 24-hour average of 97°F, solar insolation, and a decay heat loading of 24 kW within the *DSC*. This condition yields the lowest thermal margin for the fuel cladding temperature. Figure A.4.4-14 illustrates the *DSC* shell temperatures obtained from the results of the *AHSM* thermal analysis presented in Section A.4.4.2.3. Figure A.4.4-15 through Figure A.4.4-17 present a summary of the temperature distributions in the basket and fuel cladding predicted for the 104°F storage condition.

Figure A.4.4-18 illustrates the velocity profile through the center of the modeled segment of the *DSC*. The profile demonstrates the expected result of a global circulation pattern up through the vertical channels between the fuel assemblies and then downward along the shell to the bottoms of the vertical channels. Further, as expected, the flow in the horizontal channels between the fuel assemblies is very limited with the exception of the channels surrounding the fuel assemblies in the corners of the fuel basket. The maximum flow velocity seen in the center of the fuel basket is less than 1 foot per second. The peak flow velocity of approximately 2.3 feet per second occurs on the left and right sides of the basket where the flow is choked down as it passes between the outermost corner of the fuel assemblies and the *DSC* shell.

Table A.4.4-4 and Table A.4.4-6 present a summary of the *DSC* shell and basket component temperatures, respectively, for the normal and off-normal conditions. The predicted peak fuel cladding temperatures are shown in Table A.4.4-7. Examination of the results shows that all temperatures are well within their allowable temperature limits.

Figure A.4.4-27, provides the temperature distribution along a vertical cross-section of the basket for the 104°F storage condition.

A.4.4.4.3.2 24PT4-DSC Basket Thermal Analysis Results Inside TC

The design basis analysis of the thermal performance in the *TC* is conducted for the off-normal condition of transfer with a peak daily temperature of 117°F, the use of a sun shade, and a decay heat loading of 24 kW within the *DSC*. This condition yields the lowest thermal margin for the fuel cladding temperature. Figure A.4.4-19 illustrates the associated *DSC* shell temperatures obtained from the analysis of the *DSC* in the transfer cask. As seen, a uniform *DSC* shell temperature of 443°F is conservatively used for this condition. Figure A.4.4-20 to Figure

A.4.4-22 present a summary of the temperature distributions in the basket and fuel cladding predicted for the analyzed condition.

Figure A.4.4-23 illustrates the velocity profile through the center of the modeled segment of the DSC. The velocity profiles are essentially similar to those seen in Figure A.4.4-18 for the analyzed condition within the AHSM except for the magnitude of the peak velocity. The peak velocity seen in this analysis is lower than the evaluation for the AHSM due to the conservative assumption of absence of a temperature variation around the circumference of the DSC shell. As such, the buoyancy forces available to drive the flow pattern are less. As with the analysis in the AHSM, the peak flow velocity of approximately 1.7 feet per second seen for the evaluated operation in the transfer cask occurs on the left and right sides of the basket where the flow is choked down as it passes between the outermost corner of the fuel assemblies and the DSC shell.

Table A.4.4-4 and Table A.4.4-6 present a summary of the DSC shell and basket component temperatures, respectively, for the normal and off-normal conditions. Table A.4.4-7 presents the calculated maximum fuel cladding temperatures. Examination of the results shows that all temperatures are well within their allowable temperature limits.

Figure A.4.4-28, provides the temperature distribution along a vertical cross-section of the basket for the 117°F transfer condition.

A.4.4.5 Test Model

The detailed, conservative evaluations described above for the AHSM, TC, and 24PT4-DSC ensure that the Advanced NUHOMS® System is capable of dissipating the design basis heat load. The conservative approach precludes the necessity to perform thermal testing.

A.4.4.6 Maximum Temperatures

The peak temperatures for the 24PT4-DSC structural components are listed in Table A.4.4-4 and Table A.4.4-6 for the range of operating conditions. The peak fuel cladding temperatures are listed in Table A.4.4-7 for the full range of operating conditions.

Temperatures for AHSM normal and off-normal conditions are provided in Table A.4.4-2 and Table A.4.4-3.

A summary of these results for the normal and off-normal conditions are provided in Table A.4.1-1 and Table A.4.1-2, respectively.

A.4.4.7 Minimum Temperatures

For the minimum daily averaged temperature condition of 0°F ambient for the normal condition and -40°F for the off-normal condition, the resulting component temperatures will approach 0°F and -40°F, respectively, if no credit is taken for the decay heat load. Since the 24PT4-DSC materials, including confinement structures and welds, continue to function at this temperature (structural materials are stainless steel, or carbon steel), the minimum temperature condition has no adverse effect on the performance of the Advanced NUHOMS® System during storage. See

Technical Specifications for controls applicable to moving a loaded TC/24PT4-DSC as a function of temperature and location.

A.4.4.8 Maximum Internal Pressure

Based on the results of the 24PT4-DSC thermal analysis, the initial pressure of the helium fill gas during loading operations, and the characteristics of the fuel assemblies being stored, a conservative prediction of the maximum gas pressure within the 24PT4-DSC cavity during normal conditions is determined.

The characteristics of the fuel assemblies are given in Table A.4.4-9. The parameters in Table A.4.4-9 are used to determine the amount of fuel rod fill gas and fission gas moles for 24 CE 16x16 Zircaloy clad fuel assemblies.

Based on the basket temperature results in Table A.4.4-6 and the fuel cladding temperature results of Table A.4.4-7, the maximum pressure in the 24PT4-DSC cavity for normal conditions will occur while in the TC at peak summer ambient condition.

An average helium temperature is calculated for determining the DSC pressure by averaging the model mesh temperatures as follows:

$$T_{gas\ aver} = \frac{\sum (T_{element} \cdot V_{element})}{\sum V_{element}}$$

The resulting maximum average helium temperature for the normal *and off-normal conditions* are given in Table A.4.4-10.

The helium pressure during the backfill operation is limited to 7 psig (6.0 psi + 1.0 psi, -0.0 psi per Technical Specification 3.1.2.b). For this condition, a uniform helium temperature of 230°F is assumed, which is approximately equal to the maximum temperature of water in the TC/DSC annulus expected during the loading operations. This assumption is conservative for the following reasons; (1) the assumption of a lower temperature will yield the maximum number of moles of helium gas at the time of backfill and, thus, the maximum predicted canister pressure at steady-state conditions, and (2) the canister and fuel assemblies have ample time during decontamination, welding, blowdown, and vacuum drying described in Chapter A.8 to heatup. The quantity of helium fill gas is then calculated using the ideal gas equation.

For normal *and off-normal* conditions, 1% *and 10%* failure of the fuel rods, *respectively*, is assumed. For the ruptured rods, 100% release of the fuel rod fill gas and 30% release of the fission gas is assumed, based on guidance in Reference [A4.2]. Based on this guidance, the maximum normal *and off-normal* pressures *are* calculated using the ideal gas law and is presented in Table A.4.4-10.

A.4.4.9 Maximum Thermal Stresses

The maximum thermal stresses are presented in Chapter A.3 for the 24PT4-DSC basket and shell assemblies. The AHSM thermal stresses are presented in Chapter 3. The cases that were evaluated for the AHSM and 24PT4-DSC are listed in Table A.4.4-8.

Figure A.4.4-24, Figure A.4.4-25 and Figure A.4.4-26 depicting the thermal gradients across the spacer discs, show the gradients used in the structural analyses (labeled ANSYS) versus those predicted by the CFD analysis (labeled FLUENT™). From these figures it is clear that the CFD analysis gradients are bounded by the ANSYS analysis gradients used in the structural analysis. Therefore, the spacer disc structural analysis is conservative. The controlling thermal gradients for the shell are the transfer cask cases which were not impacted by the CFD analysis. The increase in AHSM component temperatures was minimal with respect to associated stress margins, therefore, the CFD analysis results had no impact on the AHSM thermal stresses.

A.4.4.10 Evaluation of System Performance for Normal Conditions of Storage and Transfer

The thermal analysis for normal *and off-normal* storage and transfer *conditions* concludes that the 24PT4-DSC design meets all applicable requirements. The maximum *component* temperatures calculated using conservative assumptions are within the criteria set forth. The predicted maximum fuel cladding temperature is well below the allowable fuel temperature limits given in Table A.4.1-1 and Table A.4.1-2. The comparison of the results with the allowable material temperature ranges is *also provided* in Table A.4.1-1 and Table A.4.1-2.

Table A.4.4-1
AHSM Bulk Air Temperatures

AHSM Inlet Air Temperature (°F)	$\Delta T_{air}^{(2)}$
-40	80
104 ⁽¹⁾	99

Notes:

- (1) *These values represent maximum inlet air temperatures. A conservative 24-hour average as determined in Section 4.1 was used in the analysis.*
- (2) $\Delta T_{air} = \text{AHSM outlet temperature} - \text{AHSM inlet temperature}$

Table A.4.4-2
AHSM Thermal Analysis Results Summary

Operating Condition (°F)	T_{amb} (°F)	$T_{con,max}$ (°F)	$T_{hs,max}$ (°F)	$T_{sup,max}$ (°F)
<i>Normal</i>	104	232	314	281
<i>Off-Normal</i>	-40	80	180	170
	117	242 ⁽¹⁾	324 ⁽¹⁾	291 ⁽¹⁾
<i>Blocked Vent Transient⁽³⁾</i>	-40	243	426	526
	117	392 ⁽²⁾	542	615

- (1) Conservatively extrapolated from the normal 104°F case by adding the difference in daily average ambient temperature (107-97=10) to all peak component temperatures.
- (2) 392°F is above the 300°F limit given in Reference [A4.2] - Testing will be performed to document that concrete compressive strength will be greater than that assumed in structural analyses.
- (3) 40-hour blocked vent data conservatively reported. Maximum blocked vent time per Tech Specs is 25 hours.

Nomenclature used in table

T_{amb} *Ambient temperature*
 $T_{con,max}$ *Maximum concrete temperature*
 $T_{hs,max}$ *Maximum heat shield temperature*
 $T_{sup,max}$ *Maximum AHSM support structure temperature*

Table A.4.4-3
AHSM Peak Component Temperatures at Normal/Off-Normal Conditions

Component	117°F Off-Normal Extrapolated⁽¹⁾ Results	104°F Storage Condition	-40°F Storage Condition
<i>DSC Support Rail</i>	291	281	170
<i>Inner Heat Shield</i>	324	314	180
<i>Upper Heat Shield</i>	286	276	136
<i>Upper Back Wall</i>	232	212	61
<i>Roof Vault</i>	242	232	80

(1) Conservatively extrapolated from the normal 104°F case by adding the difference in daily average ambient temperature (107-97=10) to all peak component temperatures.

Table A.4.4-4
24PT4-DSC Maximum Shell Temperatures for Normal/Off-Normal Conditions

Position on DSC	DSC Shell Temperature (°F)					
	Inside AHSM @ 117°F ⁽²⁾	Inside AHSM @ 104°F	Inside AHSM @ -40°F	Inside TC @ 125°F ⁽¹⁾	Inside TC @ 104°F	Inside TC @ -40°F ⁽¹⁾
0° to 7.5°	377.0	367.0	279.3	443	439	146.0
7.5° to 22.5°	378.6	368.6	278.0			165.5
22.5° to 37.5°	367.0	357.0	261.9			185.0
37.5° to 52.5°	367.3	357.3	253.1			204.5
52.5° to 67.5°	381.2	371.2	261.3			224.0
67.5° to 82.5°	395.9	385.9	263.0			243.5
82.5° to 97.5°	400.0	390.0	262.7			263.0
97.5° to 112.5°	398.4	388.4	268.9			282.5
112.5° to 127.5°	408.4	398.8	287.2			302.0
127.5° to 142.5°	427.8	417.8	310.8			321.5
142.5° to 157.5°	441.9	431.9	331.6			341.0
157.5° to 172.5°	457.1	447.1	346.2			360.5
172.5° to 180°	469.3	459.3	358.7			380.0

(1) These results are taken from the previous analysis to support CofC 1004. This ambient condition is not based on a daily average temperature as was derived in Section A.4.1. Therefore, this temperature still bounds the daily average defined in Section A.4.1 for a maximum of 104°F.

(2) The 117°F storage case is extrapolated from the 104°F case by adding the difference in maximum daily average ambient temperatures between the two cases (107-97=10°F).

**Table A.4.4-5
24PT4-DSC Maximum Shell Temperatures for Accident Conditions**

Configuration Ref	T _{amb} (°F)	T _{shell} (°F)
24PT4-DSC in AHSM Blocked vent accident	117	642
24PT4-DSC horizontal in TC, Loss of sunshade and neutron shield	125 ⁽¹⁾	536
24PT4-DSC horizontal in TC, Fire transient	125 ⁽¹⁾	527

(1) *These results are taken from the previous analysis to support CofC 1004. This ambient condition is not based on a daily average temperature as was derived in Section A.4.1. Therefore, this temperature still bounds the daily average defined in Section A.4.1 for a maximum of 104 °F.*

Nomenclature used in table

T_{amb} Ambient temperature
T_{shell} 24PT4-DSC shell temperature

**Table A.4.4-6
24PT4-DSC Basket Temperature Results⁽⁴⁾**

Configuration	T_{amb} (°F)	T_{sp} (°F)	T_{sr} (°F)	T_{gs} (°F)	T_{Boral®} (°F)
24PT4-DSC in AHSM	104	653	560	662	662
24PT4-DSC in AHSM ⁽²⁾	117	663	570	672	672
24PT4-DSC in AHSM	-40	<i>Bounded by -40°F TC case</i>			
24PT4-DSC in AHSM, blocked vent accident ⁽¹⁾	117	836	738	845	845
24PT4-DSC horizontal in TC ⁽³⁾	104	663	574	670	670
24PT4-DSC horizontal in TC	-40	590	490	601	601
24PT4-DSC horizontal in TC with shade	117	668	580	675	675
24PT4-DSC horizontal in TC loss of sunshade and neutron shield accident ⁽¹⁾	117	761	673	768	768
24PT4-DSC horizontal in TC, Fire transient ⁽¹⁾	117	752	664	759	759

- (1) The accident results are extrapolated from the 117°F TC condition by increasing the component temperatures by the difference between the accident shell temperature and the 117°F TC condition shell temperature.
- (2) The 117°F storage case is extrapolated from the 104°F case by adding the difference in maximum daily average ambient temperatures between the two cases (107-97=10°F).
- (3) Interpolated between -40°F and 117°F transfer cases.
- (4) For vacuum drying case, see Table A.4.7-2.

Nomenclature used in table

- T_{amb} Ambient temperature
- T_{sp} Maximum spacer disc temperature
- T_{sr} Maximum support rod temperature
- T_{gs} Maximum guidesleeve temperature
- T_{Boral®} Maximum poison plate temperature

**Table A.4.4-7
24PT4-DSC Maximum Fuel Cladding Temperature Results⁽¹⁾**

Case	Calculated Maximum Cladding Temperature (°F)	Fuel Temperature Limit (°F)
24PT4-DSC in AHSM, 104°F ambient	697	752
24PT4-DSC in AHSM, 117°F ambient	707	1058
24PT4-DSC in AHSM, -40°F ambient	<i>Bounded by -40°F TC case</i>	1058
24PT4-DSC in AHSM, 117°F amb, blocked vent accident	880	1058
24PT4-DSC horizontal in TC, -40°F amb	636	1058
24PT4-DSC horizontal in TC, 104°F amb	707	752
24PT4-DSC horizontal in TC, 117°F amb with sunshade	712	1058
24PT4-DSC horizontal in TC, 117°F amb loss of sunshade and neutron shield accident	805	1058
24PT4-DSC horizontal in TC, Fire transient	796	1058

(1) For vacuum drying case, see Table A.4.7-2.

**Table A.4.4-8
Summary of Cases Considered for Thermal Stress Analysis**

Component	Operation	Heat Load (kW)	Ambient Temperature (°F)	Condition
24PT4-DSC Shell Assembly	Transfer	24	-40	Off-Normal
24PT4-DSC Shell Assembly	Transfer	24	100 ⁽¹⁾	Normal
24PT4-DSC Shell Assembly	Storage	24	-40	Off-Normal
24PT4-DSC Shell Assembly	Storage	24	104	Normal
24PT4-DSC Shell Assembly	Storage	24	117	Off-Normal
24PT4-DSC Basket	Storage	24	-40	Off-Normal
24PT4-DSC Basket	Storage	24	117	Off-Normal
24PT4-DSC Basket	Transfer	24	-40	Off-Normal
24PT4-DSC Basket	Transfer	24	104	Normal
24PT4-DSC Basket	Transfer	24	117	Off-Normal
24PT4-DSC Basket	Vacuum Drying	24	120	Normal

(1) These results are taken from the previous analysis to support CofC 1004. This ambient condition is not based on a daily average temperature as was derived in Section A.4.1. Therefore, this temperature still bounds the daily average defined in Section A.4.1 for a maximum of 104°F.

**Table A.4.4-9
Fuel Assembly Characteristics for Pressure Analysis**

Parameter	CE 16x16 Zircaloy Clad
Number of fuel rods	236
Maximum rod fill pressure (psig)	380 ± 15
Maximum rod void volume (in ³)	1.53
Quantity of fission gas per assy (g-moles)	44.15

**Table A.4.4-10
24PT4-DSC Cavity Pressure Analysis Summary**

Condition	$T_{He,ave}$ (°F)	n_{He} (g-mole)	n_{fill} (g-mole)	n_{fiss} (g-mole)	P (psig)	Thermal Criteria (psig) ⁽¹⁾	Pressures Used in Stress Analysis (psig) Table A.3.1-6
Normal	546.7	294.8	1.65	3.51	17.5	20	20
Off-Normal	550.1	294.8	16.5	35.13	22.3	23.4	26
Accident	713	294.8	164.59	351.3	80.7	81	90

(1) These criteria are used for thermal analyses only. The off-normal and accident thermal criteria have additional margin to account for the effect of the fission gases in the 24PT4-DSC cavity on the thermal results.

Nomenclature used in table

$T_{He,ave}$ Average helium temperature
 n_{He} Number of moles of helium backfill
 n_{fill} Number of moles of fuel rod fill gas released to 24PT4-DSC cavity
 n_{fiss} Number of moles of fission gas released to 24PT4-DSC cavity
P 24PT4-DSC cavity pressure

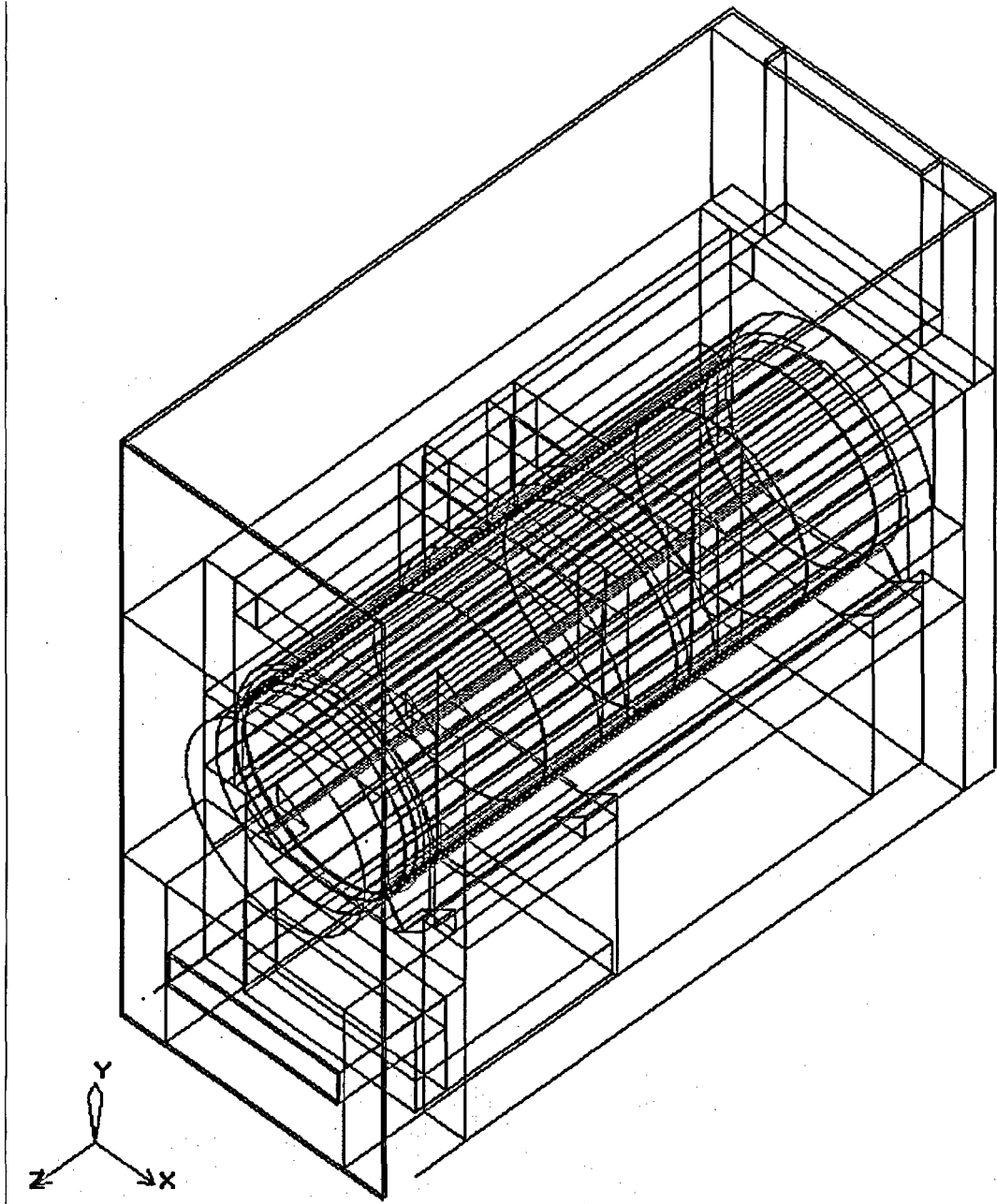


Figure A.4.4-1
Isometric, Wireframe View of the AHSM Model Layout

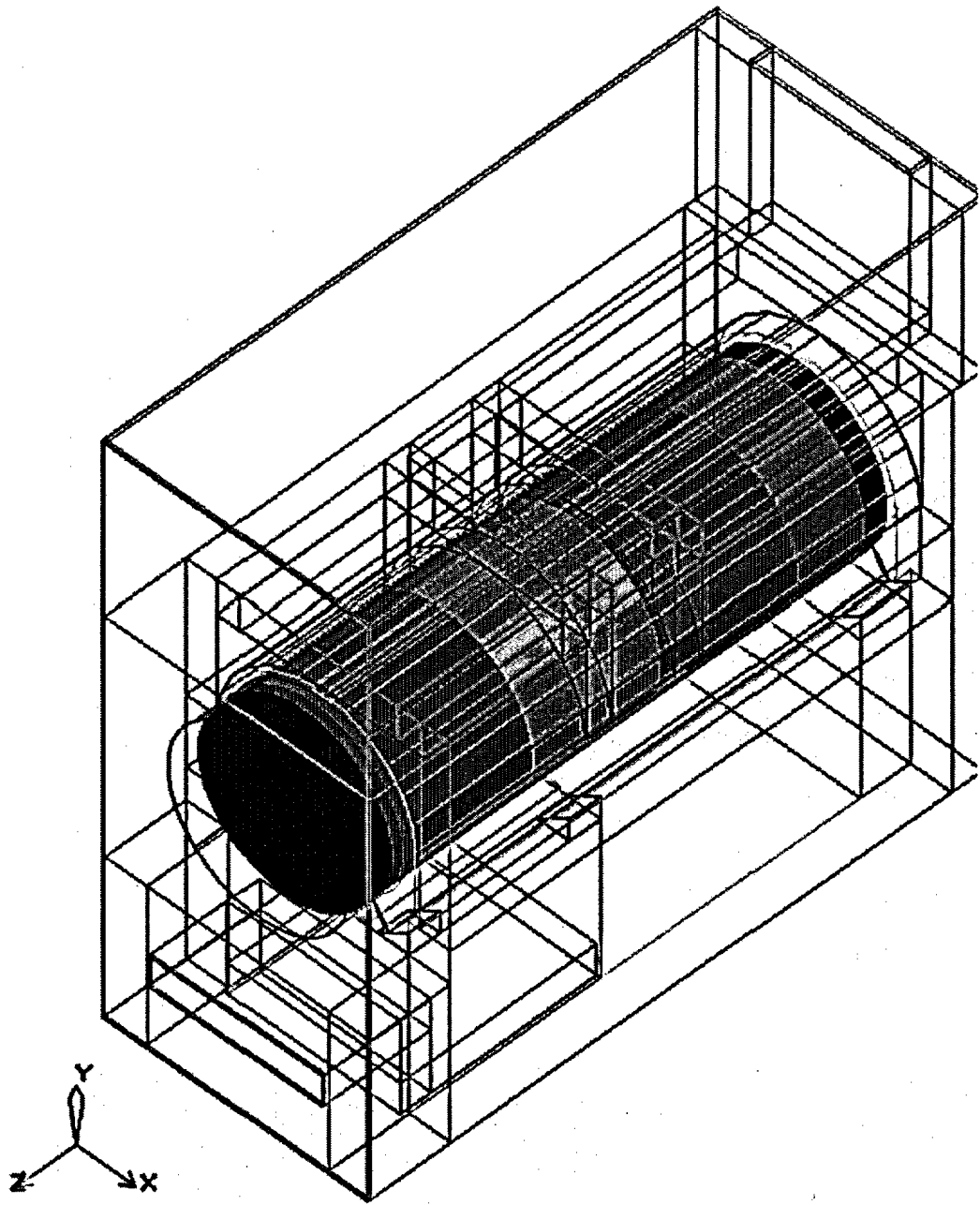


Figure A.4.4-2
Isometric View of Seven (7) Axial Segments Used to Simulate DSC within Module

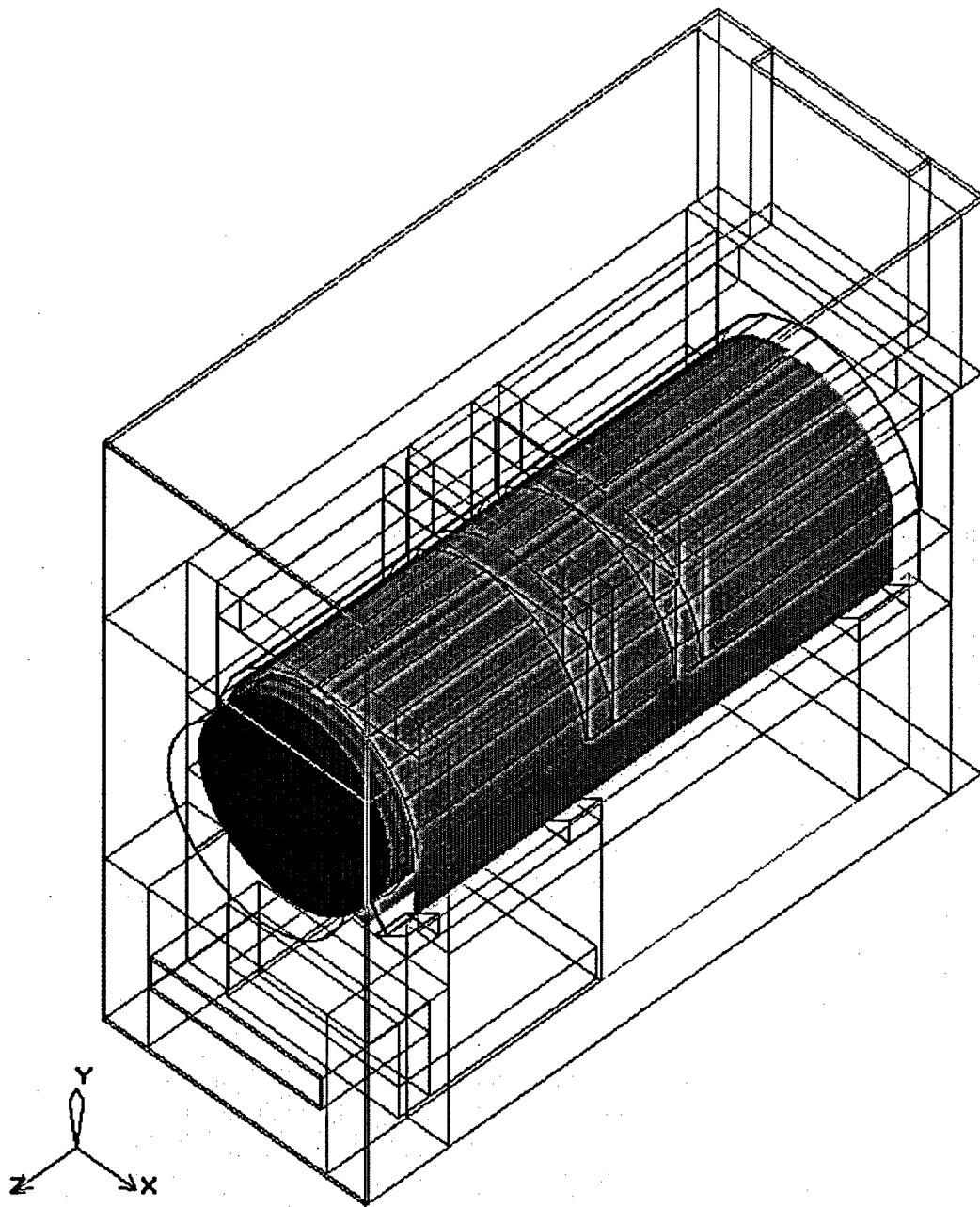


Figure A.4.4-3
Isometric View of 24PT4-DSC & Heat Shield Layout within Model

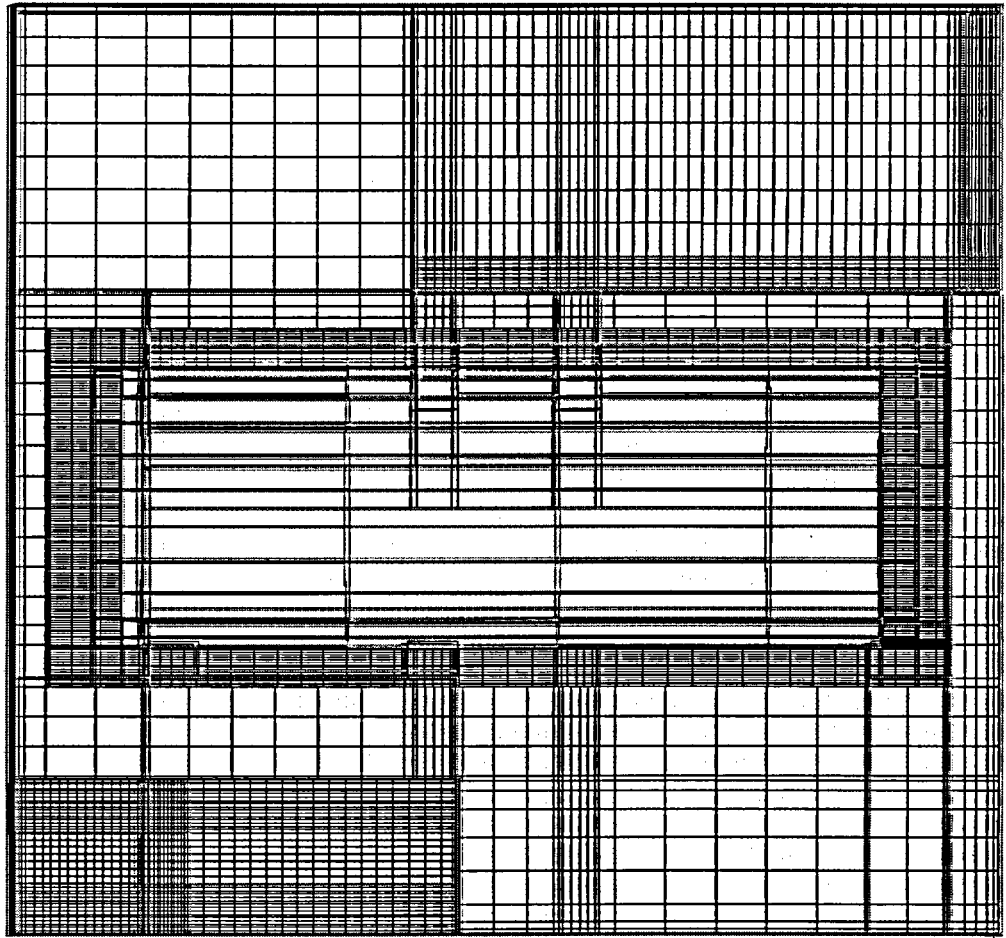
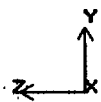


Figure A.4.4-4
Elevation View of Meshing at Z-Y Plane of AHSM

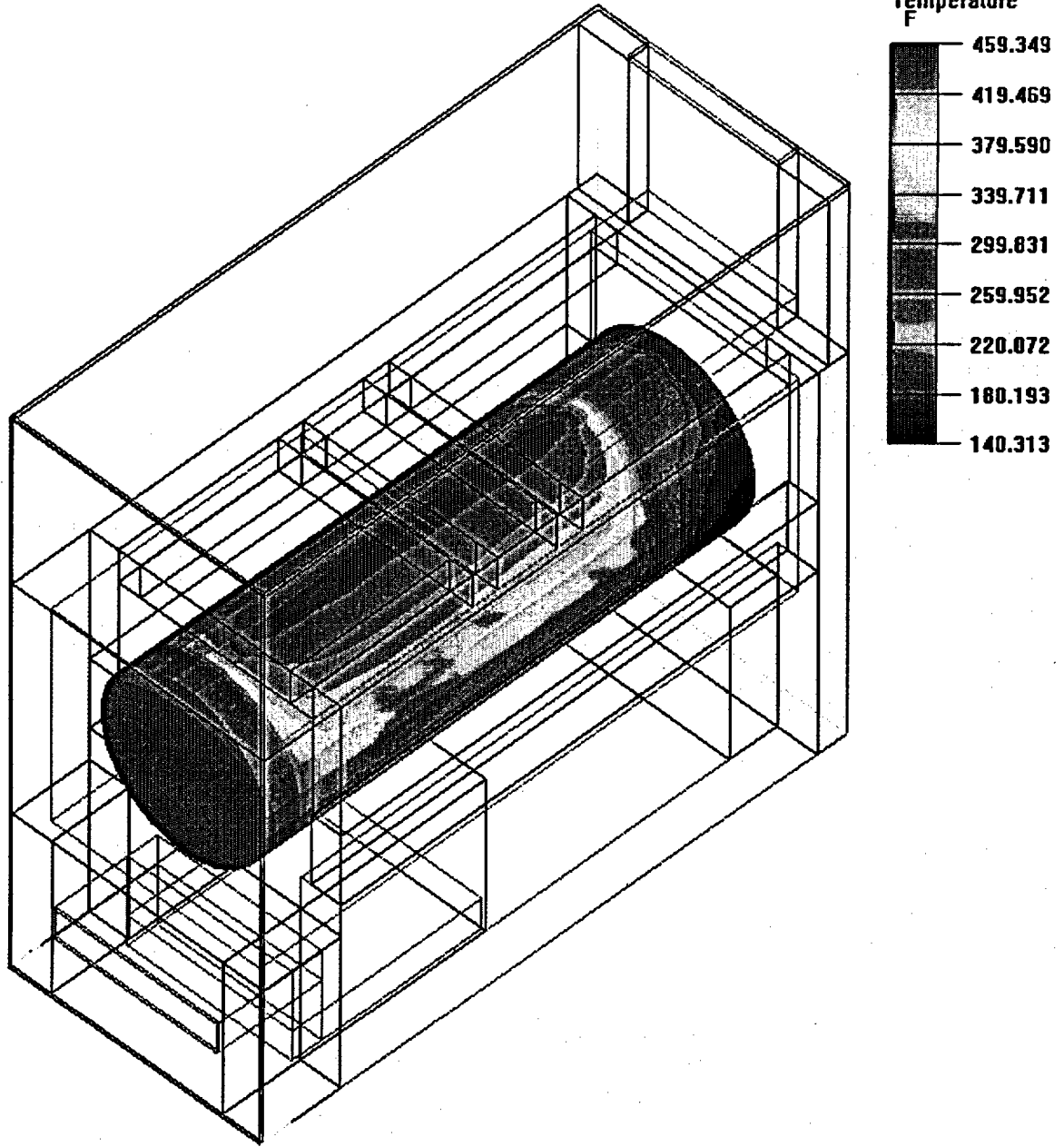


Figure A.4.4-5
Temperature Distribution on 24PT4-DSC Surface

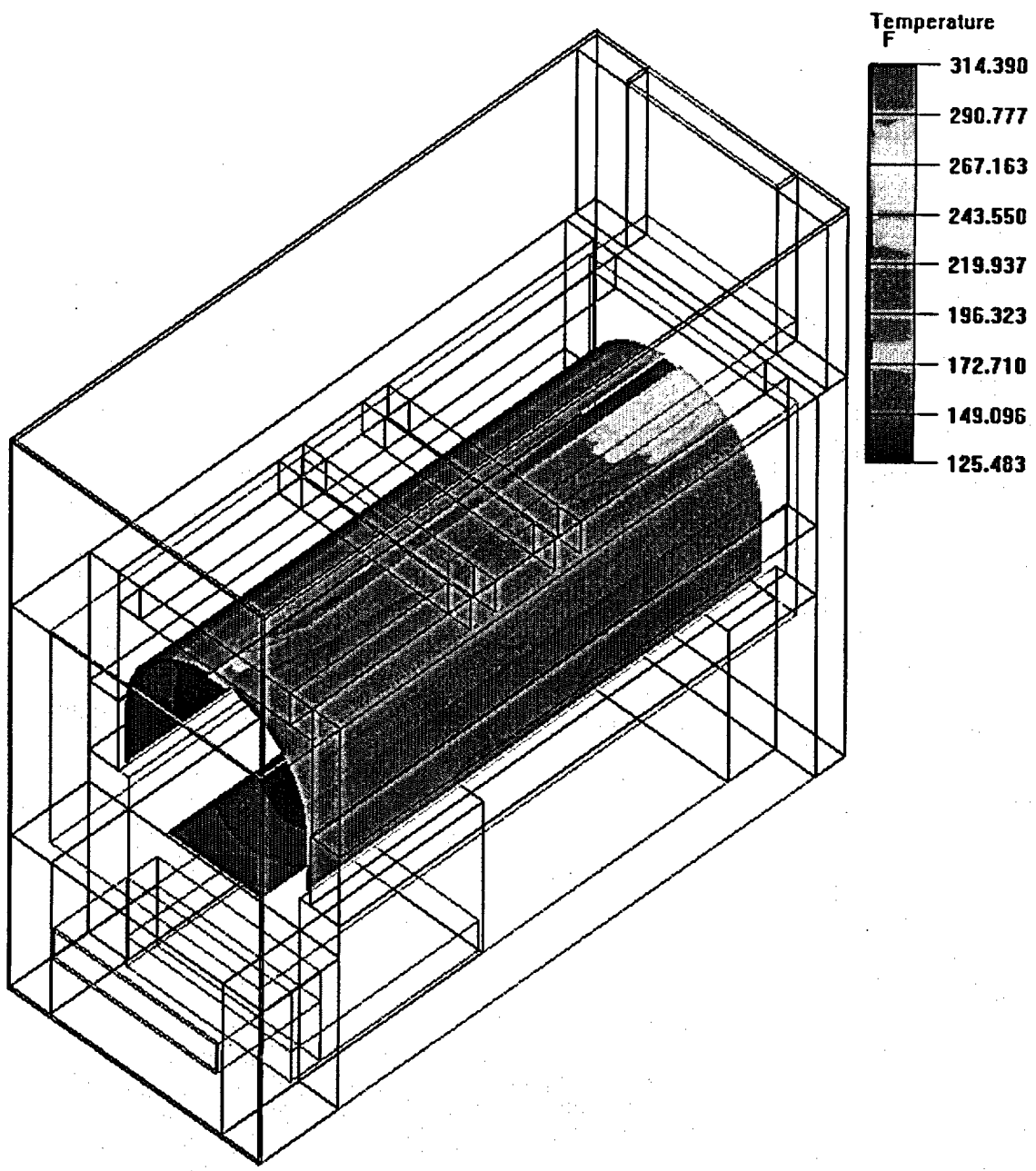


Figure A.4.4-6
Temperature Distribution on AHSM Heat Shield Surfaces

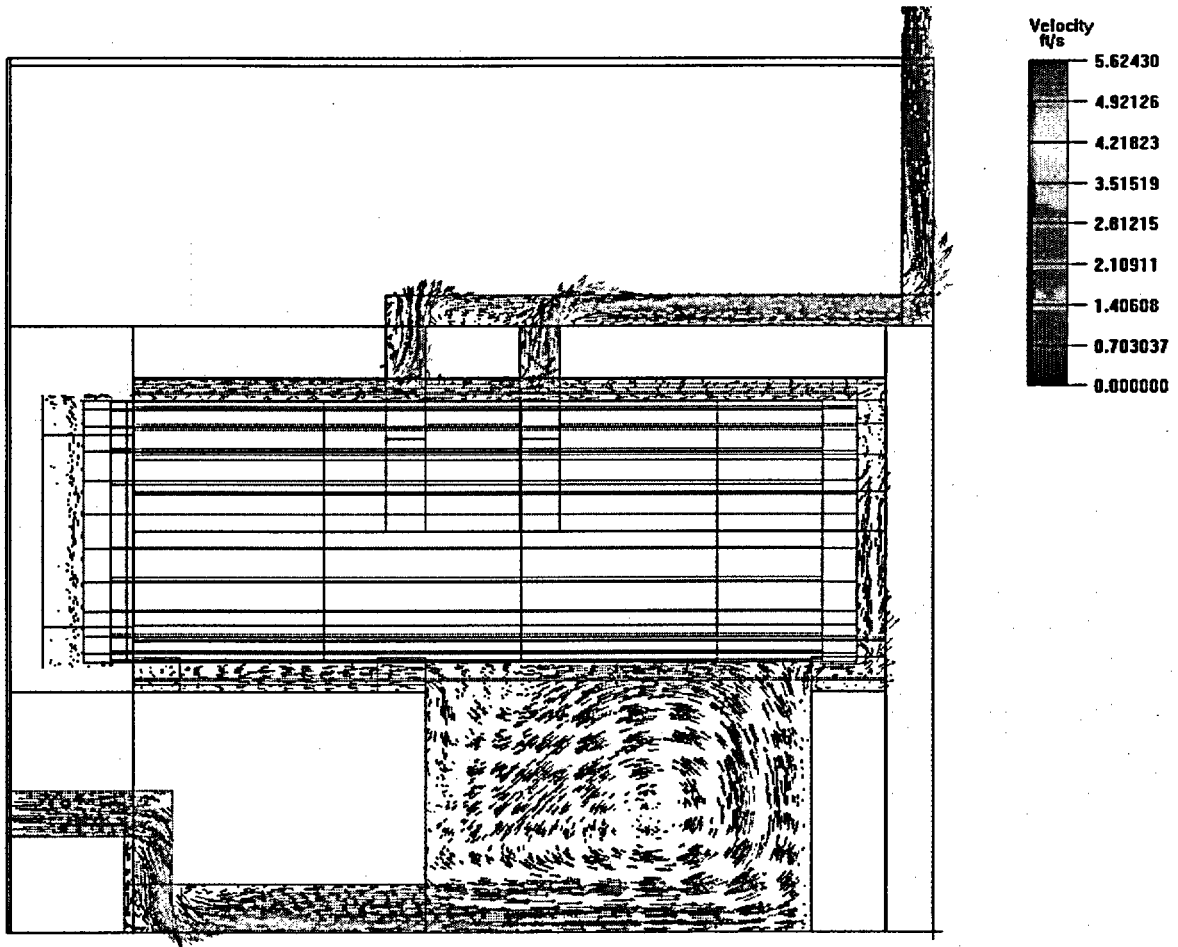


Figure A.4.4-7
Velocity Profile along Y-Z Plane at Center of AHSM

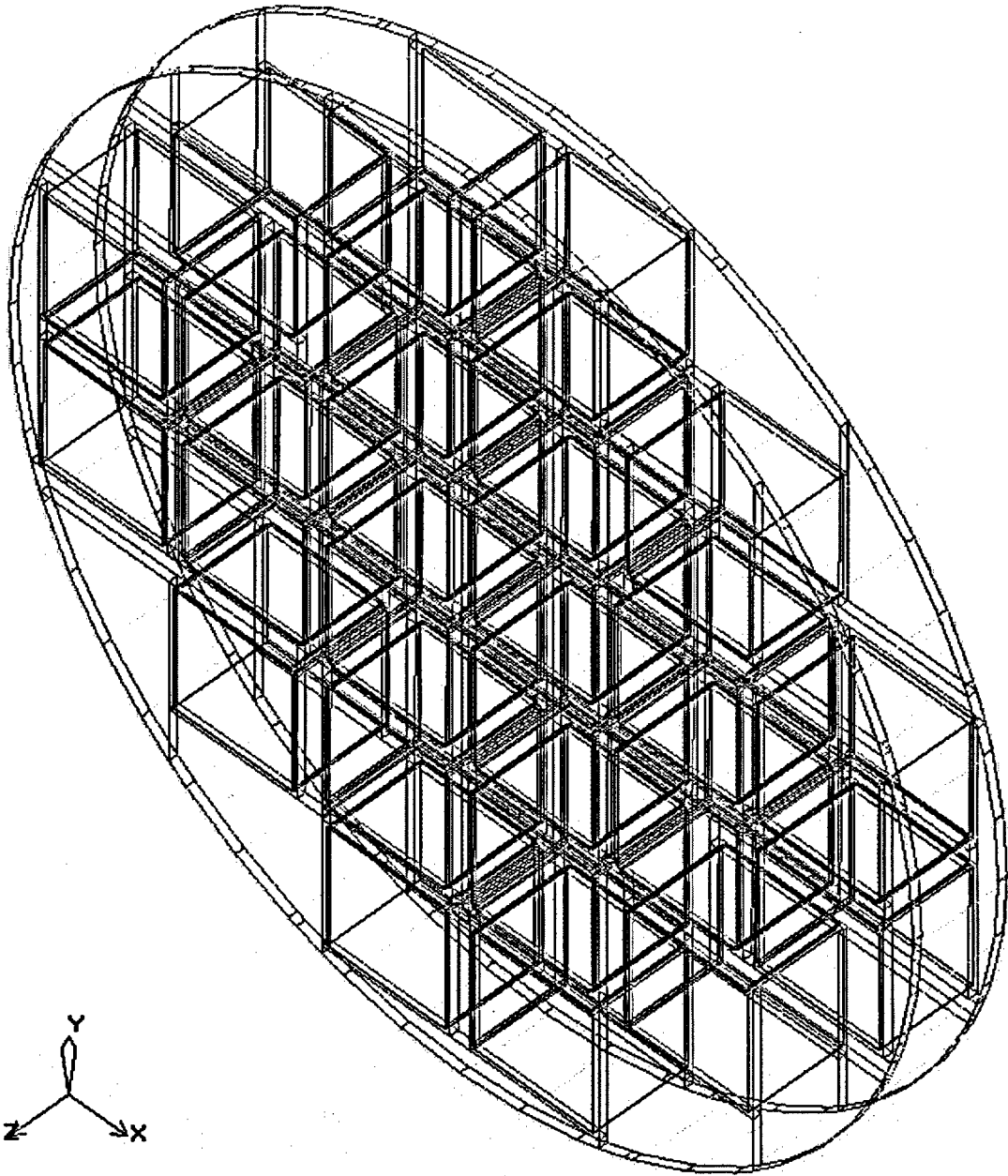


Figure A.4.4-8
Isometric, Wireframe View of Model Layout

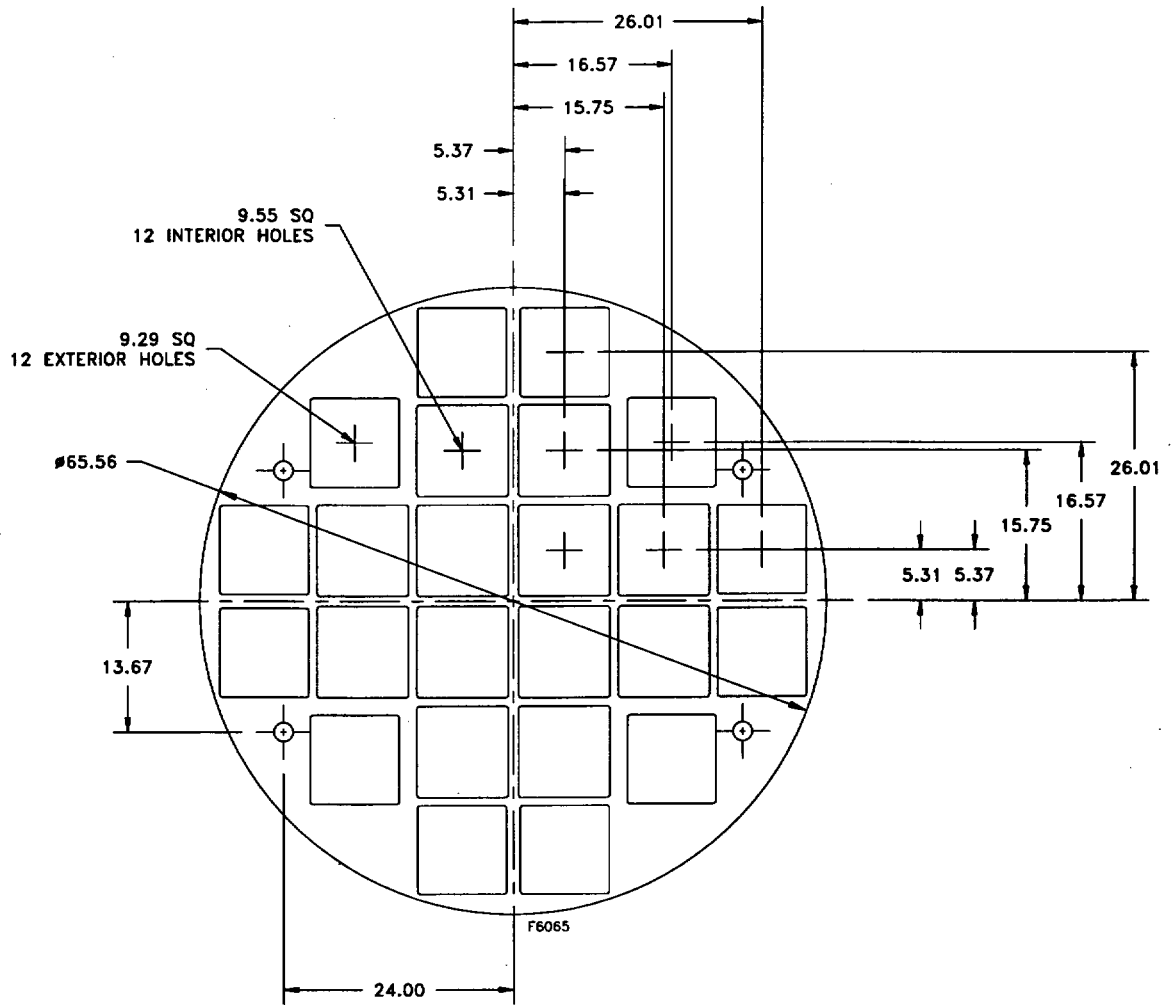


Figure A.4.4-9
24PT4-DSC Spacer Disc Schematic

Note - All dimensions are in inches

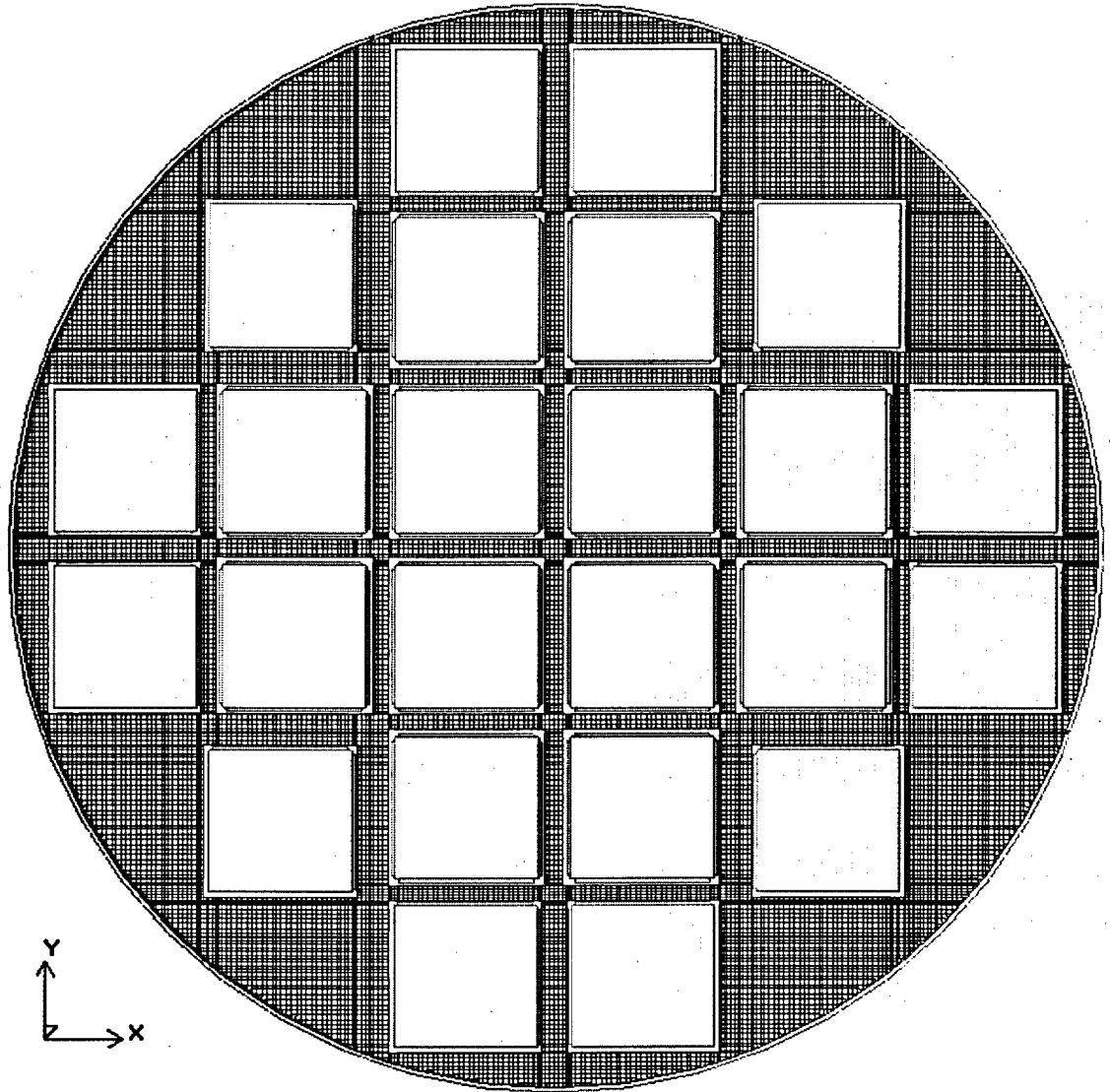


Figure A.4.4-10
Plan View of Meshing at 24PT4-DSC Spacer Disc

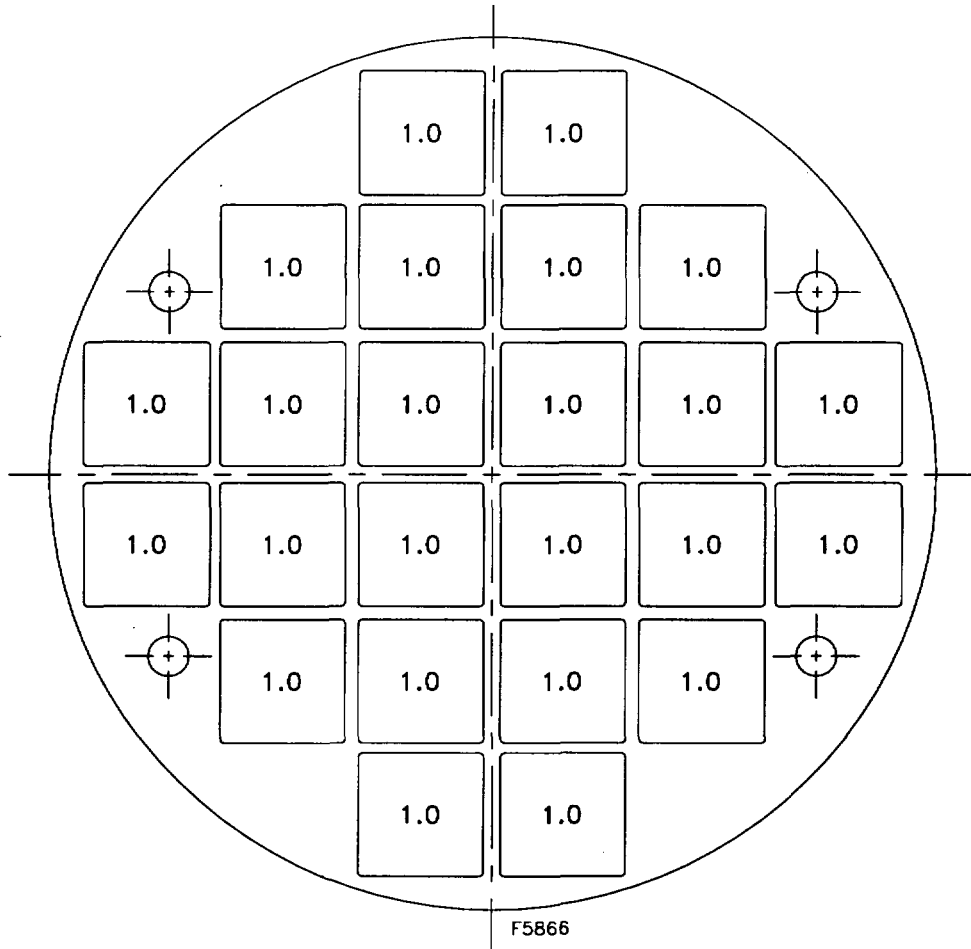


Figure A.4.4-11
24PT4-DSC HLZC #1, kW/Assembly

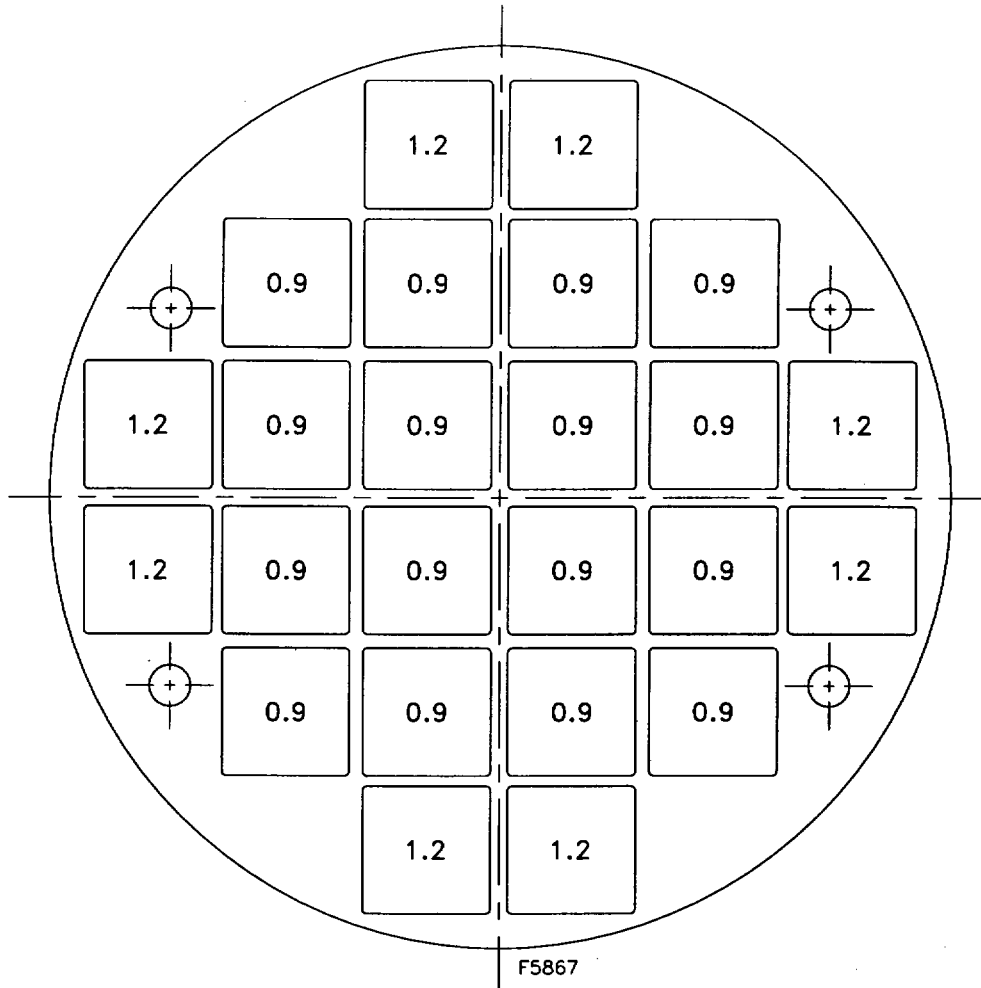
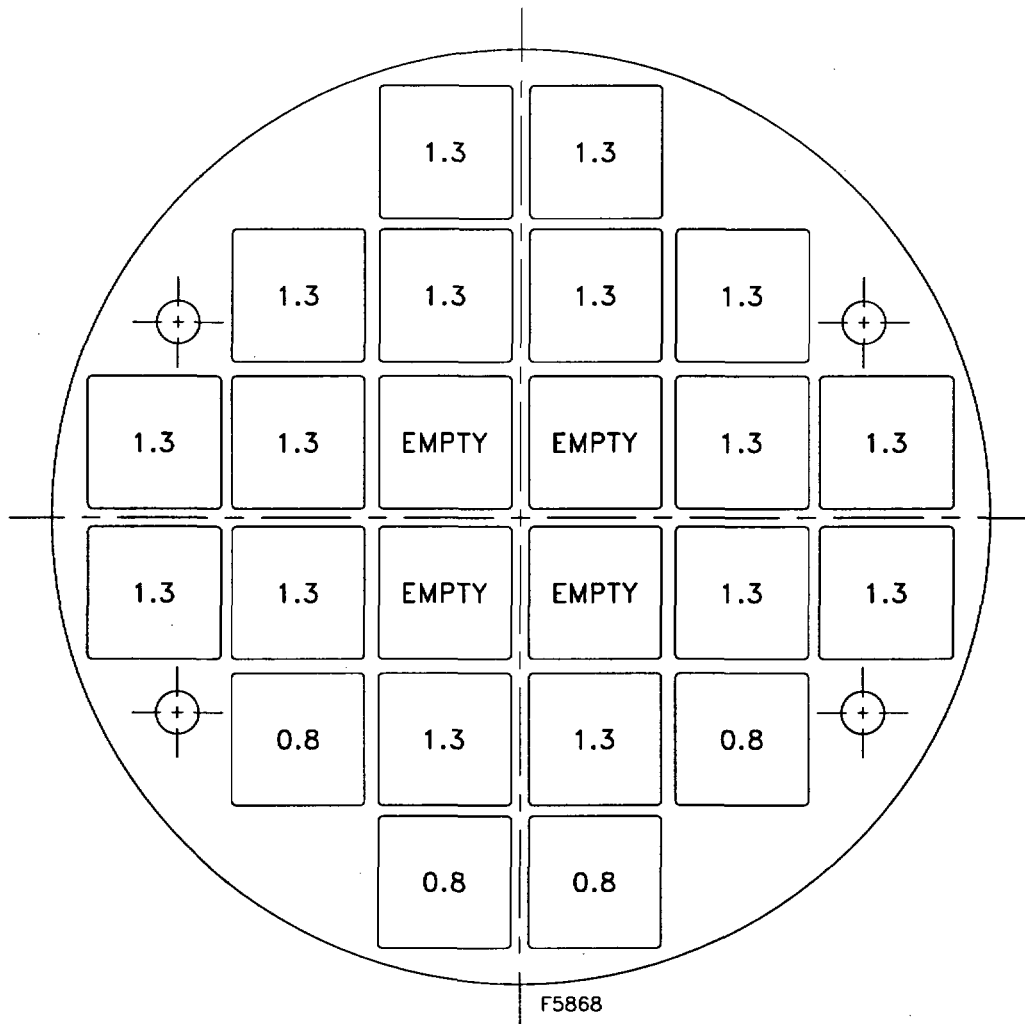


Figure A.4.4-12
24PT4-DSC HLZC #2, kW/Assembly



Notes:

1. This analyzed configuration envelopes the configuration specified for the payload in Chapter A.2 where the 1.3 kW / 0.8 kW heat load is replaced with a 1.26 kW / 0.9 kW heat load. Thermal analysis envelopes the total DSC heat load and the differential temperatures used for structural analysis.
2. Fuel Assemblies with a 0.8 kW heat load may be placed anywhere in the 12 locations along the outside periphery of the basket.

**Figure A.4.4-13
24PT4-DSC HLZC #3, kW/Assembly**

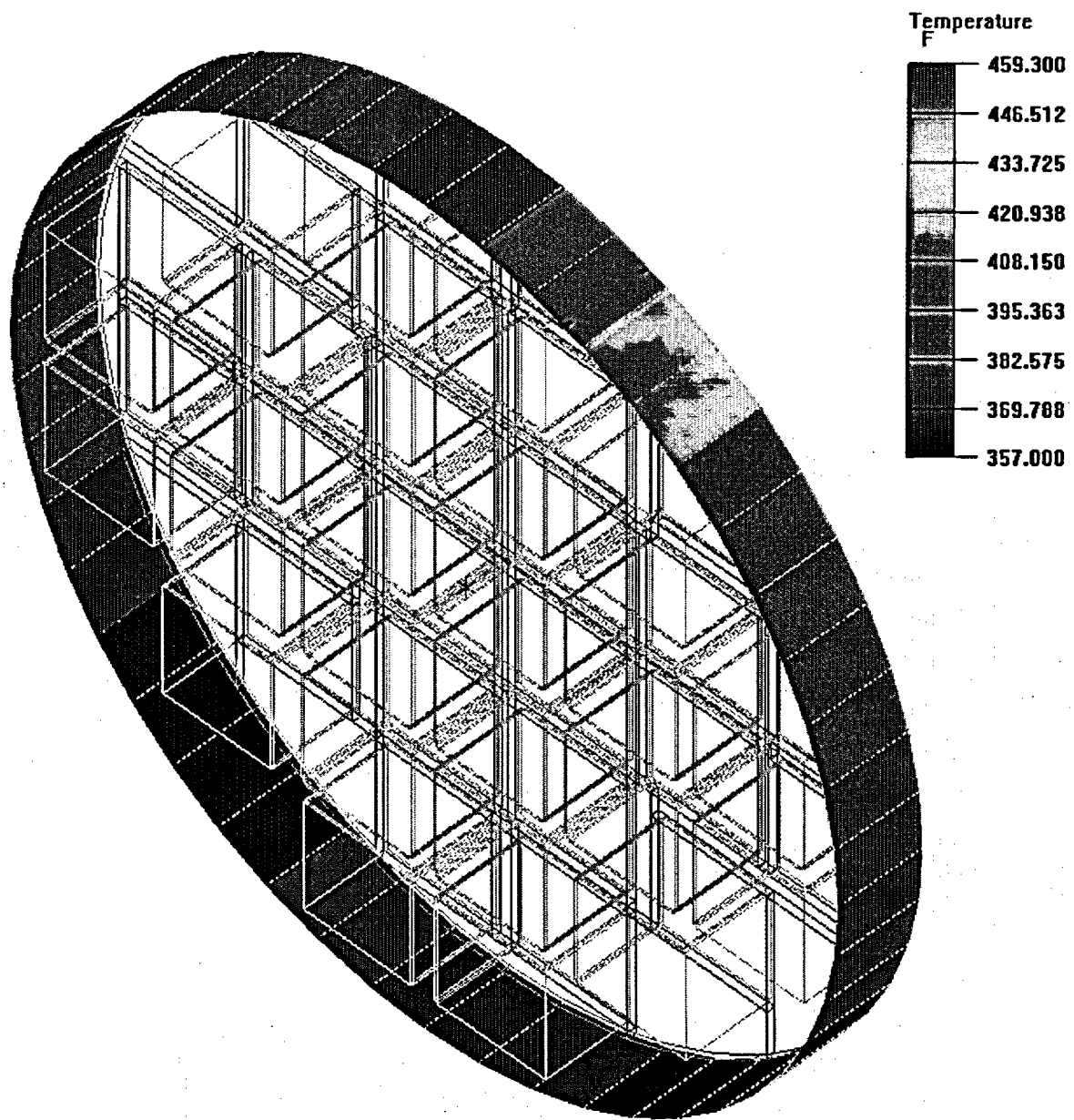


Figure A.4.4-14
24PT4-DSC Shell Temperatures, Bounding Condition in AHSM

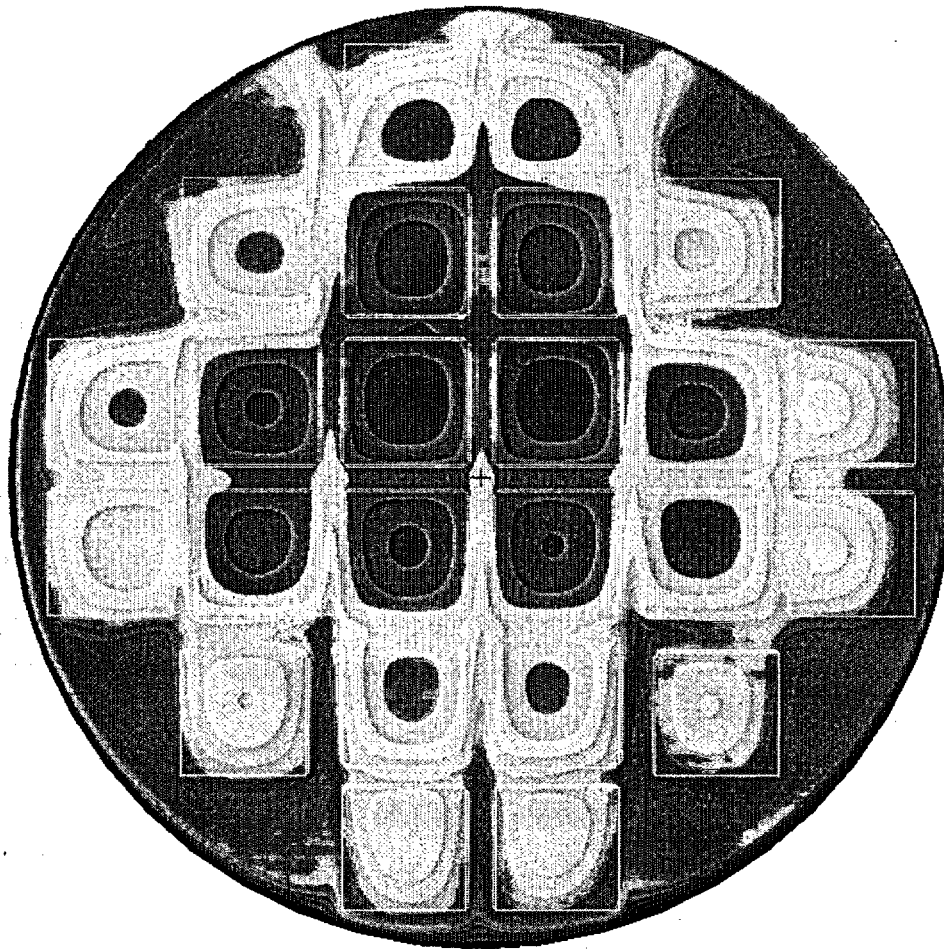


Figure A.4.4-15
Fuel Cladding Temperature Distribution within 24PT4-DSC Basket, Bounding Condition in AHSM

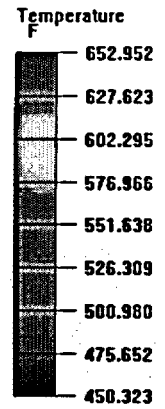
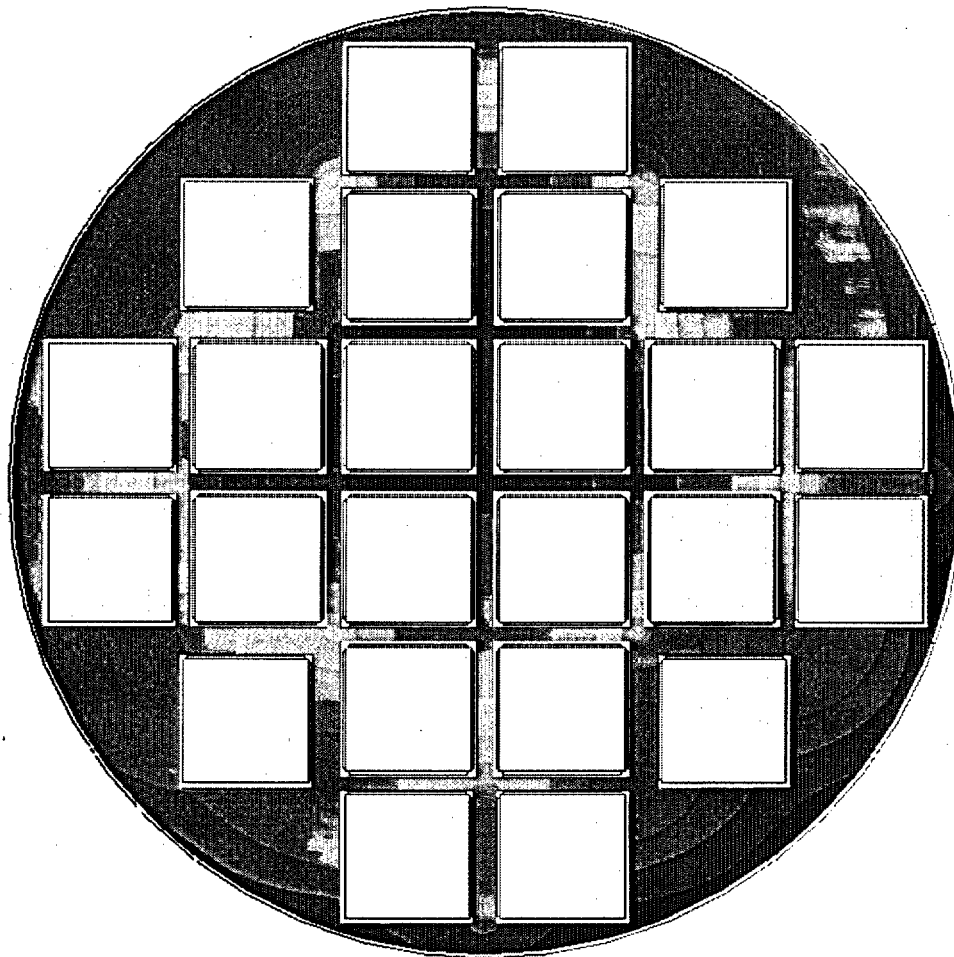


Figure A.4.4-16
24PT4-DSC Spacer Disc Temperature Distribution, Bounding Condition in AHSM

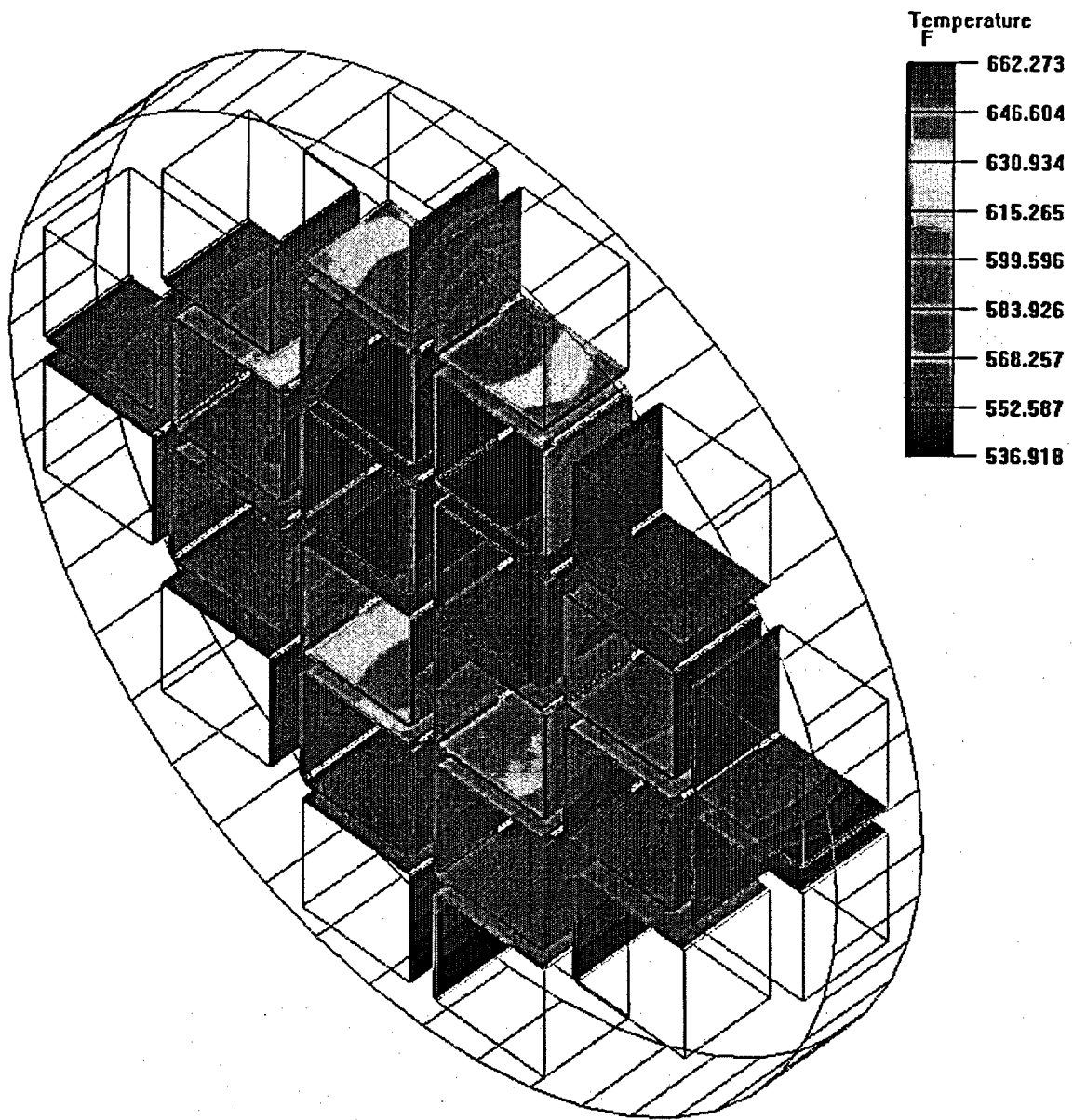


Figure A.4.4-17
24PT4-DSC Poison Sheet Temperature Distribution, Bounding Condition in AHSM

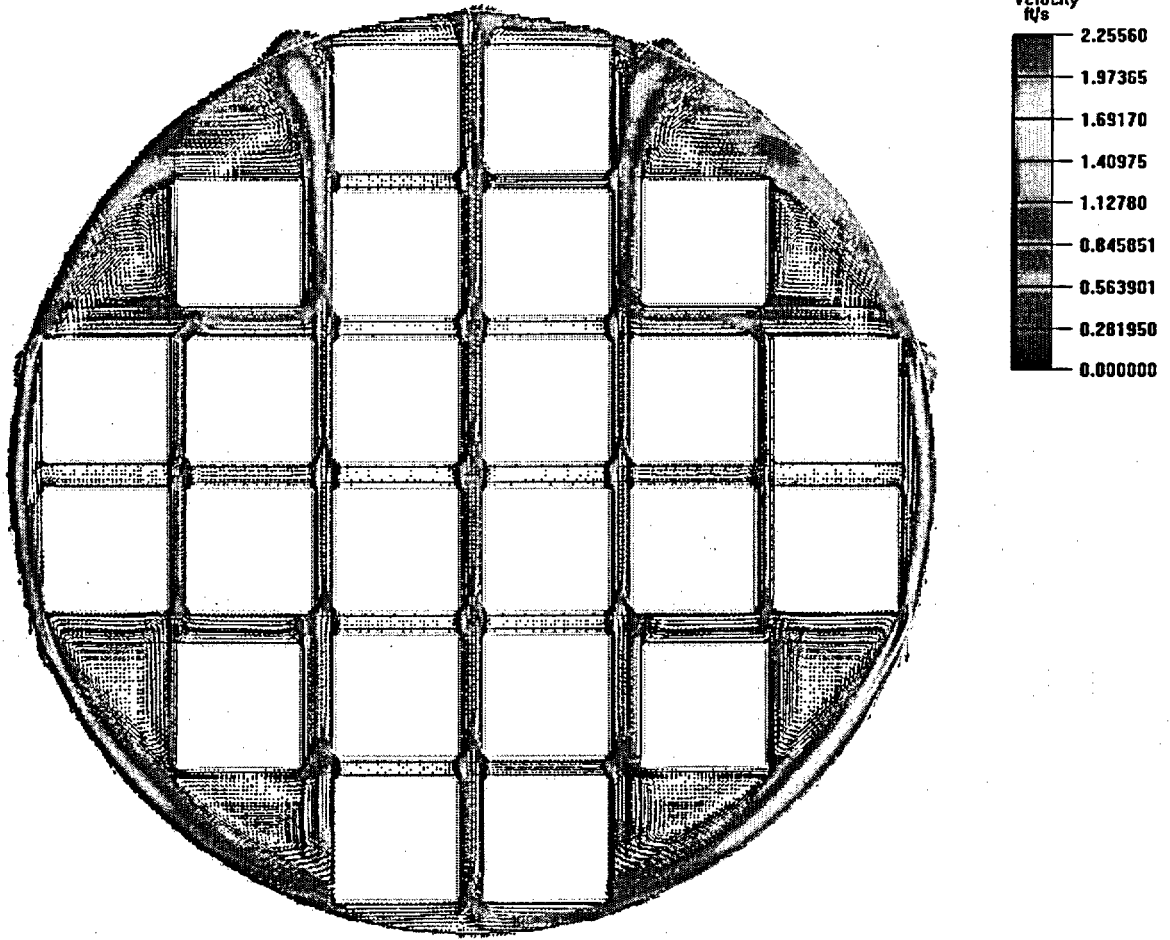


Figure A.4.4-18
Velocity Distribution within 24PT4-DSC Basket, Bounding Condition in AHSM

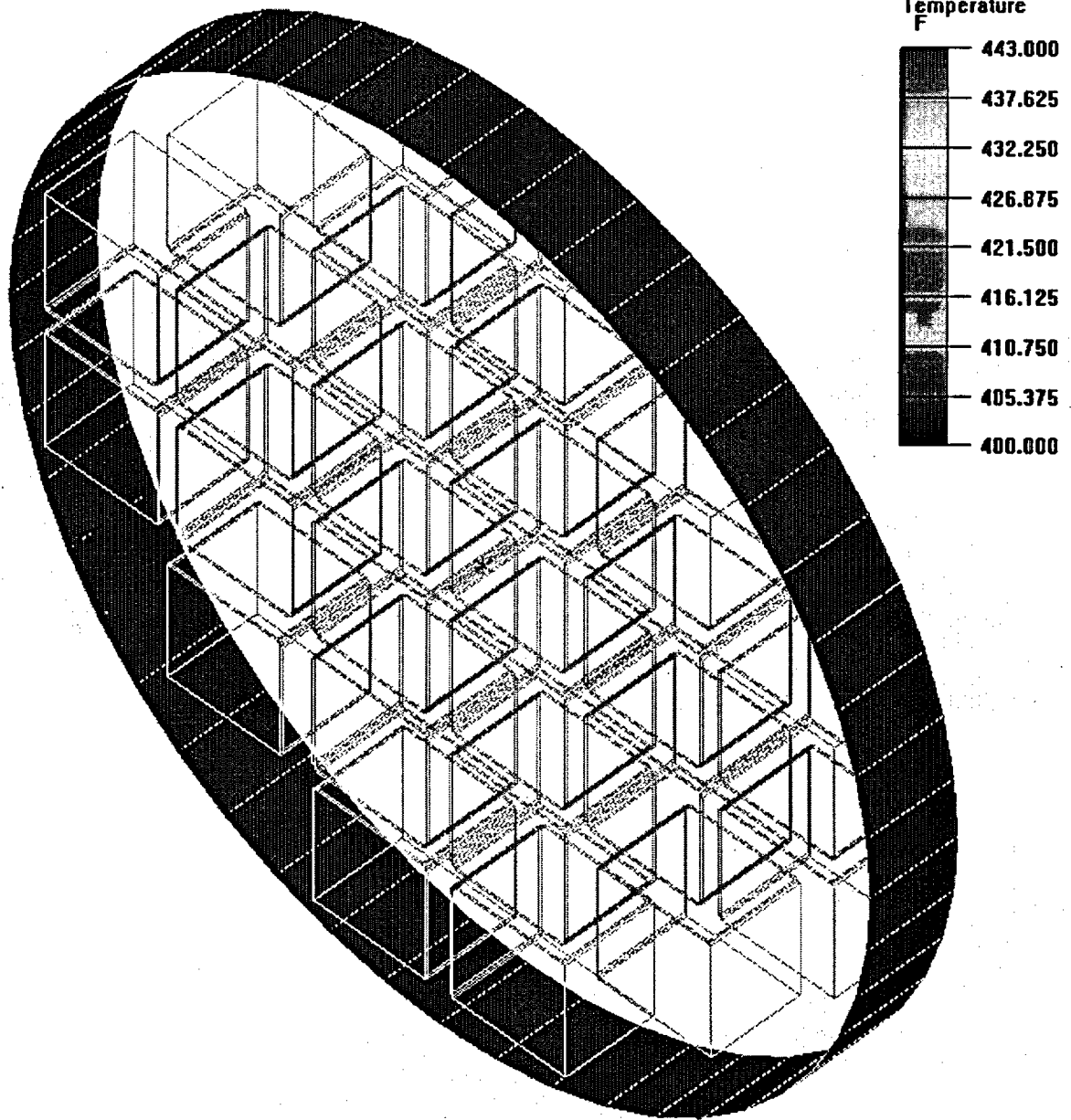


Figure A.4.4-19
24PT4-DSC Shell Temperatures, Bounding Condition in TC

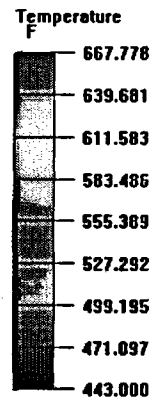
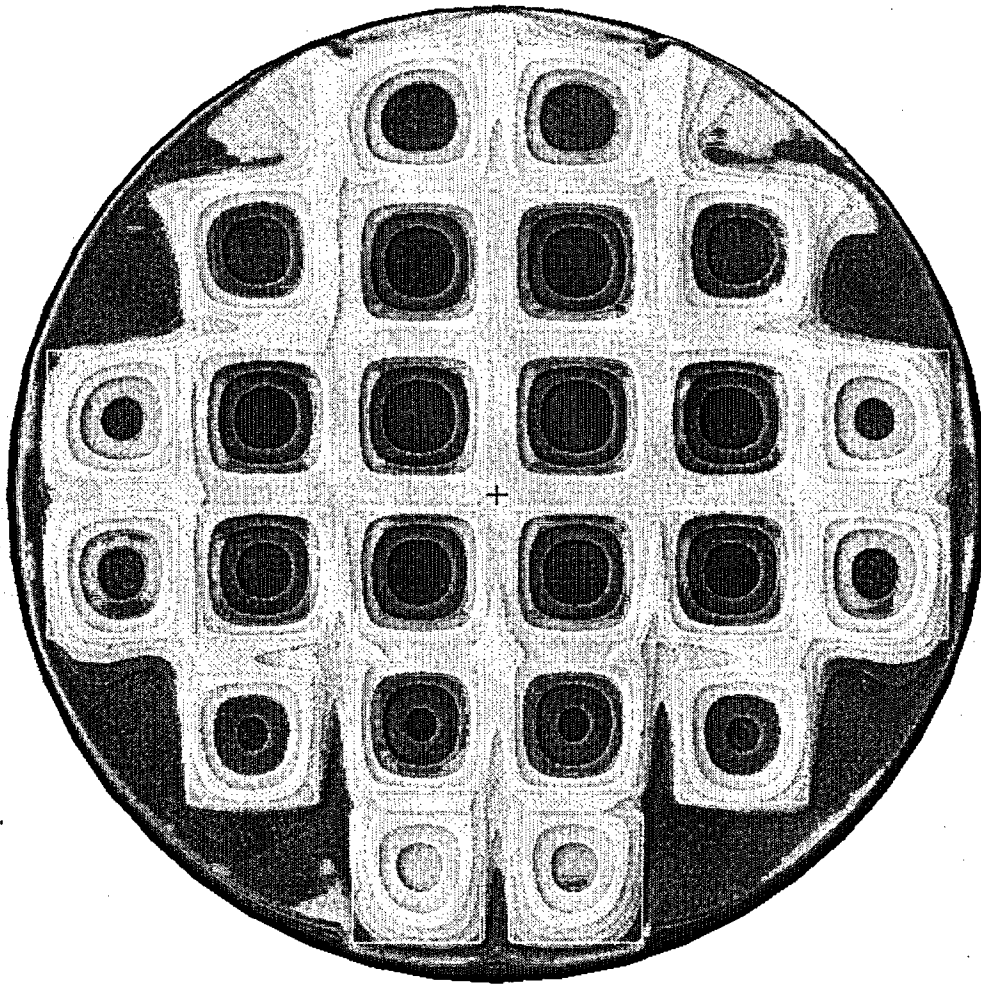


Figure A.4.4-20
Fuel Cladding Temperature Distribution within 24PT4-DSC Basket, Bounding Condition in TC

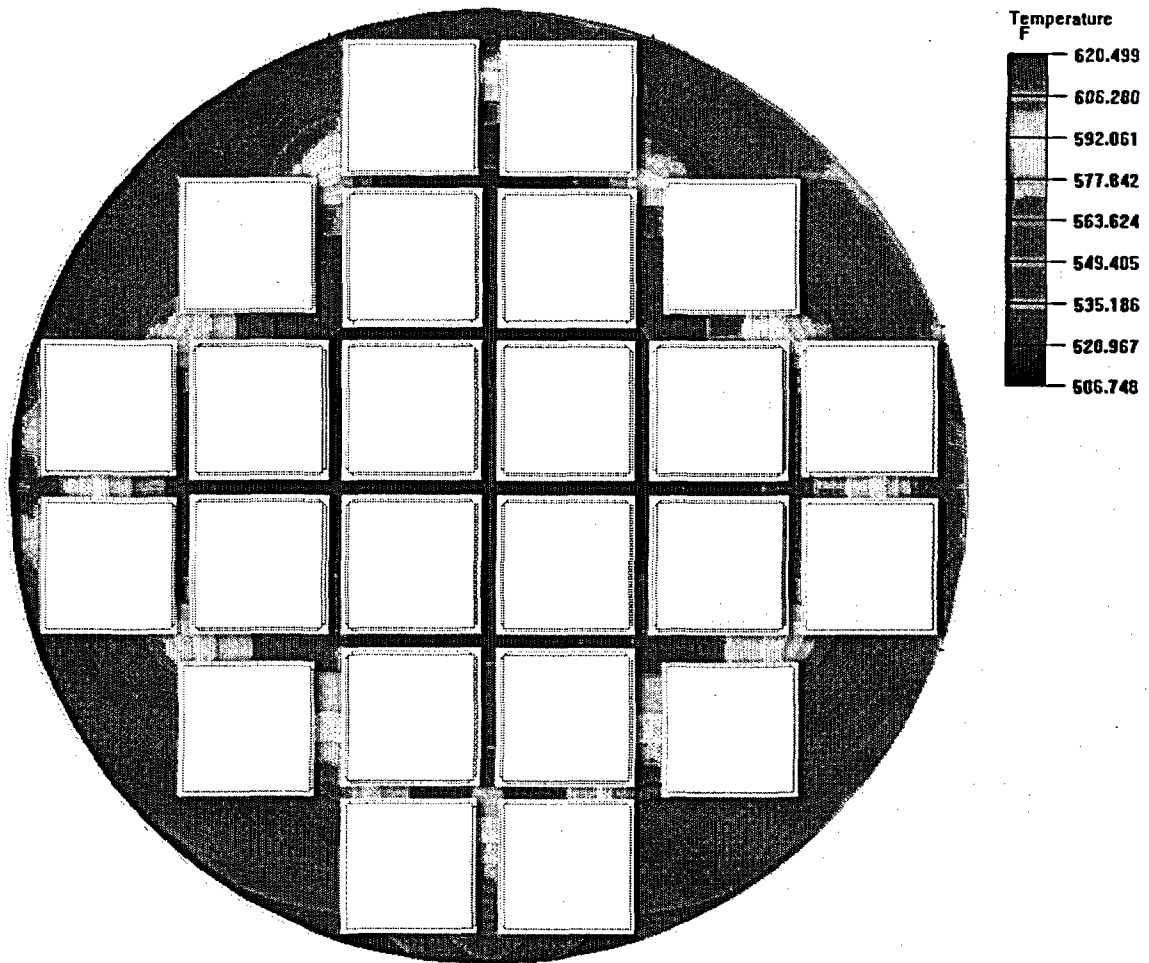


Figure A.4.4-21
24PT4-DSC Spacer Disc Temperature Distribution, Bounding Condition in TC

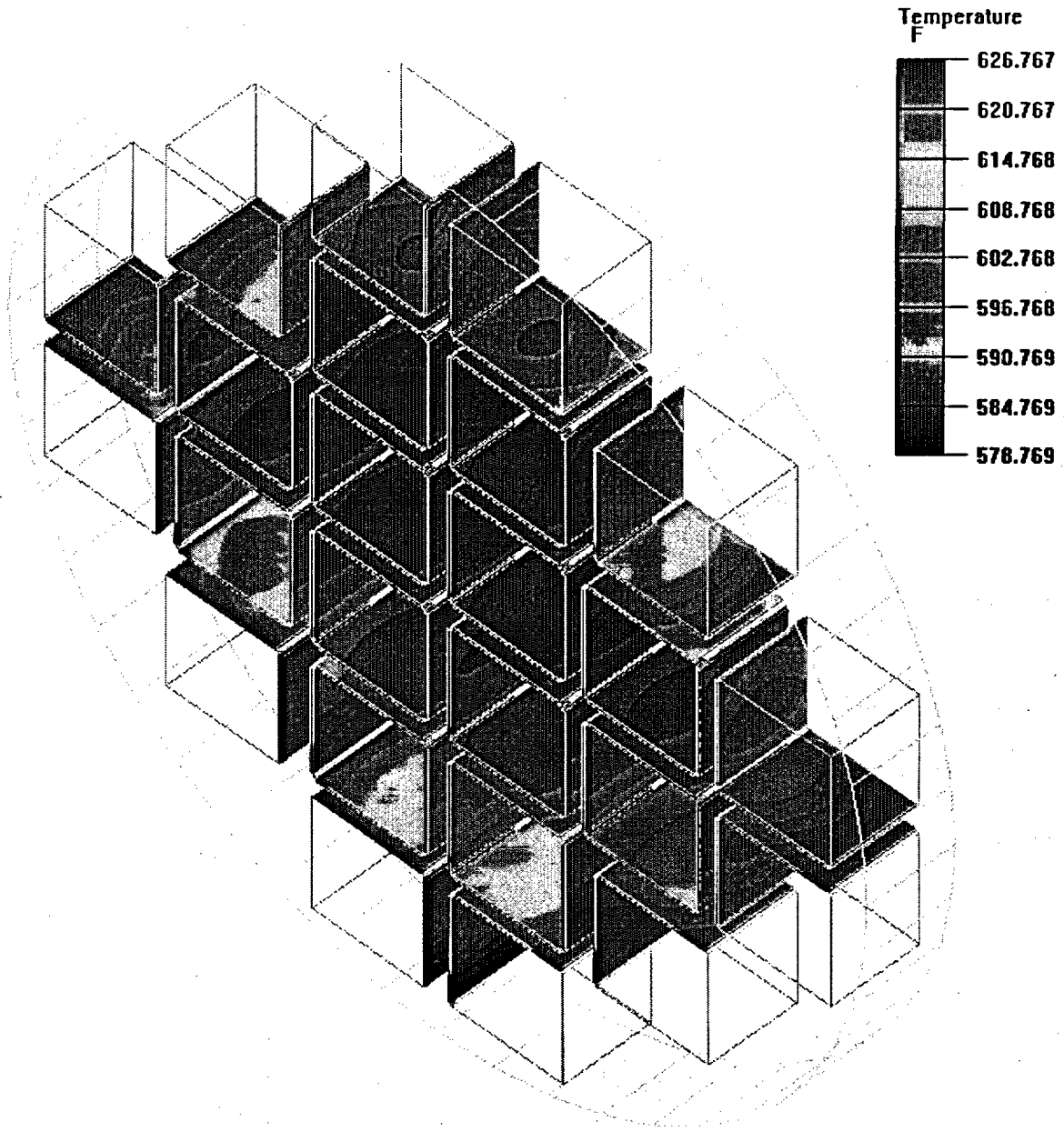


Figure A.4.4-22
24PT4-DSC Poison Sheet Temperature Distribution, Bounding Condition in TC

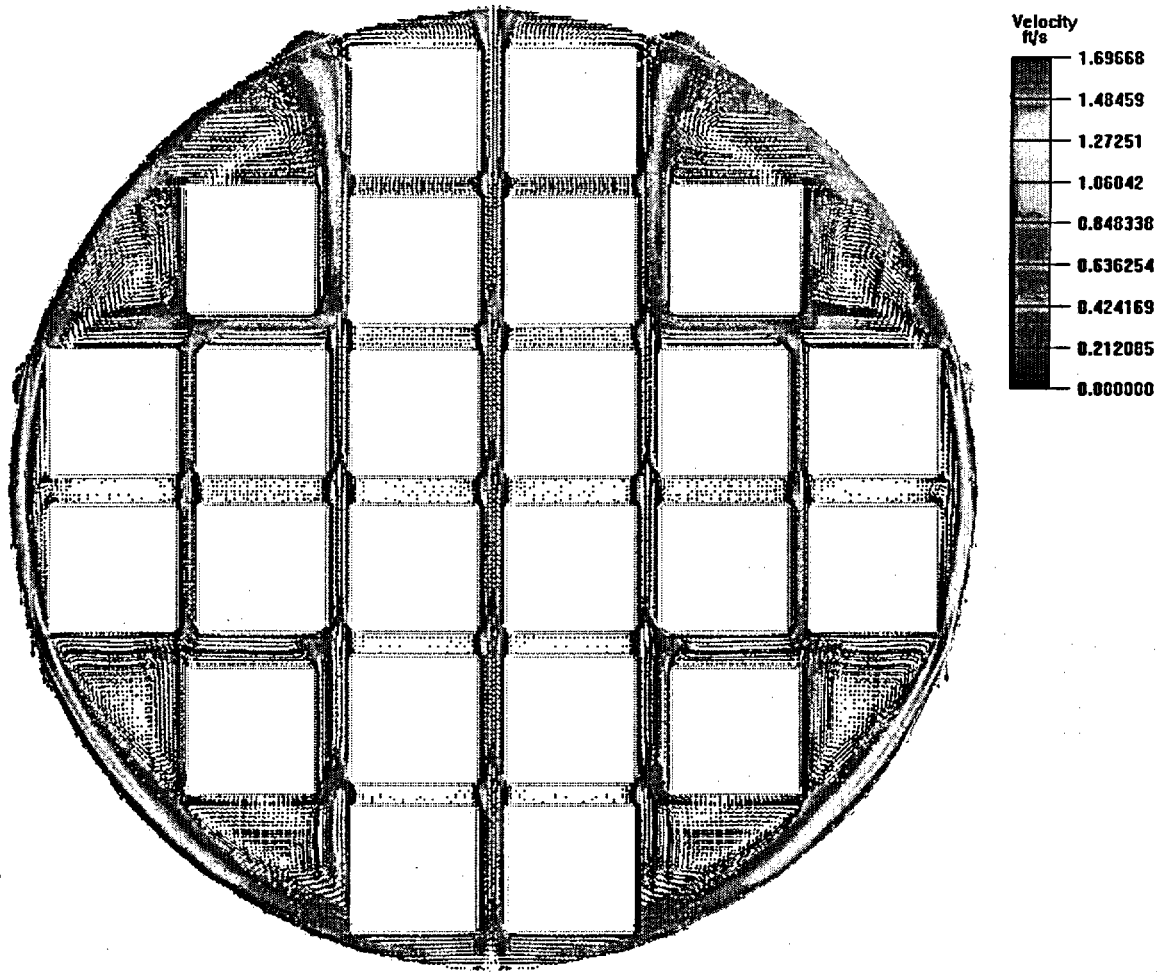


Figure A.4.4-23
Velocity Distribution within 24PT4-DSC Basket, Bounding Condition in TC

Spacer Disc Radial Temperature Distribution - HSM Storage

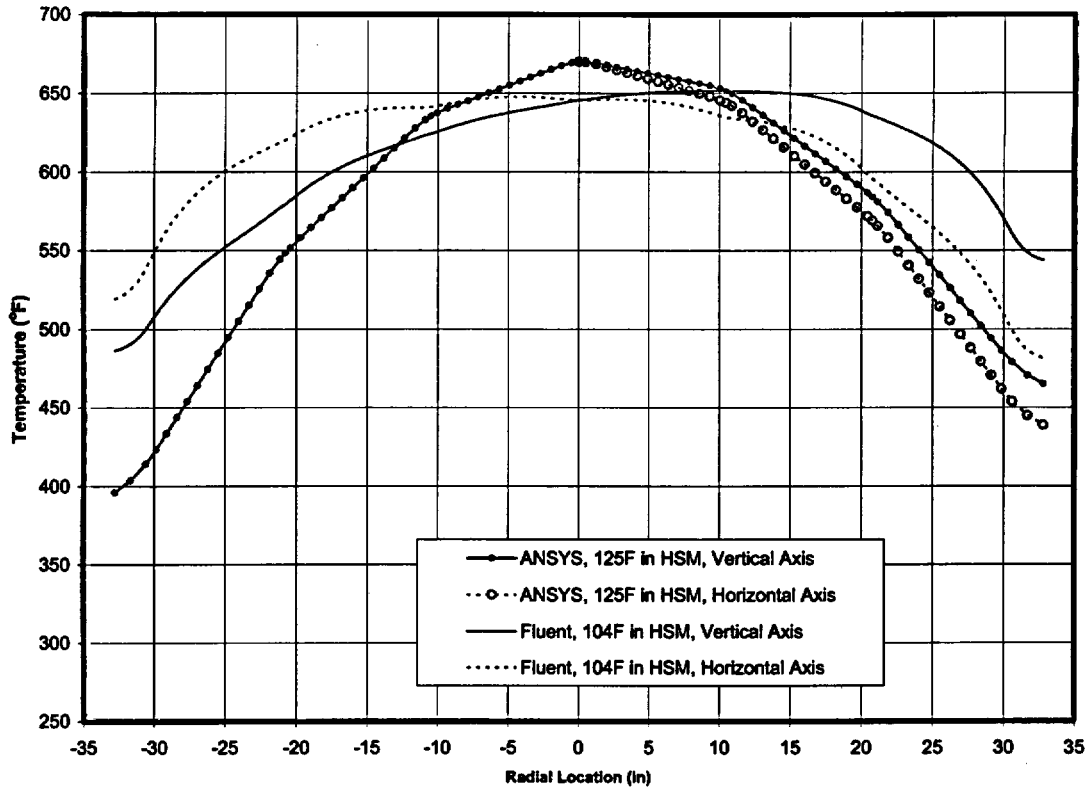


Figure A.4.4-24
Spacer Disc Radial Temperature Distribution (Storage Conditions)

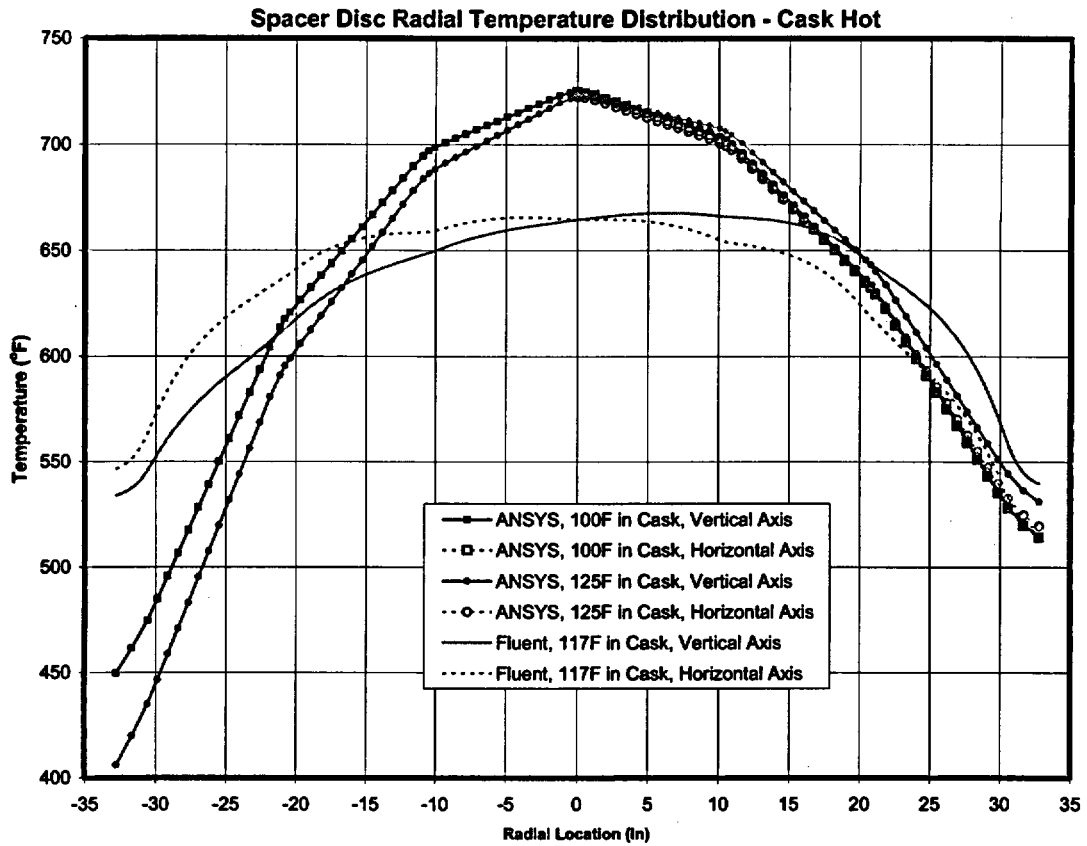


Figure A.4.4-25
Spacer Disc Radial Temperature Distribution (Transfer Conditions, Hot)

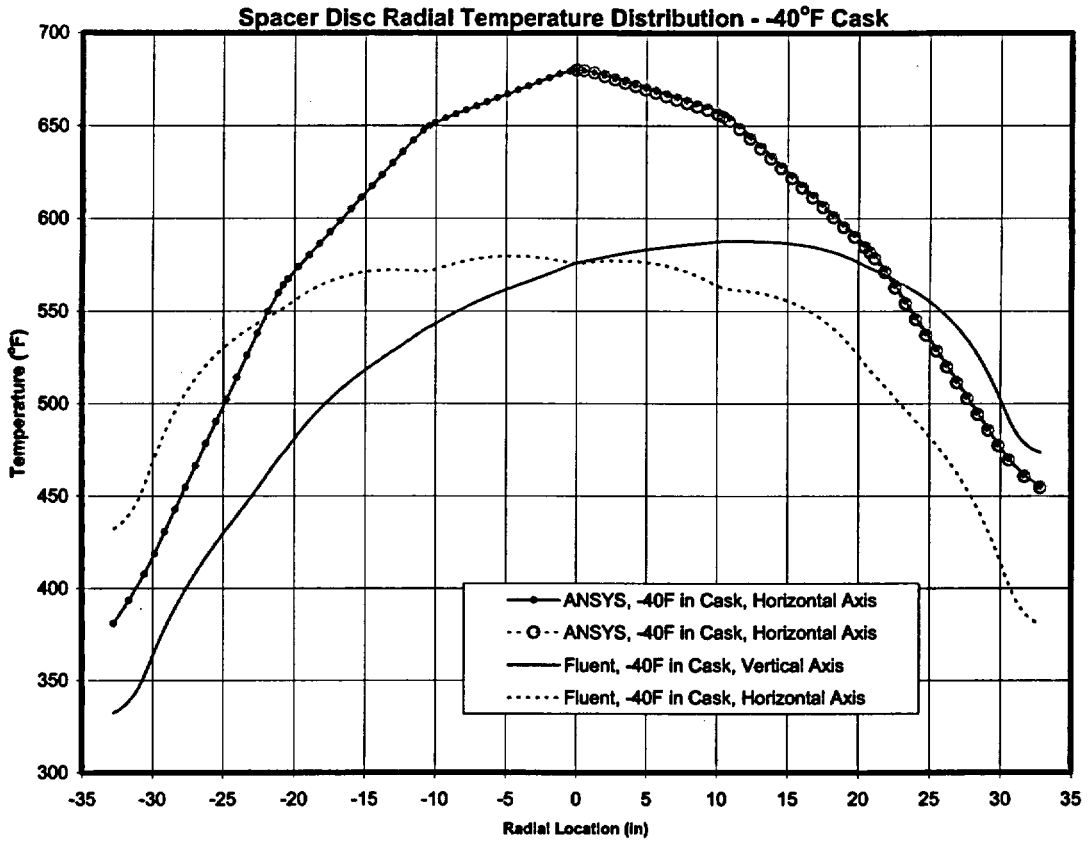


Figure A.4.4-26
Spacer Disc Radial Temperature Distribution -40°F TC

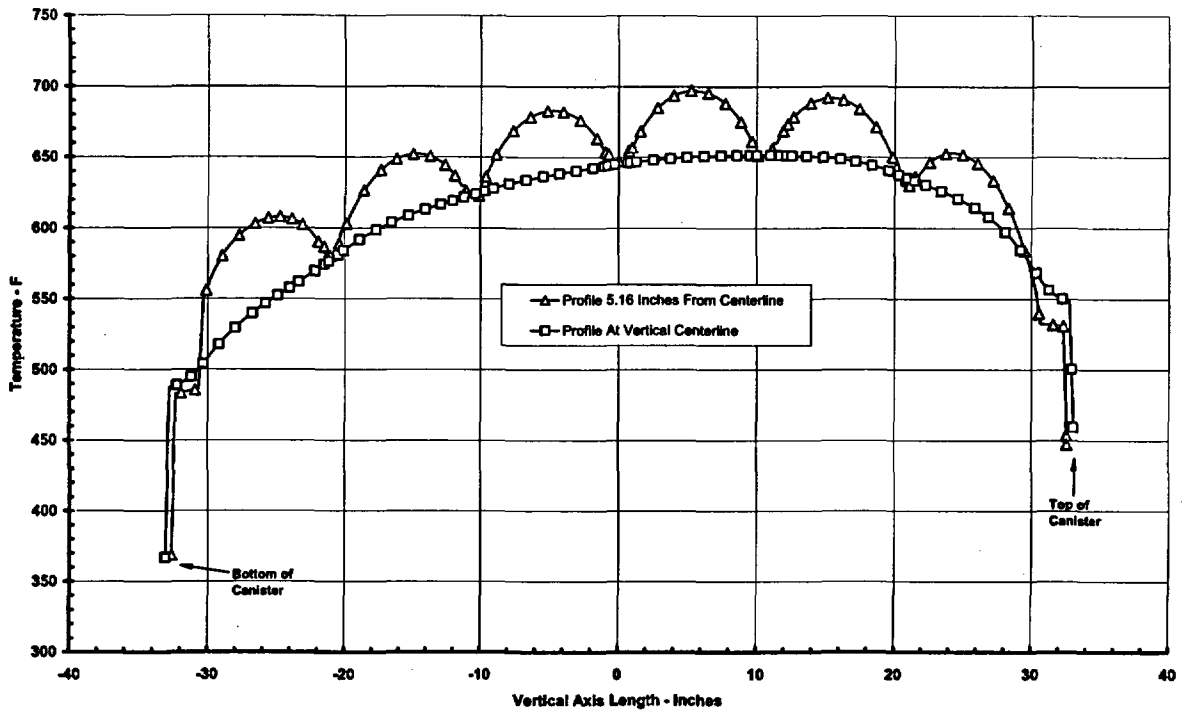


Figure A.4.4-27
Temperature along Vertical Lines through Basket, Bounding Condition
in AHSM, HLZC #1

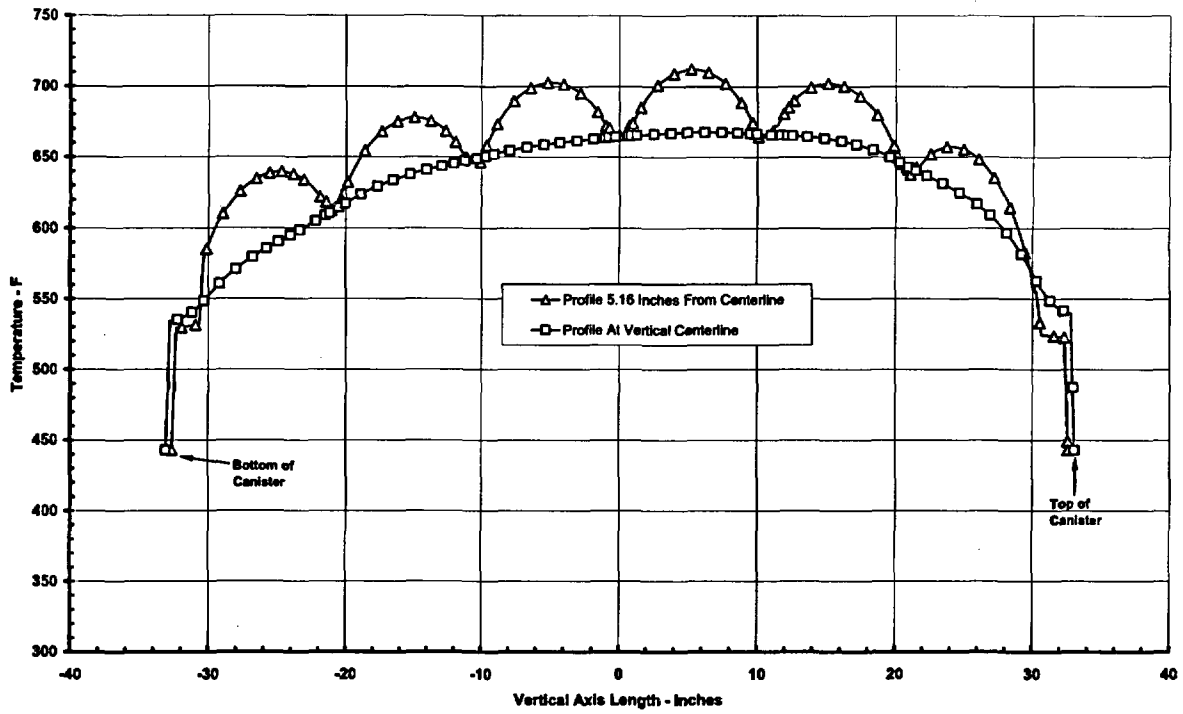


Figure A.4.4-28
Temperature along Vertical Lines through Basket, Bounding Condition in TC

A.4.5 Thermal Evaluation for Off-Normal Conditions

The thermal evaluation for off-normal condition has been combined with the evaluation for normal condition. Hence, this section has been deleted.

A.4.6 Thermal Evaluation for Accident Conditions

A.4.6.1 Accident Ambient Conditions

As with the off-normal conditions of storage *and transfer*, the accident conditions for the 24PT4-DSC components are evaluated for the extreme range of design basis ambient temperatures given in Table 4.1-1.

A.4.6.2 Blockage of AHSM Inlet and Outlet Vents

This accident conservatively postulates the complete blockage of the AHSM ventilation air inlet and outlet opening for a maximum of 25 hours concurrent with the extreme hot and cold ambient conditions given in Table A.4.1-1.

A.4.6.2.1 Cause of Accident

Since the NUHOMS[®] AHSMs are located outdoors, there is a remote probability that the ventilation air inlet and outlet openings could become blocked by debris from such unlikely events as floods and tornados. The NUHOMS[®] design features such as the perimeter security fence and the mesh screen covering of the air inlet and outlet openings reduce the probability of occurrence of such an accident. Nevertheless, for this conservative generic analysis, such an accident is postulated to occur and is analyzed.

A.4.6.2.2 Accident Analysis

The thermal effect of this accident results in increased temperatures of the 24PT4-DSC due to the blockage of the AHSM air inlet and outlet openings. The thermal model of the AHSM concrete is the *HEATING7* model described in Section 4.4.2.2.

When the inlet and outlet vents are blocked, the air surrounding the DSC in the AHSM cavity is contained (trapped) in the AHSM cavity. The temperature difference between the hot DSC surface and the surrounding cooler heat shield and concrete surfaces in the AHSM cavity will result in closed cavity convection. This closed cavity convection in the AHSM cavity is accounted for by calculating an effective conductivity of air. The AHSM cavity is modeled as a combination of separate enclosures as described below:

Enclosure 1 – space limited by 24PT4-DSC shell outer circumference and inner surface of heat shields;

Enclosure 2 – space limited by outer surface of heat shields and inner concrete surface opposite the heat shields.

The design of heat shields with an opening at top of enclosures 1 and 2 (otherwise stagnant regions) intensifies the local convection allowing air to flow.

The closed cavity convection everywhere else within AHSM is conservatively neglected.

Heat transfer within AHSM air cavity is modeled by radiation among internal surfaces and free convection with enclosure-wise film coefficient.

For enclosures of closed cavity convection, an increase of thermal conductivity of air from k_{air} , to new value k_{eff} , which accounts for a free convection, an empirical formula [A4.8] for natural convection between two concentric cylinders was applied:

$$\frac{k_{eff}}{k} = 0.386 \cdot \left(\frac{Pr}{0.861 + Pr} \right)^{1/4} \cdot (Ra_c^*)^{1/4},$$

$$Ra_c^* = \frac{\left[\ln \left(\frac{D_o}{D_i} \right) \right]^4}{\delta^3 \cdot \left(D_i^{-3/5} + D_o^{-3/5} \right)^5} \cdot Ra_\delta,$$

$$Ra_\delta = \frac{g \cdot \beta \cdot (T_i - T_o) \cdot \delta^3}{\nu^2} \cdot Pr,$$

where:

Ra_c^*, Ra_δ	–Raleigh numbers,
D_i, D_o	–inner and outer diameters of enclosure,
T_i, T_o	–wall temperature at inner and outer diameters of enclosure,
$\delta = (D_o - D_i)/2$	–thickness of enclosure,
g	–gravitational acceleration,
β	–volumetric coefficient of expansion,
ν	–kinematic viscosity,
$Pr = c_p \cdot \mu / k_{air}$	–Prandtl number,
c_p	–specific heat,
μ	–dynamic viscosity,
k_{air}	–thermal conductivity of air.

Based on Nusselt number :

$$Nu_\delta = k_{eff}/k_{air} = h \cdot \delta / k_{air},$$

a mean film coefficient h for the enclosure was calculated as:

$$h = k_{air} \cdot Nu_\delta / \delta = k_{eff} / \delta .$$

An iterative process was used to determine the mean temperatures for air property calculations. The results are given in table below:

Summary of Closed Cavity Convection Calculation

Enclosure within AHSM	OD	ID	δ	\bar{T}_{hot}	\bar{T}_{cold}	\bar{T}_{mean}	k_{air}	β	ν	Pr	Ra_{δ}	Ra_c	h
	in	in	in	°F	°F	°F	Btu/min-in-°F	1/°R	ft ² /s	-	-	-	Btu/(in ² -min-°F)
Enclosure 1 – DSC shell-heat shield gap	73	67.19	2.905	587	429	508	3.43e-5	0.00103	4.60e-4	0.679	2.39e+5	4.945e+3	3.12e-5
Enclosure 2 – Heat shield-concrete gap	77	73.21	1.895	429	316	372.5	3.04e-5	0.00120	3.58e-4	0.683	9.17e+4	1.156e+3	2.95e-5

These film coefficients were used in the HEATING 7 AHSM model to determine the transient DSC shell temperatures during blocked vent accident. The calculated DSC shell temperatures described in Chapter 4 were then used as boundary conditions for ANSYS 24PT4-DSC model to calculate the basket and fuel cladding temperatures during blocked vent transient.

The accident duration is assumed for 25 hours, at which time the air inlet and outlet opening obstructions would be cleared by site personnel and natural circulation air flow restored to the AHSM.

The temperature of the spent fuel assemblies and the 24PT4-DSC basket components will rise quickly to the higher temperature increasing heat transfer by radiation, conduction, and convection to the AHSM internal surfaces. In turn, the AHSM surface heatup is limited by the heatup of the entire AHSM. Because the heatup rate of the AHSM is much slower than that of the 24PT4-DSC or the spent fuel, the 24PT4-DSC is assumed to be at steady state at any instant in time and transferring 24 kW of heat to the AHSM. Therefore, the calculated surface temperatures of the 24PT4-DSC shell from the AHSM thermal model are used to determine the maximum 24PT4-DSC basket component and fuel cladding temperatures with a steady state evaluation of the 24PT4-DSC basket.

A transient thermal analysis of the 24PT4-DSC is performed using the 3-D ANSYS model developed in Section A.4.7.1.1, for HLZCs 1, 2 and 3.

The initial conditions for the transient analysis correspond to the steady state temperatures calculated in Section A.4.4.2.3 at the off-normal analysis extreme ambient temperatures of 117°F with insolation.

A separate CFD based blocked vent transient analysis was not performed. Instead, a comparison was made between the DSC shell temperatures predicted by the HEATING7 model (Section 4.4.2.2) and CFD model (Section A.4.4.2) at the start of the transient. This ΔT was applied to the DSC surface temperatures predicted by HEATING7 to calculate the DSC surface temperatures for the duration of transient. The individual basket component temperatures were extrapolated based on a comparison of the 117°F storage condition shell temperature and the transient shell temperature calculated above. This ΔT was then added to the CFD 117° storage condition component temperatures.

Figure A.4.6-1 and Figure A.4.6-2 present the transient temperature response during the blocked vent accident for the 24PT4-DSC shell, fuel cladding, guidesleeve, oversleeves, Boral[®], and

support rods for *the bounding HLZCs* #1 and #3, respectively. The time limit for the heat-up of the 24PT4-DSC basket components is *based on* the material temperature limit for the support rods, *guidesleeves, and oversleeves.*

The maximum 24PT4-DSC shell assembly and basket component temperatures for the blocked vent accident are given in Table A.4.4-3 and Table A.4.4-6, respectively. The maximum fuel cladding temperature for blocked vent accident is given in Table A.4.4-7.

These temperatures are below the associated safety limits for the AHSM or 24PT4-DSC *materials.* The short time exposure of the 24PT4-DSC and the spent fuel assemblies to the elevated temperatures will not cause any damage. The maximum 24PT4-DSC internal pressure during this event is calculated in Section A.4.6.6.

A.4.6.3 TC Loss of Neutron Shield and Sunshade

The TC and 24PT4-DSC are analyzed for a postulated accident in which the TC loses the annular water neutron shielding and the required sunshade during transfer at the extreme off-normal summer ambient condition. Even though such a scenario would likely result in an immediate corrective action, the duration of the accident is conservatively assumed to result in steady state temperature distributions in the TC and 24PT4-DSC. This analysis was previously performed to support the addition of the TC to the NUHOMS® design described in Reference [A4.12]. Therefore, the cask has already been analyzed for such an event.

The maximum shell temperature for this case is 536°F.

Comparison of this shell temperature of 536°F with shell temperature of 642°F for the blocked vent accident shows that the TC loss of neutron shield and sunshade accident analysis is bounded by the blocked vent analysis presented in Section A.4.6.2. Hence, end point criteria for the 24PT4-DSC under the blocked vent scenario, such as cavity pressure, fuel cladding integrity, compliance of the 24PT4-DSC structural materials with ASME B&PV Code temperature limit criteria, etc., provide a bounding analysis for the postulated accident in the TC.

A.4.6.4 Fire Accident Evaluation

The fire accident evaluation of the 24PT4-DSC is conducted under the same conditions, and in the same manner, and is described for the Advanced NUHOMS® System with 24PT1-DSC in Section 4.6.4. The results for the first 600 minutes are included in Figure A.4.6-3. The maximum calculated DSC shell temperature for the conservative fire condition analyzed is 527°F at 8000 minutes from the beginning of the transient. Comparing this to the results for the 24PT4-DSC in Table A.4.4-3 shows that this extremely conservative fire accident is bounded by the blocked vent accident. Therefore, the end point criteria of the fire for the 24PT4-DSC shell assembly, basket assembly, and fuel cladding are bounded by the blocked vent condition, including accident pressure, fuel cladding and 24PT4-DSC structural component temperatures.

Further, based on the discussion presented in Section 4.6.4, a fire at the inlet of the AHSM with a 24PT4-DSC located within the AHSM is bounded by the analysis provided for a fire accident with the 24PT4-DSC in the TC. Similarly, a fire occurring during transfer operations (i.e.,

during 24PT4-DSC transfer between the cask and AHSM) will be bounded by the cask/AHSM scenarios discussed above.

Based on the thermal analyses results and the criteria evaluated for the fire accident conditions, the 24PT4-DSC can withstand the hypothetical fire accident event without compromising its confinement integrity and fuel retrievability.

A.4.6.5 Flood Accident

The Advanced NUHOMS[®] System was evaluated for the impact of a worst case flood accident which completely covers the AHSM. The thermal consequences of such an accident are beneficial. The 24PT4-DSC shell temperatures shown in Table A.4.4-4 for the design basis decay heat are higher than the saturation temperature of water. Under these conditions, any water that contacts the 24PT4-DSC surface would eventually boil, providing an extremely effective heat removal mechanism for the 24PT4-DSC. Calculations performed using a boiling correlation show that, given the expected heat flux of the design basis heat load on the 24PT4-DSC surface, the temperature of the canister cannot differ more than 5°F from the water temperature, which is limited by the boiling process. Therefore, the thermal effects of the flood accident are bounded by the other thermal accidents which are considered.

A.4.6.6 Maximum Pressure

The methodology for calculating maximum pressure in the 24PT4-DSC cavity during accident conditions is described in Section A.4.4.8.

Based on evaluation of the basket temperature results in Table A.4.4-6 and the fuel cladding temperature results of Table A.4.4-7, the peak pressure in the 24PT4-DSC cavity for accident conditions will occur during the blocked vent condition. The resulting maximum average helium temperature for the accident case is given in Table A.4.4-10.

For accident conditions, 100% failure of the fuel rods with 100% release of the fill gas from fuel rod and 30% release of the fission gas is assumed, based on guidance in [A4.2]. The maximum accident pressure is calculated by using the ideal gas law and is presented in Table A.4.4-10. The criteria for the accident pressure is established by adding additional margin to the calculated values to account for the presence of fission gases in the 24PT4-DSC cavity which might reduce the effective cover gas conductivity, and thus increase temperatures and pressures.

A.4.6.7 Evaluation of System Performance for Accident Conditions of Storage and Transfer

The thermal analysis for storage and transfer accidents concludes that the 24PT4-DSC design meets all applicable requirements. The maximum temperatures calculated for components necessary to ensure structural integrity, confinement and retrievability of the fuel using conservative assumptions are within the criteria set forth. The predicted maximum fuel cladding temperature is well below the allowable fuel temperature limits given in Table A.4.1-3. The comparison of the results with the allowable material temperature ranges is tabulated in Table A.4.1-3.

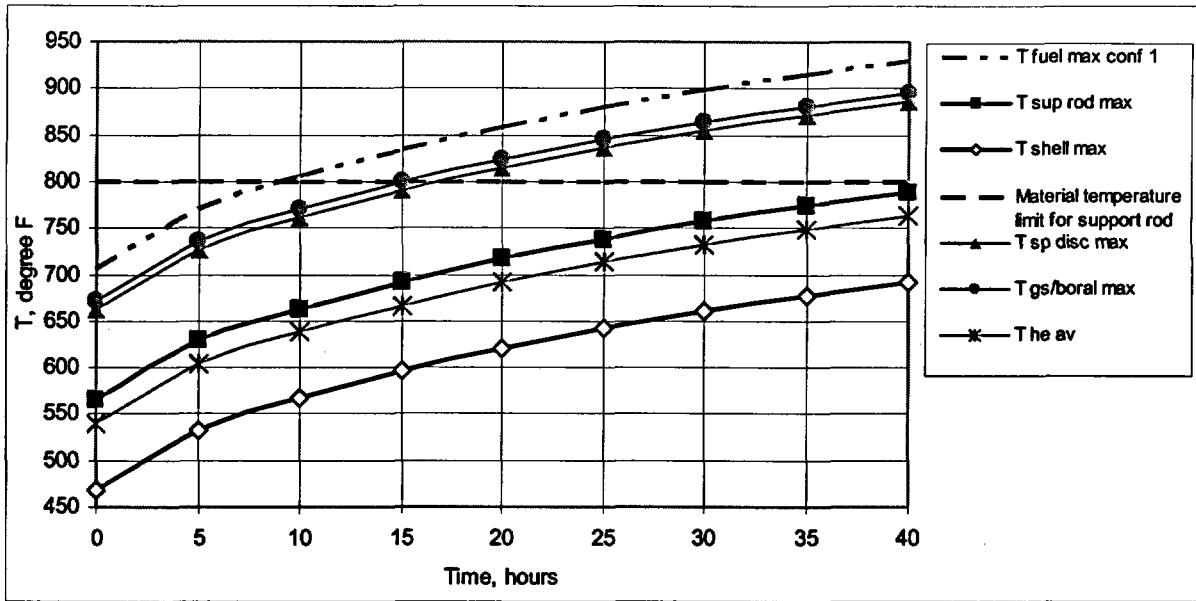


Figure A.4.6-1
Transient Temperatures of 24PT4-DSC Components during Blocked Vent Case – HLZC #1

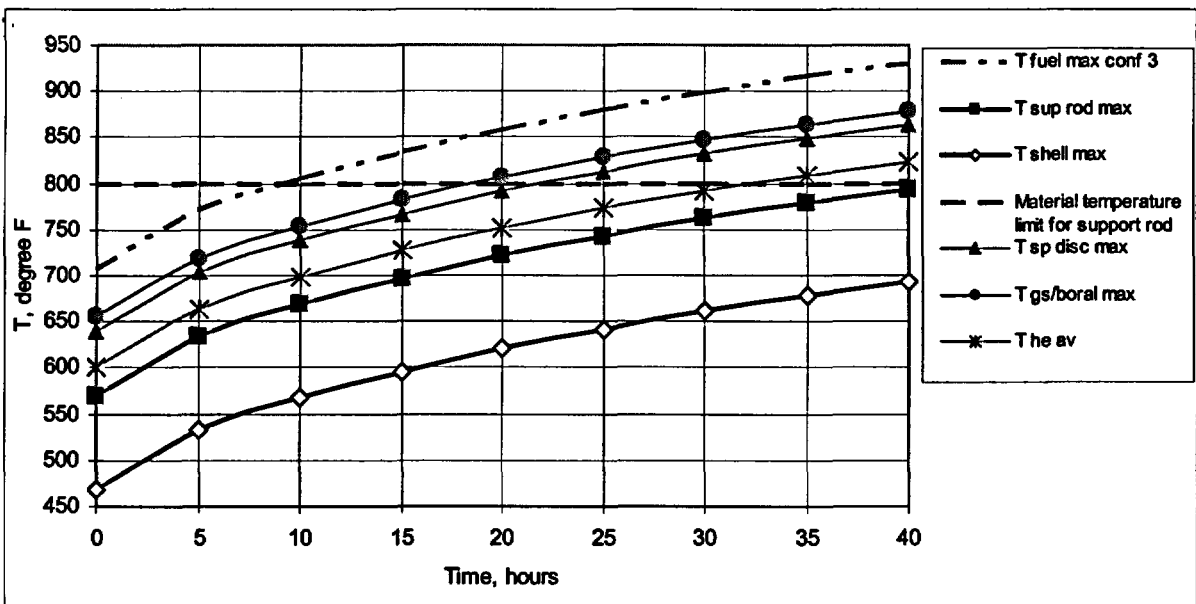


Figure A.4.6-2
Transient Temperatures of 24PT4-DSC Components during Blocked Vent Case – HLZC #3

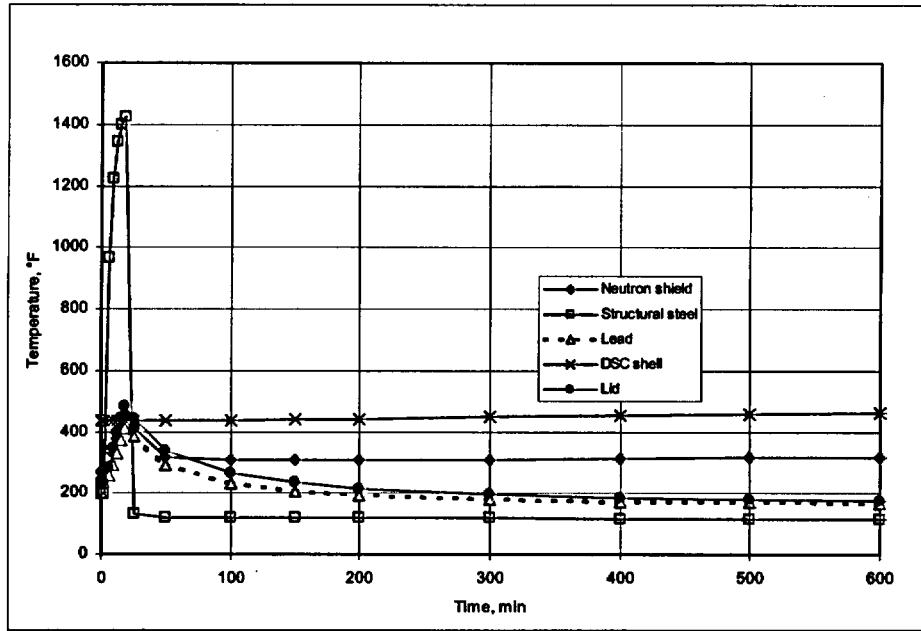


Figure A.4.6-3
OS197H Cask and 24PT4-DSC Response to Fire Accident

A.4.7 Thermal Evaluation for Loading/Unloading Conditions

All fuel transfer operations occur when the 24PT4-DSC is in the spent fuel pool. The fuel is always submerged in free-flowing pool water permitting heat dissipation. After fuel loading is complete, the 24PT4-DSC is removed from the pool, drained, dried, and backfilled with helium.

The three bounding loading conditions evaluated are (1) the heatup of the 24PT4-DSC before the cavity can be backfilled with helium (i.e., prior to blowdown), (2) the vacuum drying transient, and (3) steady state temperatures subsequent to helium backfill. Transient thermal analyses are performed to predict the heatup time history for the 24PT4-DSC components during these events.

The unloading operation considered is the reflood of the 24PT4-DSC with water.

A.4.7.1 Vacuum Drying Thermal Analysis

Analyses were performed for the vacuum drying condition in order to ensure that the steady state fuel cladding and 24PT4-DSC structural component temperatures remain below the maximum allowable material limits shown in Table A.4.7-2. In addition, a transient analysis was performed to ensure the requirements defined by ISG-11 [A4.21] for short-term operations (including vacuum during and helium backfilling operating conditions) are satisfied. According to ISG-11, the maximum fuel cladding temperature cannot exceed $T_{ISG \text{ limit}} = 400^{\circ}\text{C}$ (752°F) and the temperature difference during the thermal cycling of the cladding cannot exceed $\Delta T_{ISG \text{ limit}} = 65^{\circ}\text{C}$ (117°F).

During vacuum drying operation, water in the DSC cavity is forced out of the cavity (blowdown operation) before the start of vacuum drying. Two alternate options for the gas medium used for the water blowdown operation are evaluated.

In the first option, air is used as the gas medium to remove water and subsequent vacuum drying occurs with air environment in the DSC cavity. In the second option, helium is used as the medium to remove water and subsequent vacuum drying occurs with helium environment in the DSC cavity.

In the thermal analysis for the vacuum drying transient, either air or helium is used as the medium present in the DSC cavity during vacuum drying process. Details of the thermal analysis performed for these two alternate options are described in the following sections.

A.4.7.1.1 Analysis Model

For the vacuum drying thermal analysis, a three-dimensional slice of the 24PT4-DSC basket assembly and fuel is modeled near the center of the active fuel region using the ANSYS computer code. This case has little convection due to low pressure environment and therefore does not justify the use of a resource intensive CFD based code. The 3-D slice spans from center to center of two spacer discs to account for the radial effect of conduction through the spacer discs. Heat transfer effects along the axis of the 24PT4-DSC (third dimension) outside hottest section between two adjacent spacer disc mid-planes are conservatively neglected by applying adiabatic

boundary conditions to the axial ends of the model. The 24PT4-DSC shell surface is specified as a constant temperature boundary condition. The fuel regions inside the 24PT4-DSC are modeled as homogenous regions with internal heat sources. The effective thermal conductivity for the helium and vacuum drying cases is calculated in Section 4.9.

The ANSYS computer program [A4.15] is used to perform the thermal analysis of the 24PT4-DSC internal basket assembly and spent fuel assembly regions. Table A.4.7-1 illustrates the spacer disc layout, including the gaps between the components, simulated in the thermal model. The inside dimension of the guidesleeves used in the ANSYS model is 8.57" x 8.57", as opposed to final design configuration of 8.65" x 8.65" guidesleeve inside dimension. This deviation has a minimal impact on the transient and steady state analyses. The cutout in the spacer disc for external guidesleeves assemblies used in the ANSYS model is 9.435" instead of 9.45". A sensitivity analysis performed for 9.45" cutout shows that the 9.435" value results in conservatively higher 24PT4-DSC components and fuel cladding temperatures. Figure A.4.7-1 illustrates the axial length of the modeled basket slice.

The front and side views of the ANSYS analytical model of the 24PT4-DSC are shown in Figure A.4.7-2. Figure A.4.7-3 illustrates the layout of the finite elements used to model each of the spacer discs. Figure A.4.7-4 presents a perspective view of the finite element modeling of the 24PT4-DSC shell and guidesleeve assemblies, while Figure A.4.7-5 presents a view of the finite element modeling of the fuel assemblies.

The analysis of the guidesleeves is also applicable to the failed fuel can since their configuration is identical, except for the addition of top and bottom closures.

The heat generated within the fuel regions is assumed to be transferred to the guidesleeves and through the guidesleeve walls by conduction. The heat is then transferred through the guidesleeve assembly, including the Boral[®] sheets, oversleeves and gaps by conduction. Conservative gaps are modeled within the guidesleeve assemblies between the guidesleeves and the poison plate, between the poison plates and the oversleeves, and between the oversleeves or guidesleeves and the spacer discs. Table A.4.7-1 and Figure A.4.7-7 document the gaps between the basket components assumed within the ANSYS analytical model of the 24PT4-DSC. Radiation heat transfer across the gaps between guidesleeves and poison plates and between poison plates and oversleeves is conservatively ignored.

For the gaps between adjacent guidesleeve assemblies, heat transfer is assumed to occur by conduction and radiation. In the physical system, conduction in the axial direction would provide an additional mechanism for heat removal from the 24PT4-DSC; however, this mode of heat transfer is conservatively neglected for regions outside the hottest section between two adjacent spacer disc mid-planes. Conduction is modeled throughout the entire model. Radiation between adjacent guidesleeve assemblies, between the guidesleeve assemblies and the spacer discs, between the guidesleeve assemblies and the 24PT4-DSC shell, and between the spacer discs and the 24PT4-DSC shell is computed within the ANSYS program using the surface effect elements layout illustrated in Figure A.4.7-6.

In order to simplify the problem and reduce memory requirements and computing time, a portion of the thermal radiation was modeled using radiation link elements (link31). Radiation between the spacer discs and the 24PT4-DSC shell and radiation between the guidesleeves and the

spacer discs were modeled by this method. For these link elements, the area, view factor, emissivity, and Stefan-Boltzmann constant are defined as real constants. Because of the close proximity of the components, it is reasonable to assume a view factor of one. For the emissivity, an effective value is defined as follows [A4.8]:

$$\epsilon_{\text{eff}} = \frac{1}{\frac{1}{0.587} + \frac{1}{0.15} - 1} = 0.135$$

where 0.587 and 0.15 are the emissivity of DSC shell and spacer discs, respectively.

The area is calculated based on the total area for heat transfer divided by the total number of link elements. The thermal properties used in the ANSYS analytical model, including conductivities and emissivities, are presented in Section A.4.2.

Three different HLZCs, illustrated in Figure A.4.4-11 to Figure A.4.4-13, are evaluated. The design basis fuel decay heat ranges from 0.80 to 1.3 kW per spent fuel assembly, depending on the load configuration being analyzed. For HLZC #3, the heat load per assembly used is shown in Figure A.4.4-13. This analyzed configuration envelopes the configuration specified for the payload in Figure A.2.1-3 where the 1.3 kW/0.8 kW heat load is replaced with a 1.26 kW/0.9 kW heat load. Heat loads used in the thermal analysis envelopes the total DSC decay heat load and the differential temperatures used in structural analysis in Chapter A.3. The decay heat is applied as a volumetric heat generation uniformly distributed over the homogenous fuel regions inside the guidesleeve assemblies. The resulting volumetric heat density, including a peaking factor of 1.08, which was applied over the active fuel length, is computed as follows:

For 0.8 kW heat load.

$$\ddot{q} = \frac{0.8 \text{ kW} \cdot 1.08 \cdot 3414 \frac{\text{Btu/hr}}{\text{kW}} \cdot \frac{1 \text{ hr}}{60 \text{ min}}}{(8.57 \text{ in})^2 \cdot 149 \text{ in}} = 4.492e-3 \frac{\text{Btu}}{\text{min} \cdot \text{in}^3}$$

For 0.9 kW heat load.

$$\ddot{q} = \frac{0.9 \text{ kW} \cdot 1.08 \cdot 3414 \frac{\text{Btu/hr}}{\text{kW}} \cdot \frac{1 \text{ hr}}{60 \text{ min}}}{(8.57 \text{ in})^2 \cdot 149 \text{ in}} = 5.054e-3 \frac{\text{Btu}}{\text{min} \cdot \text{in}^3}$$

For 1.0 kW heat load.

$$\ddot{q} = \frac{1.0kW \cdot 1.08 \cdot 3414 \frac{Btu/hr}{kW} \cdot \frac{1hr}{60min}}{(8.57in)^2 \cdot 149in} = 5.615e-3 \frac{Btu}{min \cdot in^3}$$

For 1.2 kW heat load.

$$\ddot{q} = \frac{1.2kW \cdot 1.08 \cdot 3414 \frac{Btu/hr}{kW} \cdot \frac{1hr}{60min}}{(8.57in)^2 \cdot 149in} = 6.738e-3 \frac{Btu}{min \cdot in^3}$$

For 1.3 kW heat load.

$$\ddot{q} = \frac{1.3kW \cdot 1.08 \cdot 3414 \frac{Btu/hr}{kW} \cdot \frac{1hr}{60min}}{(8.57in)^2 \cdot 149in} = 7.3e-3 \frac{Btu}{min \cdot in^3}$$

A.4.7.1.2 Vacuum Drying with Air during Blowdown

Assuming that the cavity is filled with air during the vacuum drying operation provides conservative results since the void volume is typically filled with a mixture of air, water and water vapor, and no credit is taken for evaporation of water, which is a strong cooling mechanism that takes place during this operation. Air thermal conductivity does not change significantly at lower pressures, therefore, the use of a thermal conductivity for a pressure higher than 3 Torr is acceptable. As stated in Chapter A8, water is required to be in the annulus between the 24PT4-DSC and the TC during the vacuum drying process. Therefore, the 24PT4-DSC shell boundary is set to a temperature of 230°F as a conservative estimate of the shell wall temperature during this operation. A heat load of 24 kW is used in computing the maximum fuel cladding and basket component temperatures.

After vacuum drying, the DSC is backfilled with helium, the temperature of the fuel cladding drops due to the presence of helium in the DSC cavity. The steady state calculation for helium backfill shows a maximum fuel temperature of 607°F for HLZC #1 and 555°F for HLZC #3. A time limit must be placed upon vacuum drying with air to ensure that the ISG-11 transient limit of 117°F ΔT is not exceeded when the DSC is backfilled with helium. A conservative ΔT of 100°F is assumed, resulting in a maximum allowed cladding temperature of 607°F + 100°F = 707°F for the vacuum drying transient for HLZC #1 and 655°F for HLZC #3. A transient calculation demonstrates that the maximum fuel temperature reaches values of 707°F and 655°F at a time of 35 hours and 26 hours for HLZCs #1 and #3, respectively. The results are summarized in Figure A.4.7-8 and Table A.4.7-2. Therefore, the maximum duration for vacuum drying with air during blowdown is set at 35 hours and 26 hours for HLZCs #1 and #3,

respectively. The maximum temperatures for vacuum drying using air for blowdown are presented in Table A.4.7-2 for the basket structural components and fuel cladding.

A.4.7.1.3 Vacuum Drying with Helium during Blowdown

For the vacuum drying analysis *with helium, the CFD model described in Section A.4.4.4 is used with the DSC rotated to the vertical position.* Similar to air, helium thermal conductivity also remains pressure independent down to 3 Torr, [A4.23], therefore, the helium thermal conductivity at normal pressure is used for this analysis. The boundary conditions applied to the model are the same as those used for vacuum drying after blowdown by air.

The maximum fuel cladding temperature *allowed* during vacuum drying, *707°F and 655°F for HLZC #1 and HLZC #3, respectively,* do not exceed the ISG-11 limit of 752°F.

Since the similar material properties and boundary conditions applied to vacuum drying with helium during blowdown and helium backfilling operations, the maximum fuel cladding temperature of *707°F and 655°F for HLZC #1 and HLZC #3, respectively,* during helium backfilling remains unchanged after vacuum drying in helium, the ISG-11 thermal cycling temperature limit is satisfied and no time limit for vacuum drying in helium required. The results are presented in Table A.4.7-2. The maximum temperatures for vacuum drying using helium for blowdown for the basket components and fuel *are also presented in Table A.4.7-2.*

A.4.7.2 Pressure during Unloading of Cask

To unload the fuel from the 24PT4-DSC, reflooding of the cavity is required. This occurs by reducing the pressure in the 24PT4-DSC to atmospheric conditions followed by introducing water into the cavity through the drain port and venting through the vent port. Since fuel temperatures are expected to be significantly higher than the saturation temperature of water, flooding of the hot 24PT4-DSC will result in steam generation which, if not vented, will result in a higher cavity pressure.

The flow rate of water into the 24PT4-DSC during reflood is controlled during this operation so that the pressure within the 24PT4-DSC stays below the assumed 20 psig for this condition.

A.4.7.3 Cask Heatup Analysis

Heatup of the water within the 24PT4-DSC cavity prior to blowdown and backfilling with helium occurs as operations are performed to *load fuel, decon the cask and drain and dry the 24PT4-DSC.* Prevention of boiling in the Advanced NUHOMS® System is not required to ensure public health and safety for the following reasons:

1. The criticality analysis considers a wide range of moderator densities which include that of steam (Chapter A.6). Criticality limits were shown to be met at conditions of low moderator density (boiling water).
2. The cavity is always vented during the water heatup transient.

3. Although steam may be produced through boiling of the cavity water, its presence in the weld joint area during the *shield plug assembly* welding operations will be essentially blocked at the interface between the shield plug and the support ring. What little steam may be present is displaced by the argon shielding gas used in the GTAW process. This shielding gas is heavier than steam and is delivered at a sufficiently high rate (usually 30 – 50 ft³/hr) to assure that the steam is excluded from the weld joint. Finally, if moisture somehow did enter the weld area, the resulting weld bead porosity would be readily detectable by the visual inspection of each pass performed by the welding operator and the dye penetrant (PT) examination performed on the surface of the root pass.

Therefore, the only potential concern associated with steam generation is shielding. An unexpectedly high loss of water within the 24PT4-DSC cavity during these loading operations could result in increased occupational exposure. The following analysis is presented to identify to the licensees the time for the water in the 24PT4-DSC cavity to boil so that corrective action can be planned and implemented as necessary to address ALARA concerns.

The model conservatively does not credit any heat transfer in the axial direction. Homogenized effective thermal properties of the 24PT4-DSC cavity are calculated based on the weight, volume and material of the components. Radiation heat transfer within the 24PT4-DSC cavity is neglected. All temperatures in the 24PT4-DSC are initially assumed to be at the maximum spent fuel pool temperature. The exterior of the cask is assumed to radiate and convect heat to the prevailing ambient conditions of the fuel building. The analyses are performed for a building temperature of 120°F and a fuel pool temperature of 140°F. The results are tabulated in Table A.4.7-3 and shown in Figure A.4.7-9 for canister decay heat loads ranging from 12 to 24 kW. *Note that the starting time to reach boiling is based on a very conservative assumption that following the placement of the first fuel assembly in the DSC, the DSC heat load is 24 kW (i.e., all 24 fuel assemblies loaded simultaneously in the DSC).*

A.4.7.4 Pressure During Loading of Cask

The maximum pressure during cask blowdown is 20 psig. This is discussed in Chapter A.3.

Table A.4.7-1
Gaps between Components of ANSYS Model at the Spacer Disc Plane

Component of the model (Along the first column of fuel assemblies from axis Y from the top to the bottom of DSC)	Gap width, in	Total gap for composite guide sleeve regions, in	Note
Shell			See Figure A.4.7-7 for details
Gap	0.19		
Spacer disc			
Gap	0.1874		
Guide sleeve			
Exterior Fuel Assembly			
Guide sleeve			
Gap 1			
Poison plate		Gap 1 + Gap 2	
Gap 2		0.0125	
Over-sleeve			
Gap	0.1874		
Spacer disc			
Gap	0.1072		
Over-sleeve			
Gap 3			
Poison plate		Gap 3 + Gap 4	
Gap 4		0.0125	
Guide sleeve			
Interior Fuel Assembly			
Guide sleeve			
Gap 5			
Poison plate		Gap 5 + Gap 6	
Gap 6		0.0125	
Over-sleeve			
Gap	0.1072		
Spacer disc			
Gap	0.1072		
Over-sleeve			
Gap 7			
Poison plate		Gap 7 + Gap 8	
Gap 8		0.0125	
Guide sleeve			
Interior Fuel Assembly			
Guide sleeve			
Gap 9			
Poison plate		Gap 9 + Gap 10	
Gap 10		0.0125	
Over-sleeve			
Gap	0.1072		
Spacer disc			

**Table A.4.7-2
Vacuum Drying Results following Blowdown with Air or Helium**

Component Heat Load	Max Temperature during Vacuum Drying (Air Blowdown)		Max Temperature during Vacuum Drying (Helium Blowdown)		Limit Ref (°F)
	HLZC #1 @ 35 hours	HLZC #3 @ 26 hours	HLZC #1	HLZC #3	
Fuel	707	655	607	555	752 [A4.21]
Support Rod	408	394	376	386	650 [A4.4]
Guidesleeve	657	573	568	<568	800 [A4.4]
Boral [®]	657	573	568	<568	1000 [A4.4]
Spacer Disc	642	545	559	<559	800 [A4.4]

**Table A.4.7-3
Summary of Water Heatup Calculation**

Decay Heat, kW	Time, hrs*	
	$T_{\text{pool}}=140^{\circ}\text{F}$	$T_{\text{stb}}=120^{\circ}\text{F}$
12		31.4
14		25.9
16		22.2
18		19.5
20		17.4
22		15.7
24		14.3

**Time is to be conservatively measured from the time that the first assembly is loaded in the DSC to account for heatup of water in the DSC while still in the spent fuel pool.*

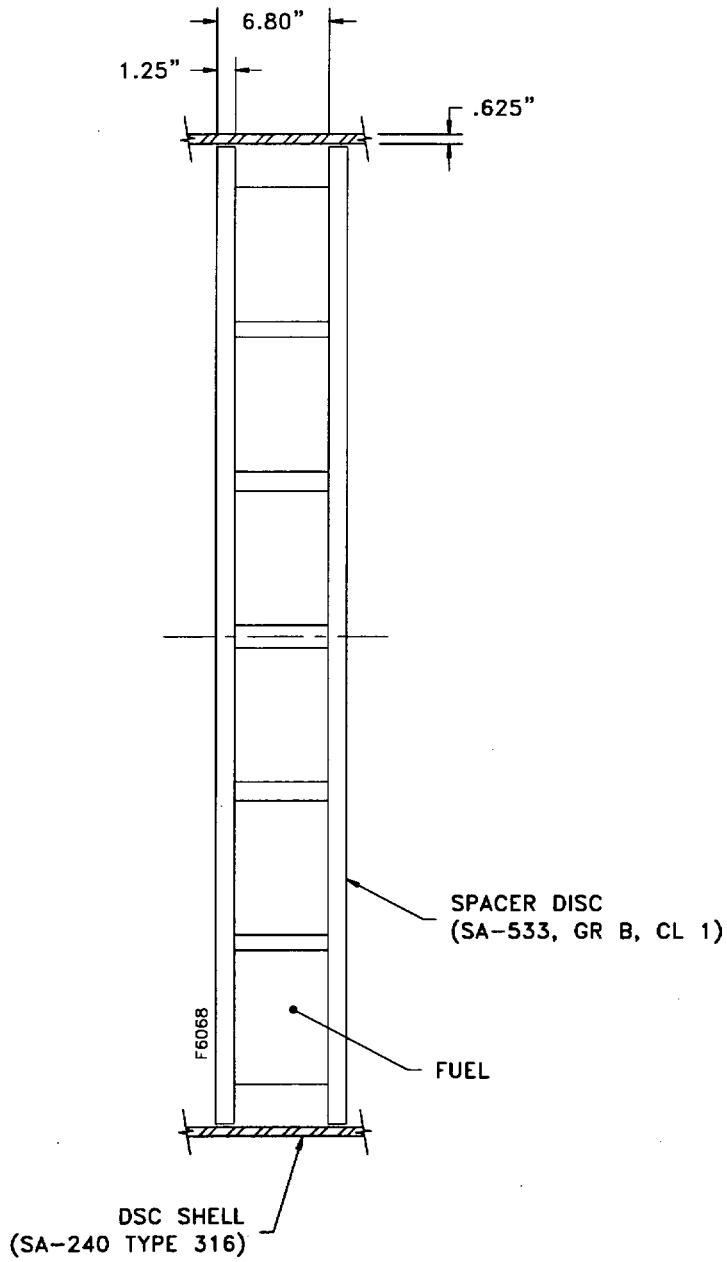


Figure A.4.7-1
Simplified Axial View of the 24PT4-DSC Basket Model

Note – All dimensions are in inches

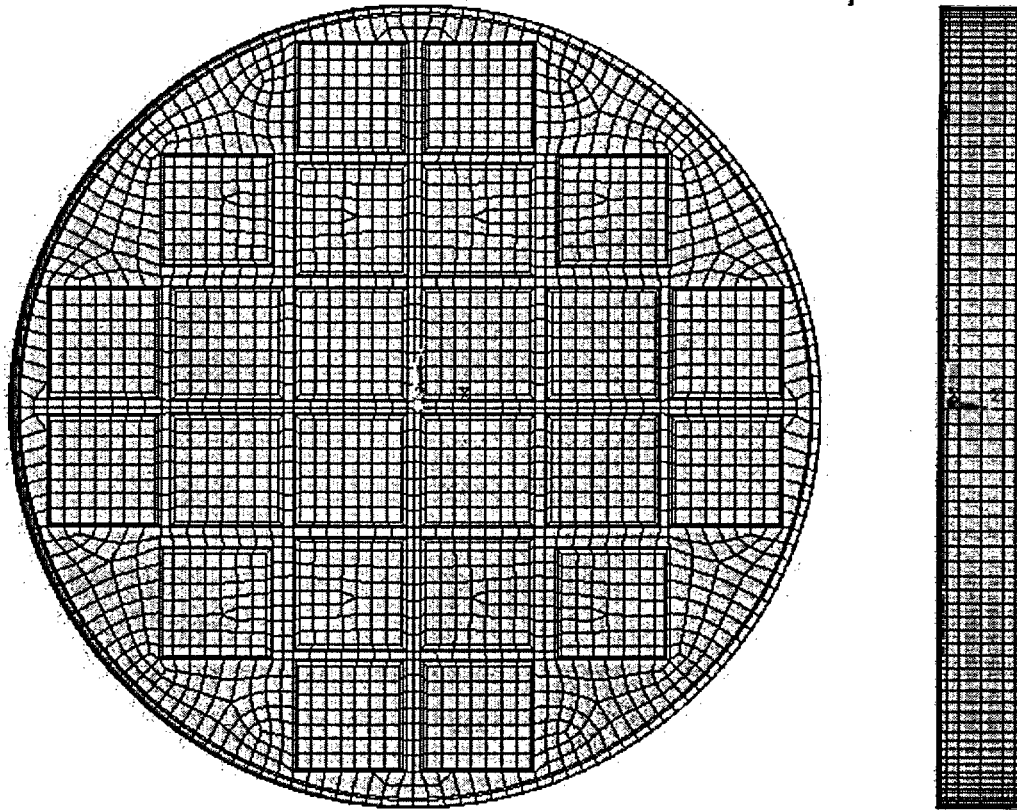


Figure A.4.7-2
24PT4-DSC ANSYS Thermal Model; Front And Side Views

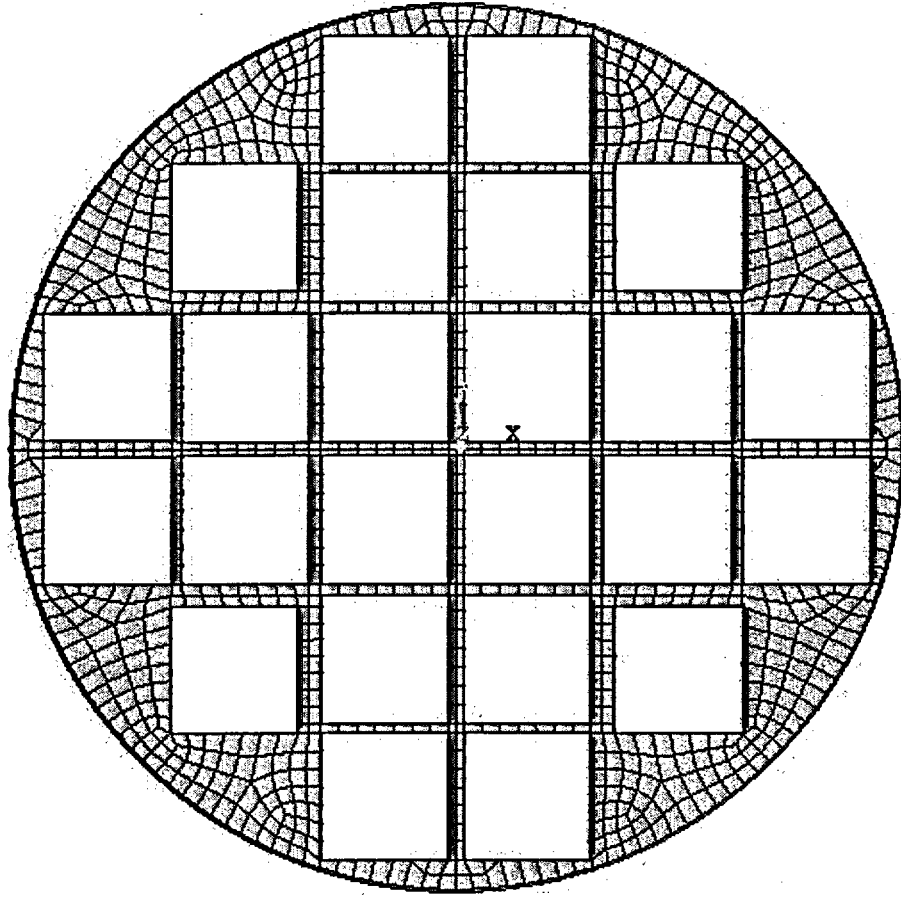


Figure A.4.7-3
24PT4-DSC ANSYS Thermal Model, Spacer Disc

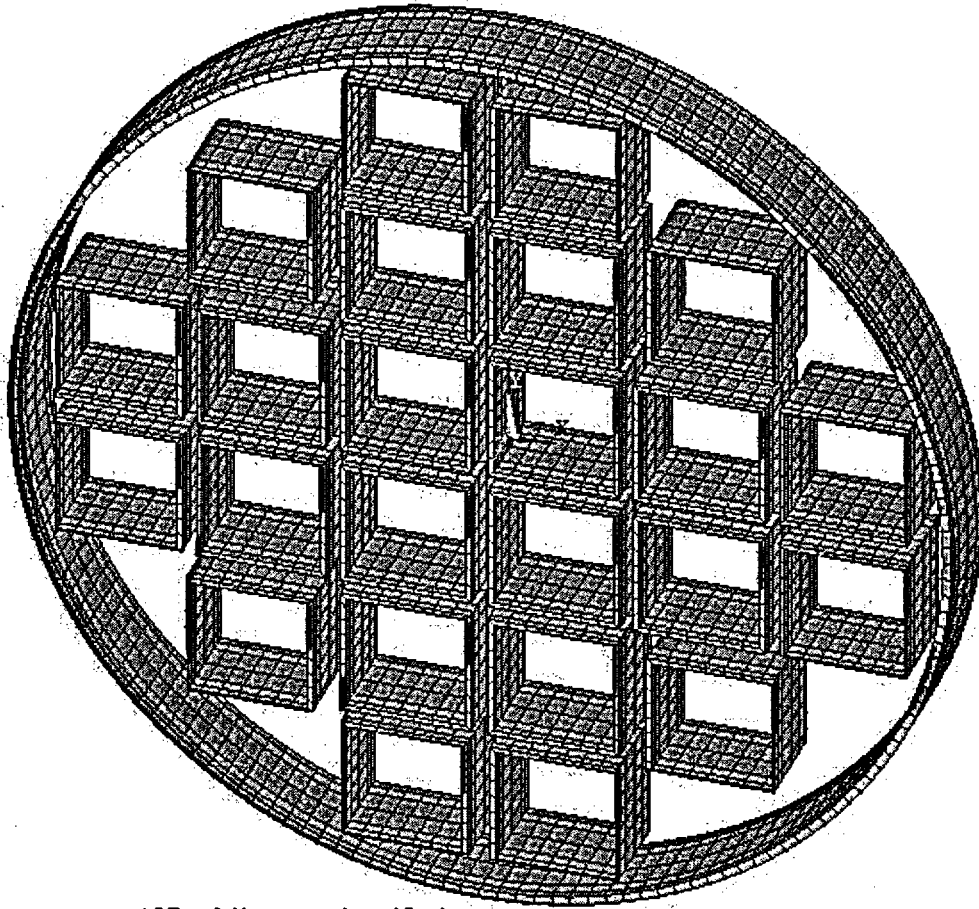


Figure A.4.7-4
24PT4-DSC ANSYS Thermal Model, Shell and Guidesleeve Assembly

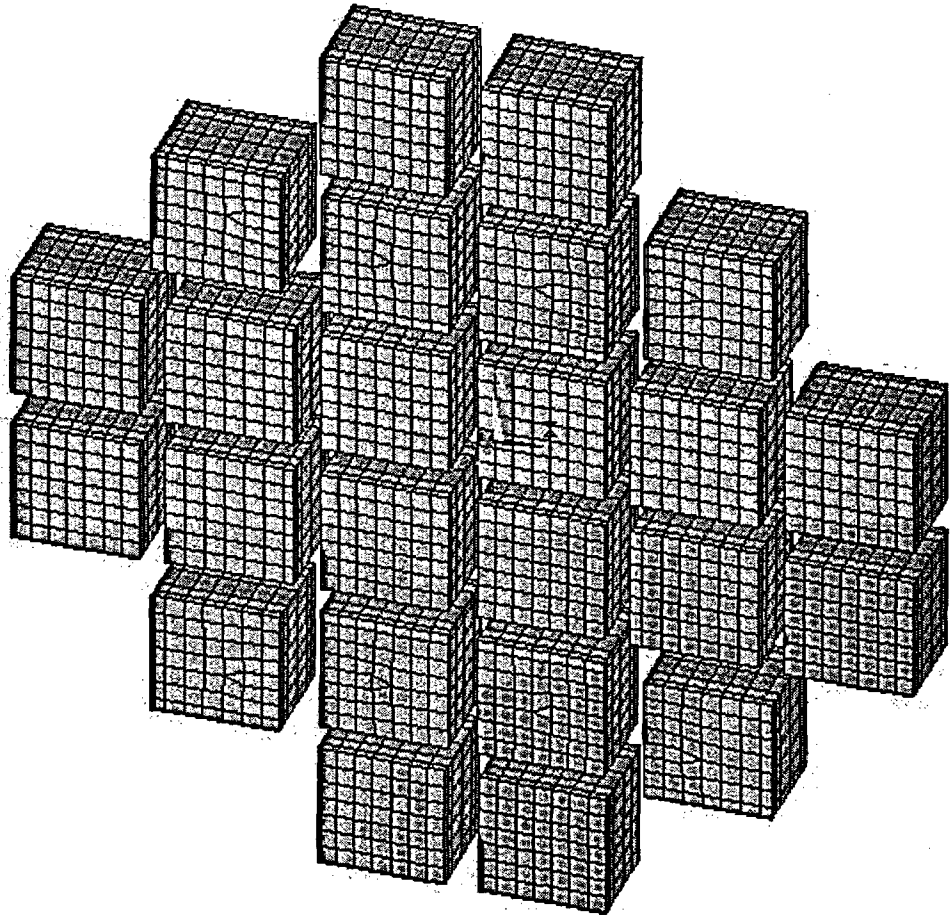


Figure A.4.7-5
24PT4-DSC ANSYS Thermal Model, Fuel Assemblies

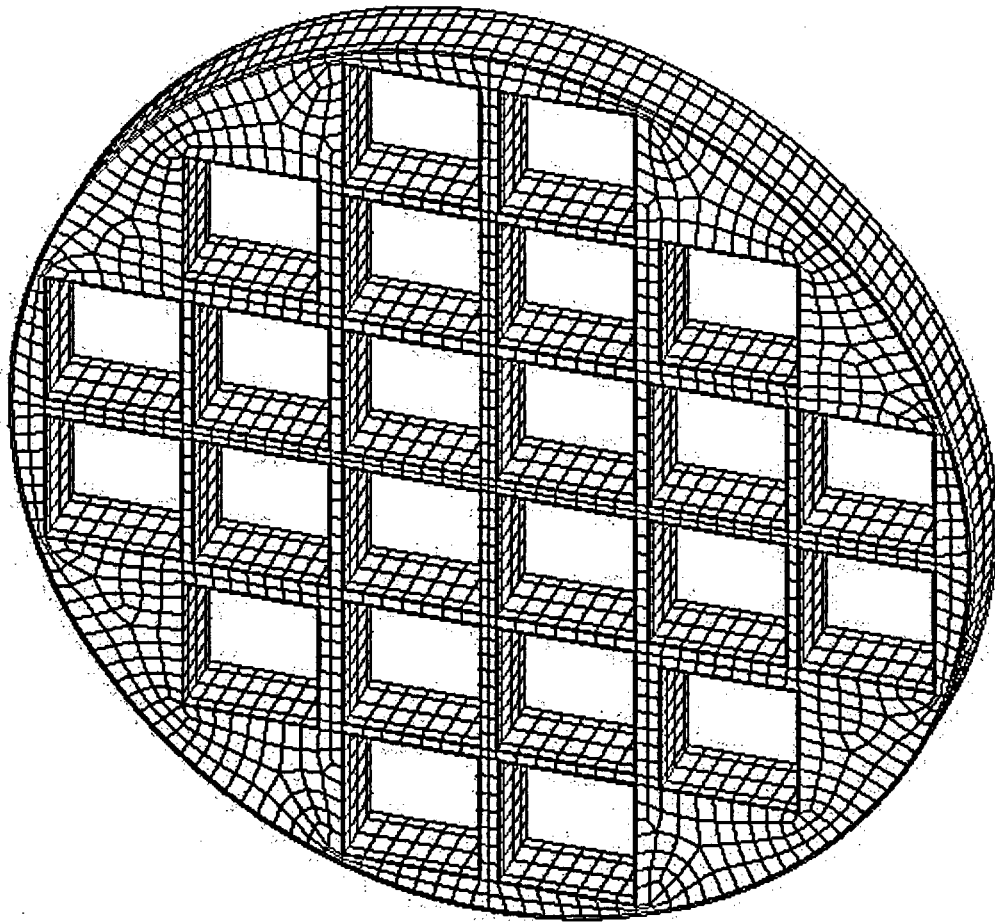


Figure A.4.7-6
Surface Elements for Radiation View Factor Calculation

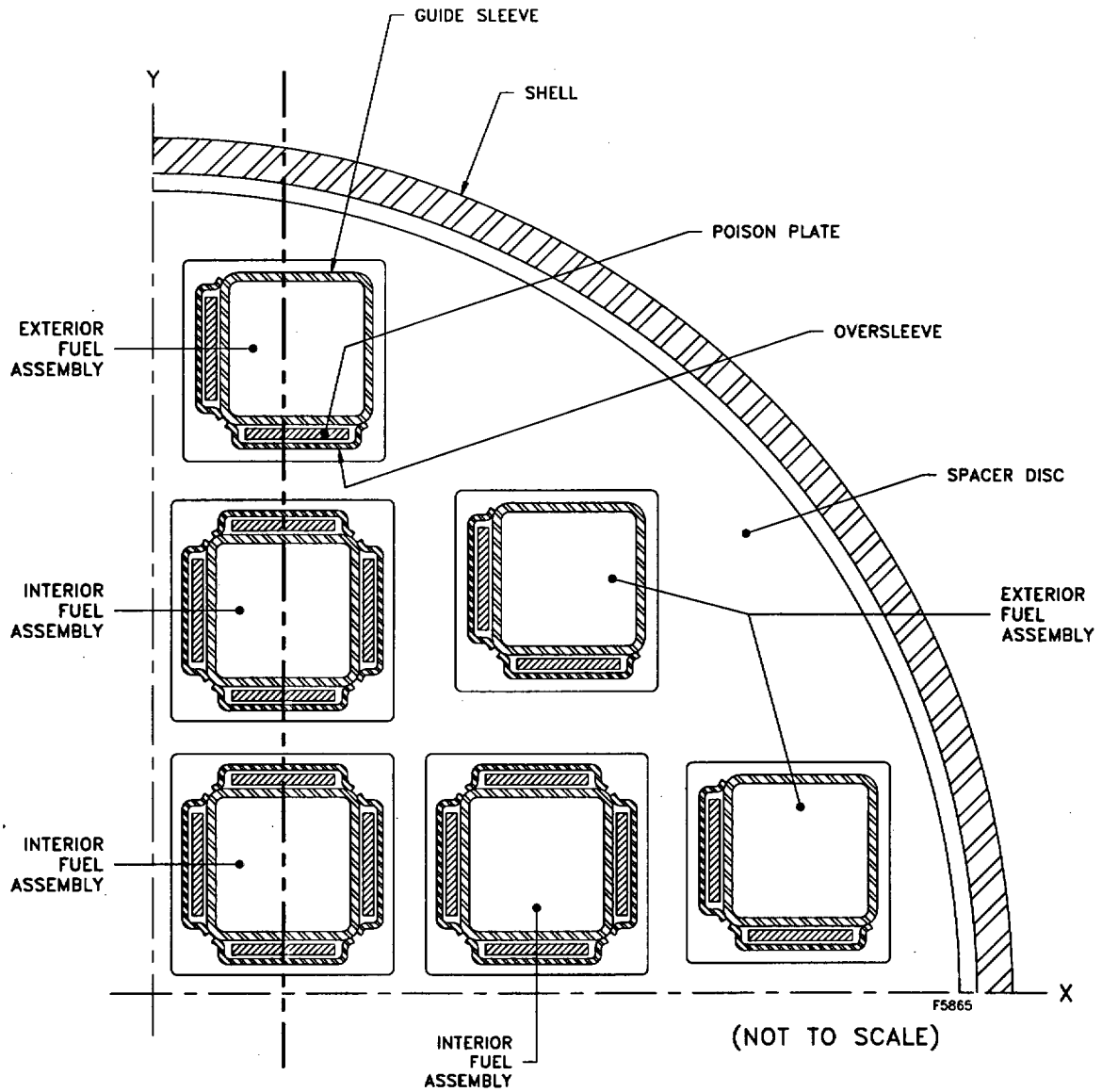


Figure A.4.7-7
Gaps between Components of ANSYS Model

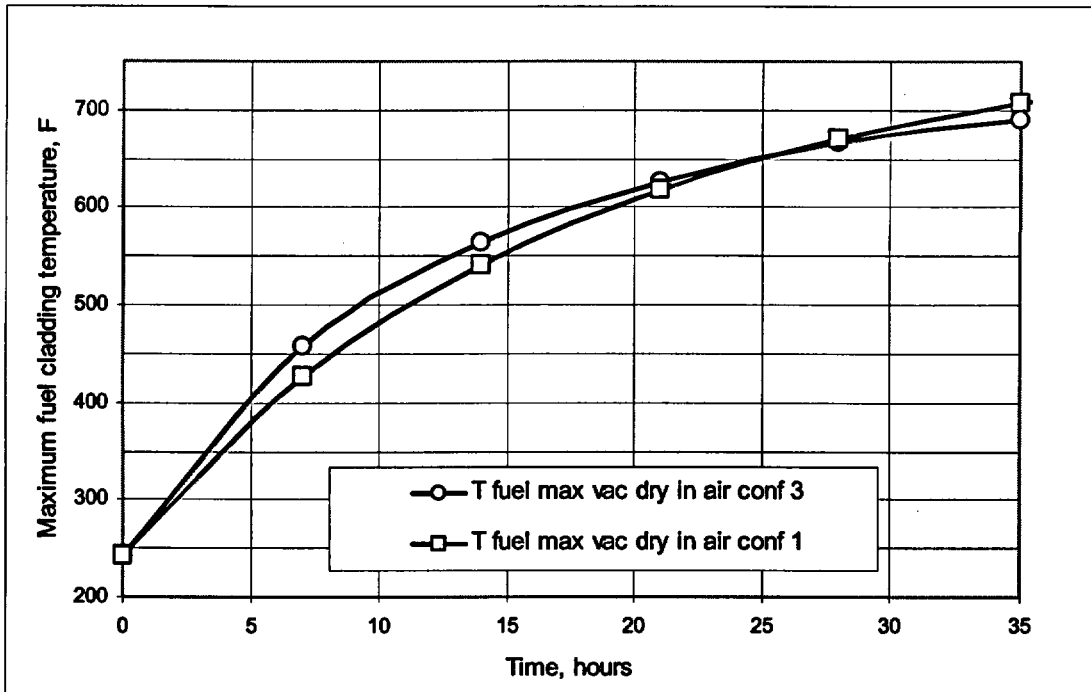


Figure A.4.7-8
Maximum Fuel Cladding Temperature during Vacuum Drying Using Air for Blowdown

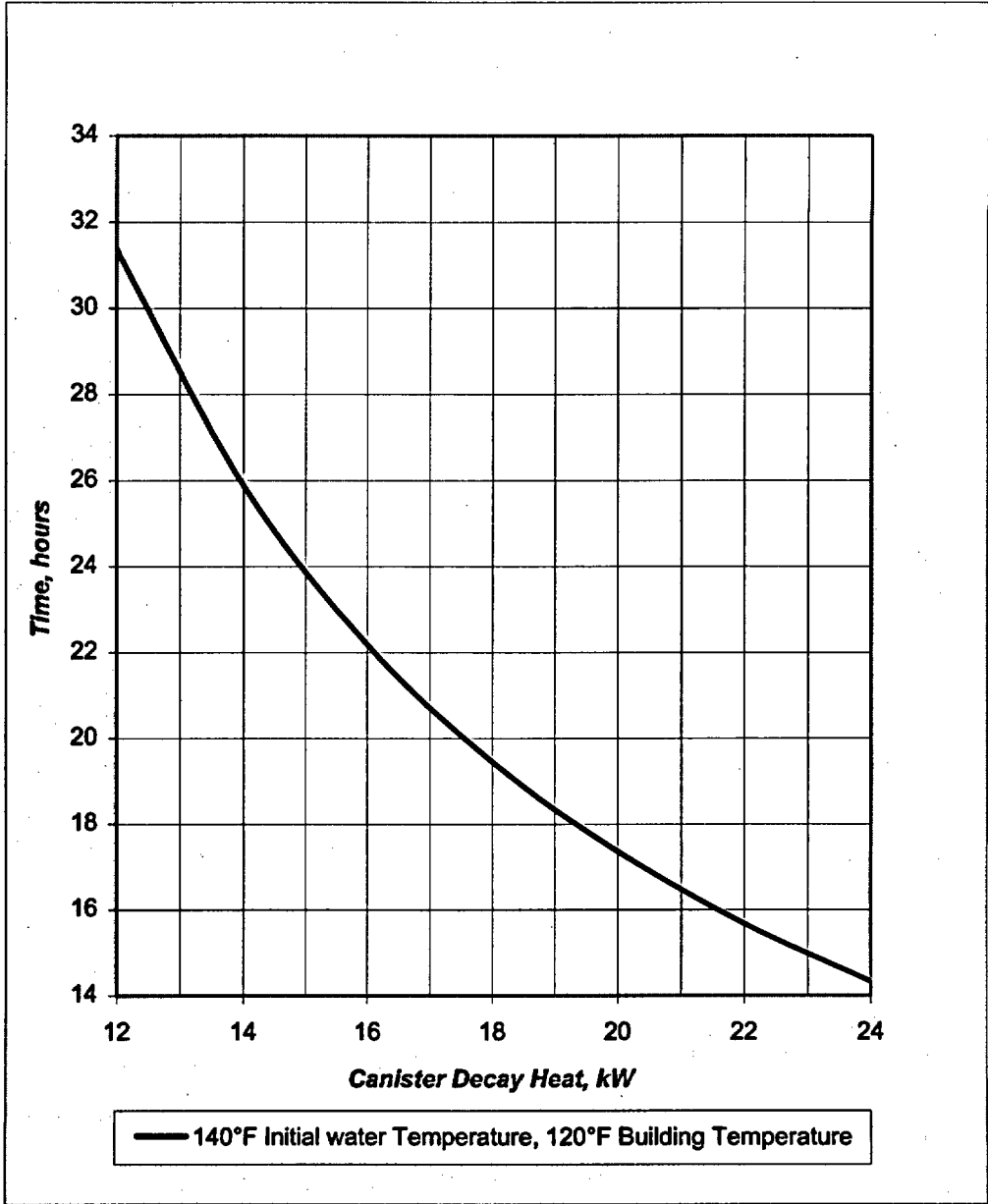


Figure A.4.7-9
Time to Reach Boiling Conditions inside 24PT4-DSC Cavity

A.4.8 Confirmatory Thermal Analysis of the 24PT4-DSC

The thermal analysis of the AHSM and 24PT4-DSC has been performed using a CFD based code. Hence, the use of an alternate code such as SINDA/FLUINT which also credits convection for performing a confirmatory analysis is unnecessary. Hence, this section has been deleted.

A.4.9 Determination of Effective Thermal Conductivity of CE 16x16 Fuel Assemblies

This section presents the methodology for the determination of transverse and axial effective thermal conductivity of the spent fuel.

The design basis thermal analysis of the 24PT4-DSC presented in Section A.4.4 models the CE 16x16 Zircalloy clad fuel assemblies as homogeneous solid regions with uniform internal heat generation. To accurately predict the temperature rise from the DSC guidesleeve to the peak pin location within each fuel assembly using this type of modeling, the effective thermal conductivity of the homogeneous solid region must be determined. The effective thermal conductivity calculation accounts for the actual geometry the fuel assembly and the fact that the heat generation occurs only within the fueled pins

A.4.9.1 Transverse Thermal Conductivity of Fuel in Helium and Vacuum

A.4.9.1.1 Methodology

The analysis methodology used for this calculation is based on the calculation approach outlined in Section 3.2.2 of reference [A4.37]. One quarter of the CE 16x16 fuel assembly and the surrounding DSC guidesleeve are modeled. The boundaries formed by the guidesleeve are assumed to be at a specified constant temperature, while symmetry conditions are assumed at the remaining two boundaries. The Thermal Desktop™ [A4.25] and SINDA/FLUINT™ [A4.24] computer programs were used to develop and exercise this detailed thermal model of the fuel assembly. Figure A.4.9-1 presents a perspective view of the modeled fuel assembly and guidesleeve segment for the CE 16x16 fuel assemblies. Figure A.4.9-2 illustrates the finite element modeling used.

The fuel assembly guide tubes are assumed to be filled with helium gas with heat transfer across the interior void volume being via radiation and conduction. Heat generated in the pellets within the fuel rods is transferred to the guidesleeves via conduction and radiation. While a gap may exist between the cladding and the fuel pellet, the associated thermal resistance is assumed to be negligible since the size of the gap is small and since, due to swelling of the pellet, it may not even exist. Further, the resistance due to this gap has an insignificant effect on the radial heat transfer within the fuel assembly.

Table A.4.9-2 presents the component thermal conductivity values assumed for the thermal modeling. Since the analysis is conducted using a series of steady-state simulations, values for density and specific heat are not required. The fuel rods are assumed to have an emissivity of 0.8 while the stainless steel guidesleeve emissivity is 0.4 per Section A.4.2.

To account for the presence of air and or steam/water vapor at low vacuum pressures, the effective fuel conductivity for vacuum conditions are computed using the thermal conductivity of air for the void spaces within the assembly and the DSC guidesleeve.

The decay heat loading is applied as a volumetric heat load assuming a 1.08 peaking factor and an active fuel length from Table A.4.9-1. The design volumetric heat loading used for the fuel assembly types are as follows:

$$\text{Design volumetric heat load} = \left[\frac{(\text{Decay Heat per Assembly}) \times (\text{Peaking Factor})}{(\text{No. of fueled rods}) \times (\text{Volume per rod})} \right]$$

For the 24PT4 with a decay heat loading of 1.0 kW/assembly:

$$\begin{aligned} \text{Volume per rod} &= \text{Active Fuel Length} \times \pi \times (\text{Fuel rod OD} - 2 \times \text{Cladding Thickness})^2 / 4 \\ &= 149" \times \pi \times (0.382 - 2 \times 0.025)^2 / 4 \\ &= 12.89889 \text{ in}^3 \end{aligned}$$

$$\begin{aligned} \text{24PT4 Design volumetric heat load w/ 1.0 kW} &= \left[\frac{(1000 \text{ watts}) \times (1.08)}{(236) \times (12.89889 \text{ in}^3)} \right] \\ &= 0.35478 \text{ watts/in}^3 \end{aligned}$$

A.4.9.1.2 Effective Transverse Thermal Conductivity Calculation

The thermal model described above was exercised for nine guide sleeve temperature levels (i.e., 150, 200, 275, 350, 425, 500, 575, 650, and 725 °F) for the case with helium backfill and eleven guide sleeve temperature levels (i.e., the previous nine levels plus 800 and 875 °F) for the vacuum drying condition. The resulting peak temperatures are presented in Table A.4.9-3. In accordance with the development of the equation for effective conductivity presented on page II-127 of [A4.36] and equation 6.1-5 of [A4.37], the effective thermal conductivity can be computed as:

$$k_{\text{effective}} = \left[\frac{0.29468 \times \text{Volumetric Heat Generation Based On Assembly Width} \times \left(\frac{\text{Assembly Width}}{2} \right)^2}{(T_{\text{peak}} - T_{\text{sleeve}})} \right]$$

This equation can be restated as:

$$k_{\text{effective}} = \left[\frac{0.29468 \times \text{Decay Heat Loading For Modeled Section} \times 4}{4 \times \text{Length of Modeled Segment} \times (T_{\text{peak}} - T_{\text{sleeve}})} \right]$$

The decay heat loading computed from the model, the length of the modeled segment (i.e., 0.5 inches), and the noted peak temperature and boundary sleeve temperature are substituted to yield the computed effective thermal conductivity. Table A.4.9-3 presents the computed effective thermal conductivity for each guide sleeve boundary temperature under the helium filled and vacuum drying conditions.

For use in finite element modeling, Section 6.2.2 of [A4.37] recommends that the effective thermal conductivity values be made a function of the mean assembly temperature, or $(T_{peak} + T_{sleeve})/2$. Figure A.4.9-3 illustrates the correlation between the computed effective thermal conductivity and the median assembly temperature for the helium filled conditions, while Figure A.4.9-4 illustrates the correlation for the vacuum drying condition. The recommended effective thermal conductivity for PWR fuel assemblies from Table S-2 of [A4.37] is also presented in the figures for comparison purposes.

Table A.4.9-4 presents the same effective thermal conductivity data in Table A.4.9-3, but interpolated for specific values of the median assembly temperature.

A.4.9.2 Axial Thermal Conductivity of Fuel

The axial fuel conductivity is assumed to be limited to the cladding conductivity weighted by its fractional area as required in NUREG 1536 [A4.2].

$$K_{axl} = (K_{zirc})(A_{zirc}/A_{eff}) \quad (1)$$

$$K_{zirc} = \text{Conductivity of Zircaloy 4}$$

$$A_{eff} = (8.70") \times (8.70") = 75.69 \text{ in}^2$$

$$A_{zirc} = \text{Cross section area of Zircaloy cladding in the fuel assembly}$$

Equation (1) is used to calculate axial effective conductivity. The results are presented in Table A.4.9-5.

The axial thermal conductivity values presented in Table A.4.9-5 assume the pin geometry and number of fueled pins for the CE 16x16 Zircaloy clad fuel assembly for the 24PT4-DSC and are adjusted by the cross-sectional area of the fuel region to account for the fact that the fuel assemblies are treated as homogenized regions within this modeling. For example, at a temperature of 392 °F, the effective axial conductivity is computed as:

$$k_{axial \text{ direction}} = 236 \text{ pins} \times \frac{\pi}{4} \left((0.382")^2 - (0.382" - 2 \times 0.025")^2 \right) * 0.0115 \frac{\text{Btu}}{\text{min} - \text{in} - ^\circ \text{F}} + (8.57" \times 8.57")$$

$$k_{axial \text{ direction}} = 0.001017 \frac{\text{Btu}}{\text{min} - \text{in} - ^\circ \text{F}} @ 392^\circ \text{F}$$

Backfill gas property does not have any effect on the axial effective fuel conductivity. Therefore, identical axial effective fuel conductivity values can be used for helium and vacuum conditions.

Table A.4.9-1
Summary of Design Data For CE 16x16 Fuel Assembly Type

Parameter	
<i>Number of fuel rods</i>	236
<i>Number of guide tubes</i>	5
<i>Pellet diameter (in.)</i>	0.325
<i>Active fuel length (in.)</i>	149
<i>Cladding thickness (in.)</i>	0.025
<i>Fuel rod OD (in.)</i>	0.382
<i>Fuel rod pitch (in.)</i>	0.506
<i>Guide tube OD (in.)</i>	0.98
<i>Guide tube thickness (in.)</i>	0.040

Note: Assembly geometry obtained from References [A4.33] and [A4.34].

Table A.4.9-2
Thermal Properties Used in Calculation of Fuel Effective Conductivities

Temperature (°F)	Conductivity (BTU/min -in-°F)
Zircalloy [A4.35]	
200	0.0109
300	0.0115
400	0.0121
500	0.0126
600	0.0131
800	0.0142
Fuel Pellet, UO₂ [A4.35]	
200	5.537e-3
300	5.038e-3
400	4.622e-3
500	4.270e-3
600	3.968e-3
700	3.707e-3
800	3.478e-3
Type 304/304L Stainless Steel (See Section A.4.2)	
Helium (See Section A.4.2)	
Air (See Section A.4.2)	

Table A.4.9-3
CE 16x16 Computed Effective Transverse Thermal Conductivity

Conditions	DSC Guidesleeve Temperature, °F	Assembly Peak Temperature, °F	Assembly Median Temperature, °F	Effective Transverse Thermal Conductivity, (Btu/min-in-°F)
Helium Filled	150	234.8	192.4	0.000349
	200	279.5	239.8	0.000372
	275	345.9	310.5	0.000418
	350	413.2	381.6	0.000469
	425	481.2	453.1	0.000527
	500	550	525.0	0.000592
	575	619.7	597.4	0.000662
	650	690.1	670.1	0.000738
	725	761	743.0	0.000823
Vacuum Drying Conditions	150	347.6	248.8	0.000150
	200	376.3	288.2	0.000168
	275	423.5	349.3	0.000199
	350	475.2	412.6	0.000237
	425	530.9	478.0	0.000280
	500	589.8	544.9	0.000330
	575	651.5	613.3	0.000387
	650	715.5	682.8	0.000452
	725	781.4	753.2	0.000525
	800	848.9	824.5	0.000606
	875	917.6	896.3	0.000695

Table A.4.9-4
CE 16x16 Fuel Assembly Transverse Thermal Conductivities

Median Temperature (°F)	K (Btu/min-in-°F)	
	Helium Filled	Vacuum Conditions
200	0.000353	0.000127
275	0.000395	0.000161
350	0.000446	0.000200
425	0.000504	0.000245
500	0.000570	0.000296
575	0.000641	0.000355
650	0.000717	0.000421
725	0.000802	0.000496
800	0.000886	0.000578
875	—	0.000669

Table A.4.9-5
CE 16x16 Axial Thermal Conductivity

Temperature (°F)	Axial Thermal Conductivity (Btu/min-in-°F)
122	9.374E-04
212	9.640E-04
302	9.905E-04
392	1.017E-03
482	1.048E-03
572	1.079E-03
662	1.132E-03
752	1.185E-03

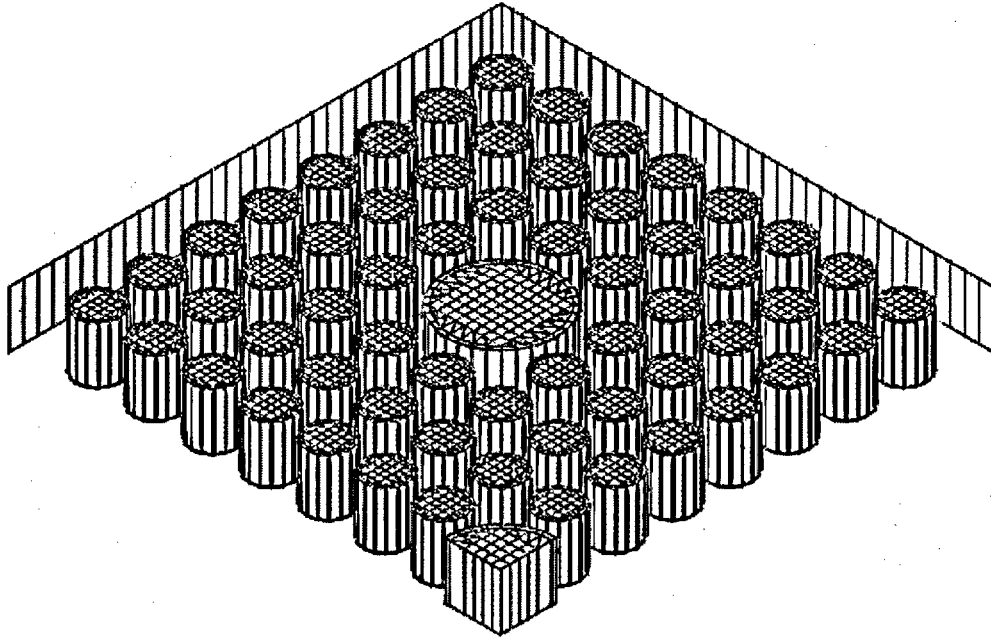


Figure A.4.9-1
Perspective View of CE 16x16 Thermal Model (1/4 Segment)

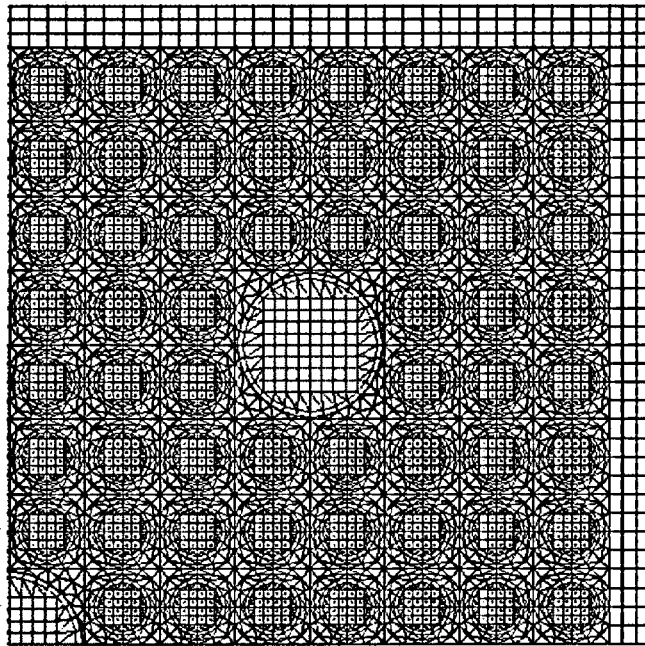


Figure A.4.9-2
Finite Element Modeling of 1/4 Segment CE 16x16 Assembly

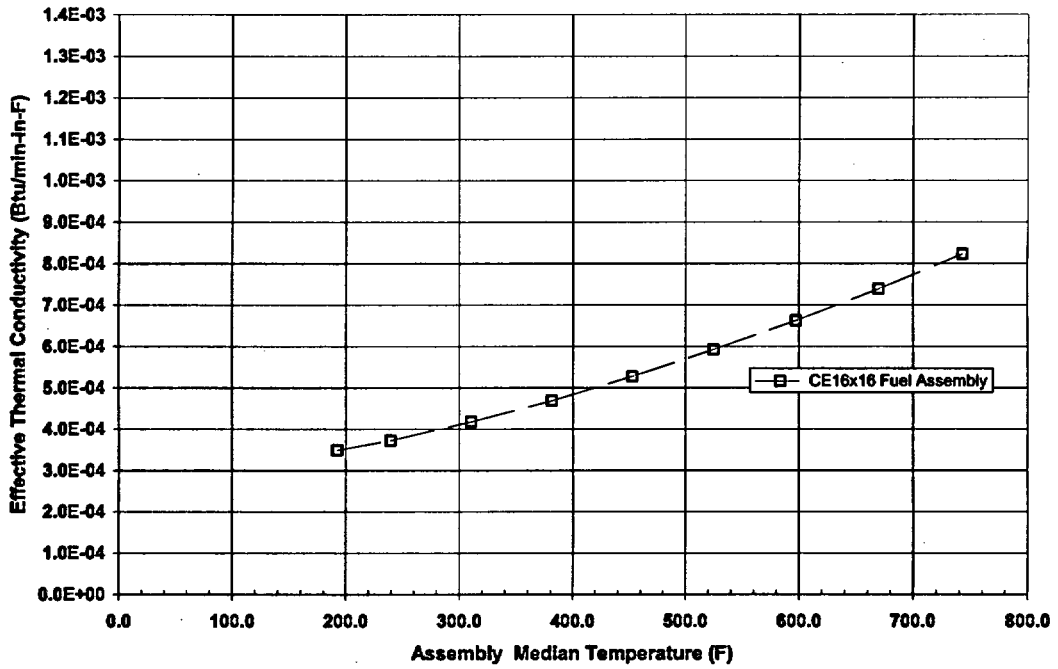


Figure A.4.9-3
Effective Transverse Thermal Conductivity for 1.0 kW CE 16x16 Fuel Assembly – Helium Filled Condition

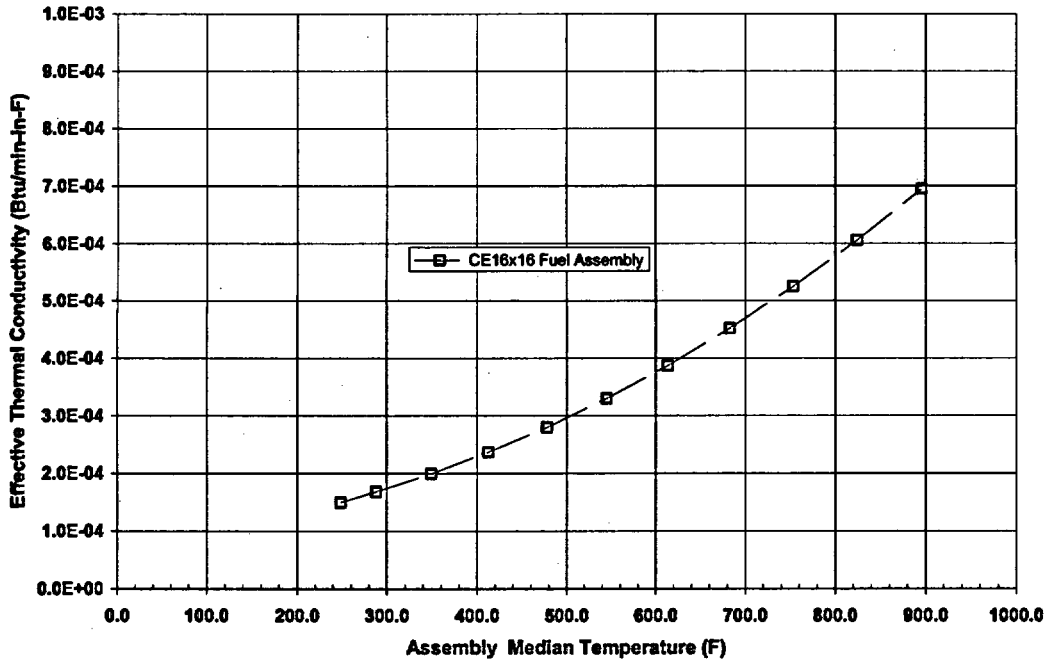


Figure A.4.9-4
Effective Transverse Thermal Conductivity for 1.0 kW CE 16x16 Fuel Assembly – Air Filled Condition

A.4.10 Validation of FLUENT™/ICEPAK™ Computer Codes against NUHOMS®-7P Test Data

The applicability of the FLUENT™ and ICEPAK™ software codes for predicting the thermal-hydraulic performance of a Horizontal Storage Module (HSM) was validated using full scale test results for the NUHOMS®-7P HSM. This performance testing [A4.20] was conducted during 1988 and 1989 using a combination of electrical heaters and actual spent fuel assemblies to establish the thermal performance of both the horizontal storage module and the NUHOMS®-7P DSC housed within it. While the design and decay heat loading of the NUHOMS®-7P HSM varies from a typical AHSM module, the general arrangement and thermo-physical principles driving the airflow through the module are similar for both designs.

Figure A.4.10-1 illustrates the layout of the NUHOMS®-7P storage module array as tested. As seen, the test setup consisted of three (3) horizontal storage modules (HSMs) arranged side-by-side. The figure also illustrates the placement of the two (2) inlet vents and two (2) outlet vents per module.

Figure A.4.10-2 provides an overview of the geometry of the NUHOMS®-7P HSM used for the testing. Each module is 263" long and 144" high, excluding the outlet shielding blocks. The sidewall thickness is 24" between adjacent modules, but increased to 42" at the exposed outside walls of the module's array to provide additional shielding. The exposed front and back walls of the modules are 36" thick. The interior cavity of the module is 43" wide and 102" high.

Figure A.4.10-3 to Figure A.4.10-7 illustrate the thermocouple locations used in the testing [A4.20]. The numbers in the figures represent the thermocouple identification number per the legend provided in each figure. Only the center module and one side module were instrumented for the test. The combined measurement uncertainty for the thermocouples, the extension wires, and the data acquisition system was estimated at $\pm 4^{\circ}\text{C}$ (7°F). No airflow data is available from the [A4.20] test report.

The material properties used for this analysis are taken from Section A.4.2. The soil below the base mat of the HSM module is assumed to have a constant earth temperature of 70°F .

The modeling of the 7P-DSC in the NUHOMS®-7P HSM was based on the geometry shown in Figure A.4.10-2, and conducted using the Icepak™ module which is a fully interactive, object-based graphical interface that allows complex geometries to be modeled and meshed using a combination of shapes in a 'building block' approach.

Figure A.4.10-8 provides an isometric wire frame view of the thermal-hydraulic model developed for this evaluation. The model represents the center module of the array depicted in Figure A.4.10-1. The +x axis of the model's coordinate system extends across the 67" width from the centerline of the sidewall between the first and second modules to the centerline of the sidewall between the second and third module. The +y axis is aligned with the elevation of the module with the 0 dimension at the top of the base mat and the maximum 144" dimension at the top of the module's roof. The +z axis extends 263" from the back of the module to the front face of the module.

As seen from Figure A.4.10-8, the model accurately captures the geometry of the twin inlet vents. The dimensions and offset turns of the modeled duct match the actual flow path within the HSM. A screened opening with a loss coefficient of 0.58 is assumed [A4.30]. The model also includes an accurate representation of the forward air distribution plenum within its triple air ducts leading to the main vault within the HSM, the I-beam support structure, and the two exhaust air ducts leading to the roof of the HSM.

The final flow turn within the outlet shielding blocks, the outlet opening, and the wire mesh at the screened exhaust openings are not specifically modeled in order to simplify the modeling and since the flow losses associated with these flow path items have been well defined by experimental testing [A4.30]. Instead, a combined flow loss factor for these items is applied as a flow resistance element at the outlet [A4.30].

While a symmetry plane could have been assumed along a y-z plane through the center of the module, a full 3-D model is used since radiative exchange is a major heat transfer mode within the HSM module and a symmetry model would not permit the correct calculation of the view or shape factors. The concrete walls and roof of the module are modeled using a combination of block shapes.

The modeling of the DSC within the HSM module is accomplished using two, 24-sided polygons that are 8-inches long to represent the bottom and top shield plugs. The 161.75-inch long, 0.5-inch thick shell of the DSC over the length of the fuel basket is represented by twenty four (24) polygons that are arranged to simulate the cylindrical shape of the DSC. The DSC is simulated using polygons in order to divide the surface of the DSC into individual facets to facilitate an accurate calculation of the radiation view factor over various portions of the DSC using the surface-to-surface radiation modeler that is part of the Icepak™ software..

Since the DSC basket is not specifically modeled, the decay heat loading is simulated as a uniform heat flux applied over the length of the DSC shell between the shield plugs. The heat shields are modeled using thin conducting plate elements.

The ability of the FLUENT™ program to create non-conformal computational meshes is used to increase the mesh density in those areas requiring greater fluid flow and/or thermal resolution and decrease the mesh density in those areas (i.e., within the concrete walls, etc.) that do not experience large thermal gradients. A total of approximately 980,600 mesh elements are used for the analysis. Figure A.4.10-9 illustrates an elevation view of the mesh profile along the y-z plane through the center of the module. The non-conformal nature of the mesh is again evident from the figure with the mesh density being significantly higher in the region of the inlet plenum, the DSC shell and shield plugs, and the outlet exhaust ducts and much lower elsewhere.

A direct simulation of insolation on the outer surface of the HSM could not be included in the selected modeling approach due to program limitations on the number of boundary conditions that could be applied. Therefore, the simulation of the insolation was addressed by increasing the reference temperature used to compute the convective and radiation heat transfer exchange from the affected surfaces to the ambient to a level sufficient to account for the equivalent surface heating due to insolation.

The Icepak™ and FLUENT™ codes were used to compute the buoyancy driven convection heat transfer within the HSM enclosure. The analysis was conducted using first order discretization solver scheme as an initial solution. This initial solution was used as a re-start file for a refined solution using a second order discretization solver scheme.

Figure A.4.10-10 to Figure A.4.10-12 present a summary of the surface temperature distributions predicted for the analyzed decay heat loading of 5,320 Watts within the DSC and the measured ambient condition of 77°F. Table A.4.10-1 presents a comparison of the test measured temperatures at the thermocouple locations and corresponding predicted temperatures at the same locations as obtained from the CFD model results. The results from the test are presented in both degrees Centigrade to match the documented results in the test report [A4.20] and in degrees Fahrenheit to match the modeling units used for the CFD model. The CFD predicted results are rounded to the nearest whole degree since the exact location of the thermocouple is uncertain and since the model accuracy does not support reporting to the tenth of a degree.

Figure A.4.10-10 presents a perspective view of the predicted temperature profile on the DSC surface and for the DSC support structure. A comparison of the measured vs. predicted temperatures at seven different locations on the exterior of the DSC shell (i.e., thermocouple IDs C-2-01 through C-2-13) is provided in Table A.4.10-1. A review of the temperatures in the table shows that the predicted shell temperatures consistently bound the measured temperatures. At the single location on the side of the DSC (i.e., thermocouple ID C-2-02), the predicted shell temperature is 17°F higher than the test measurement.

As shown in Table A.4.10-1 predicted temperatures along the bottom of the DSC are 30 to 65°F higher than the test measurements (i.e., thermocouple ID C-2-03, C-2-11, and C-2-13). A review of the predicted flow pattern near the bottom of the DSC shows the expected region of low airflow between the DSC support rails will tend to raise the temperatures along the bottom of the DSC. One possible explanation for the over-prediction of the temperatures on the bottom side of the DSC is that the predicted region of low airflow was not as severe or extensive as that predicted due to the support rail geometry differences that are not captured by the CFD model. Any increase in airflow in this region could significantly reduce the temperatures along the bottom of the DSC.

A comparison of the predicted heat shield temperatures to the test measurements is provided in Table A.4.10-1 at five (5) locations (i.e., thermocouple IDs HS-2-43 to HS-2-47).

Figure A.4.10-12 illustrates the computed temperature distribution within the sidewall and the rear wall of the module and through the roof slab. A comparison to the test measurements is provided in Table A.4.10-1 at ten (10) locations (i.e., thermocouple IDs H-2-04 to H-2-23). As seen from the table, the maximum measured concrete temperatures predictably occur on the underside of the roof slab (i.e., thermocouple IDs H-2-11, H-2-21, and H-2-25).

The CFD model predicted sidewall temperature midway between modules conservatively bounds the measured temperature by 16°F (i.e., thermocouple ID H-2-04), under estimates the inside surface temperature by 3°F (i.e., thermocouple ID H-2-05), and over estimates the inside surface temperature at the intersection of the sidewall and roof slabs (i.e., thermocouple ID H-2-10) by

22°F. While the test report [A4.20] is silent on this, it is suspected that the measured data at thermocouple ID H-2-10 is too low given the trend in the adjacent thermocouple locations.

The CFD model predicted roof exterior temperatures are within 4°F at the center of the module (i.e., thermocouple ID H-2-17), bounds the measured temperature by 9°F midway between adjacent modules (i.e., thermocouple ID H-2-16), and under predicts the measured temperature by 12°F near the exhaust vents (i.e., thermocouple IDs H-2-19 and H-2-23). The bounding temperatures achieved in the center of the module would indicate that the methodology used for estimating the insolation load on the roof surface was appropriate. The under estimate achieved for the concrete temperatures near the exhaust vents is probably related to the lack of modeling of the final turn in the exhaust flow under the shielding blocks. The model assumes that the exhaust air flows straight upwards into the ambient. In reality, the horizontal flow of the relatively hot exhaust air will provide some level of heating the concrete surface as it exits the screened opening.

The test [A4.20] used six (6) thermocouples to monitor the exit air temperature from the two exhaust vents. These thermocouples (i.e., thermocouple IDs H-2-29, H-2-30, and H-2-31 for the rear exhaust vent and thermocouple IDs H-2-35, H-2-36, and H-2-37 for the front exhaust vent) indicate an average exhaust temperature of 119°F for the rear vent and 116°F for the front vent. In contrast, the CFD analysis indicates an average exhaust temperature of 140°F for the rear vent and 136°F for the front vent, or a temperature rise through the HSM that is approximately 50% higher than that indicated by the test results. A likely explanation is that, given the location of the thermocouples at the face of the screened outlet and the relatively low flow rate through the openings, a significant level of mixing with the ambient air probably occurred. The CFD model predicts a total flow rate of approximately 0.32 lbm/sec, evenly split between the left and right inlets.

Figure A.4.10-13 and Figure A.4.10-14 provide representative illustrations of the airflow profile within the HSM. The figures demonstrate that relatively even flow distribution is achieved over the length of the DSC. Areas of flow re-circulation are present in the forward and main air plenums beneath the DSC and between the support rails for the DSC.

In conclusion, the methodology used to predict the thermal-hydraulic performance within a horizontal storage module has been validated (benchmarked) against full scale test results for the NUHOMS[®]-7P horizontal storage module. With the exception of one test point (i.e., thermocouple C-2-13), the predicted absolute temperatures are within 10% of the absolute test measured temperatures. Since this deviation between predicted and test data at the thermocouple C-2-13 location is in the conservative direction (i.e., hotter predicted temperature) and since the average error across all 28 thermocouple locations is less than 3%, the CFD model results are deemed to be acceptable.

While the design and decay heat loading of the NUHOMS[®]-7P storage module varies from the current generic designs for the AHSM module and its heat loading, the general arrangement and thermo-physical principles driving the airflow through the module are similar. As such, validation of the FLUENT[™] 6.1 / ICEPAK[™] 4.1 CFD analysis against the NUHOMS[®]-7P test data also provides validation of the codes for providing an accurate representation of the temperature levels and distribution within the generic AHSM module.

**Table A.4.10-1
Test Vs. Predicted Temperatures for 7P DSC in HSM**

Thermocouple ID	Thermocouple Location Description	Test Temperature, °F (°C)	Icepak™/FLUENT Predicted Temperature, °F
C-2-01	Top of DSC, 9'-3" from front of HSM	239.9 (115.5)	250
C-2-02	Side of DSC, 9'-3" from front of HSM	197.4 (91.9)	214
C-2-03	Bottom of DSC, 9'-3" from front of HSM	162.5 (72.5)	192
C-2-10	Top of DSC, 5'-2" from front of HSM	212.5 (100.3)	231
C-2-11	Bottom of DSC, 5'-2" from front of HSM	145.8 (63.2)	182
C-2-12	Top of DSC, 15'-6" from front of HSM	203.7 (95.4)	245
C-2-13	Bottom of DSC, 15'-6" from front of HSM	133.0 (56.1)	198
H-2-04	Midway between adjacent modules, slightly above vertical centerline of DSC, 9'-3" from front of HSM	103.1 (39.5)	119
H-2-05	Inside wall of module, at vertical centerline of DSC, 9'-3" from front of HSM	121.5 (49.7)	119
H-2-10	Inside corner of module's vault, 9'-3" from front of HSM	101.7 (38.7)	124
H-2-11	Inside surface of module's roof, center of module, 9'-3" from front of HSM	124.5 (51.4)	136
H-2-16	Roof surface, midway between adjacent modules, 9'-3" from front of HSM	83.5 (28.6)	92
H-2-17	Outside surface of module's roof, center of module, 9'-3" from front of HSM	88.7 (31.5)	93
H-2-19	Outside surface of module's roof, center of module, 15'-6" from front of HSM	108.7 (42.6)	97
H-2-21	Inside surface of module's roof, center of module, 15'-6" from front of HSM	132.3 (55.7)	135
H-2-23	Outside surface of module's roof, center of module, 5'-2" from front of HSM	109.0 (42.8)	97
H-2-25	Inside surface of module's roof, center of module, 5'-2" from front of HSM	130.6 (54.8)	137
H-2-29	Right side of rear vent exit (looking aft), approximately 8" from side	117.9 (47.7)	134
H-2-30	Center of rear vent exit (looking aft)	120.9 (49.4)	141
H-2-31	Left side of rear vent exit (looking aft), approximately 8" from side	119.1 (48.4)	134
H-2-35	Right side of front vent exit (looking aft), approximately 8" from side	114.4 (45.8)	136

Table A.4.10-1
Test Vs. Predicted Temperatures for 7P DSC in HSM
 (Concluded)

Thermocouple ID	Thermocouple Location Description	Test Temperature, °F (°C)	Icepak™/FLUENT Predicted Temperature, °F
<i>H-2-36</i>	<i>Center of front vent exit (looking aft)</i>	<i>120.4 (49.1)</i>	<i>146</i>
<i>H-2-37</i>	<i>Left side of front vent exit (looking aft), approximately 8" from side</i>	<i>113.9 (45.5)</i>	<i>137</i>
<i>HS-2-43</i>	<i>Horizontal heat shield, center of module, 5'-2" from front of HSM</i>	<i>143.4 (61.9)</i>	<i>157</i>
<i>HS-2-44</i>	<i>Vertical heat shield, approx. 8" up from bottom, 9'-3" from front of HSM</i>	<i>108.7 (42.6)</i>	<i>113</i>
<i>HS-2-45</i>	<i>Horizontal heat shield, center of module, 7'-2" from front of HSM</i>	<i>148.3 (64.6)</i>	<i>156</i>
<i>HS-2-46</i>	<i>Horizontal heat shield, center of module, 9'-3" from front of HSM</i>	<i>150.3 (65.7)</i>	<i>158</i>
<i>HS-2-47</i>	<i>Horizontal heat shield, center of module, 15'-6" from front of HSM</i>	<i>140.0 (60.0)</i>	<i>154</i>

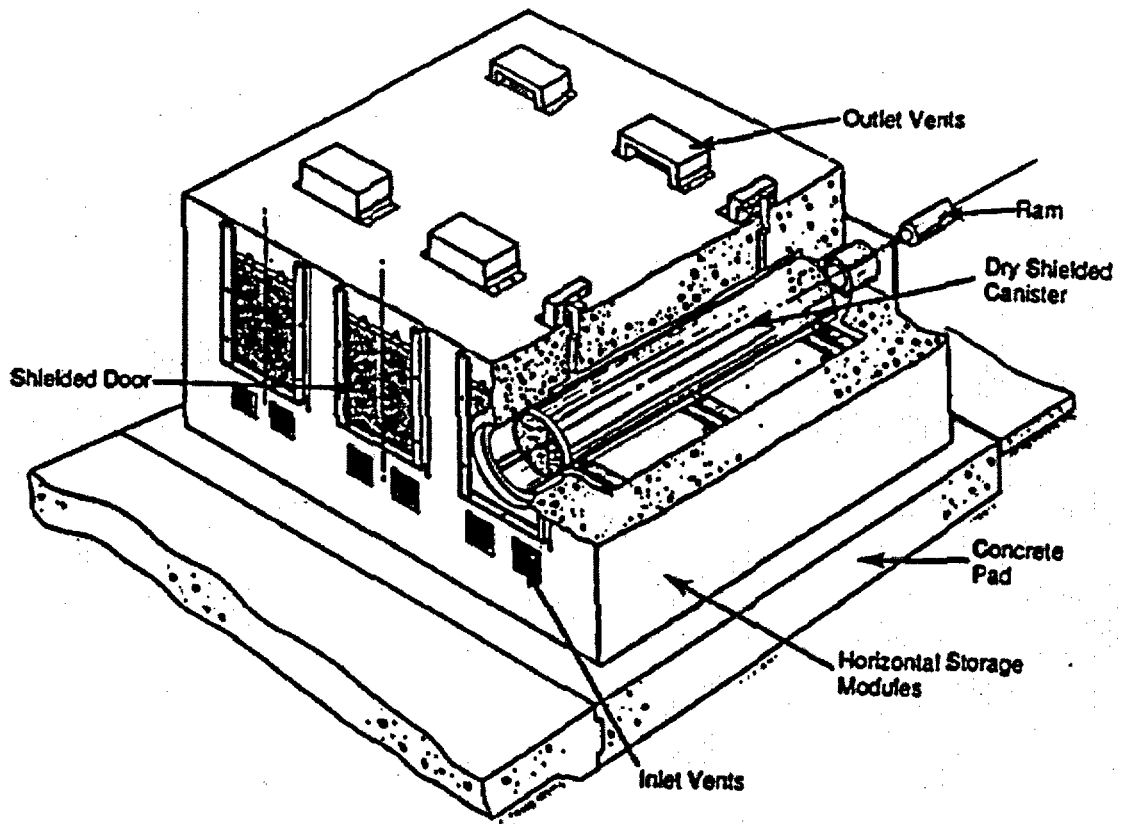


Figure A.4.10-1
Layout of NUHOMS®-7P HSM Array for Performance Testing

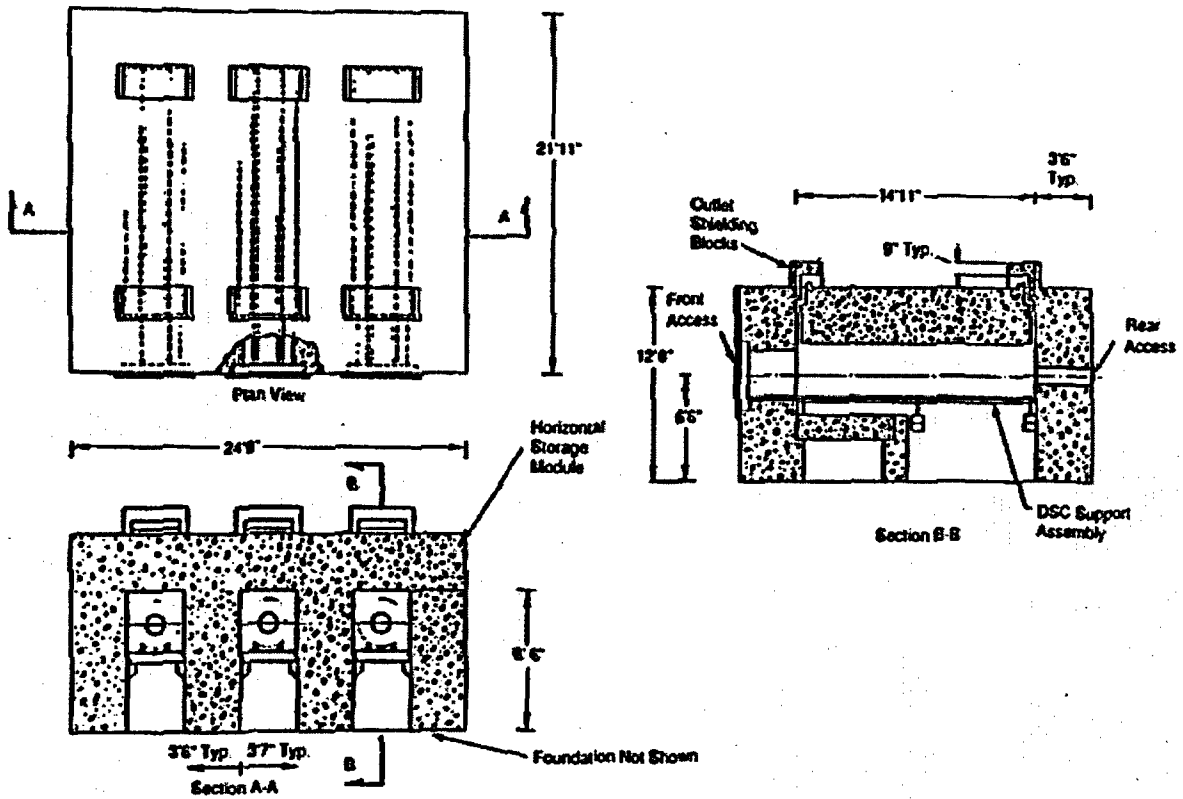


Figure A.4.10-2
General Geometry of NUHOMS®-7P Horizontal Storage Module

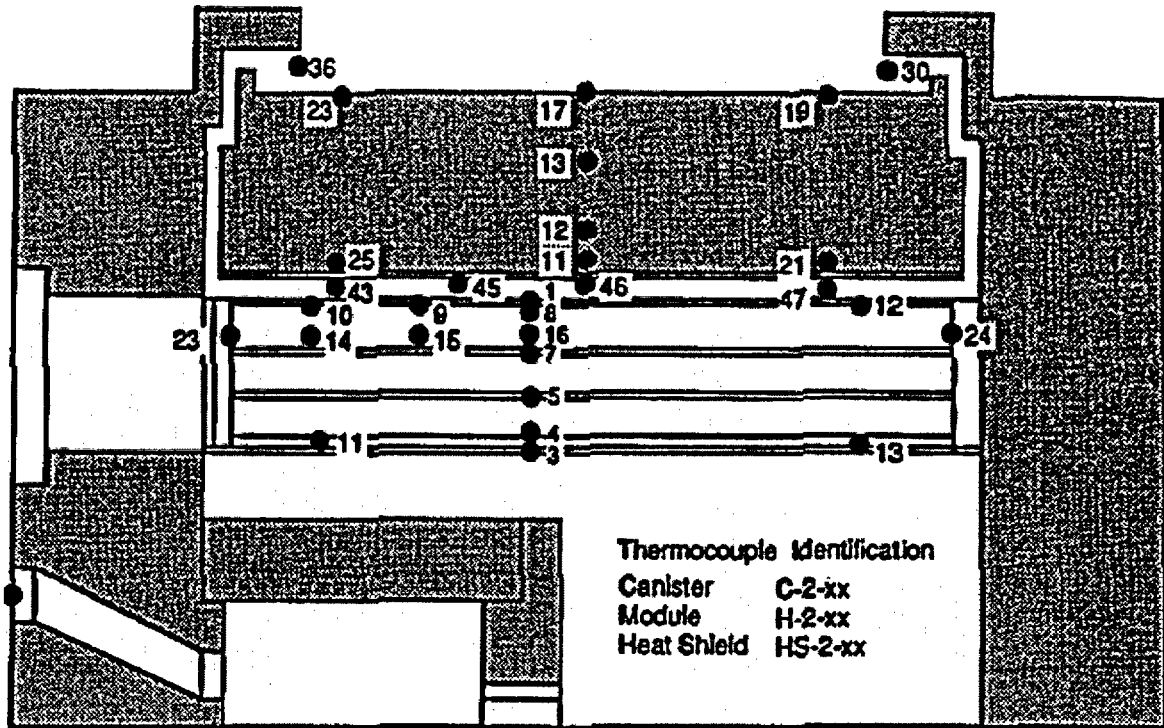


Figure A.4.10-3
Thermocouple Location in Center Module (HSM-2)

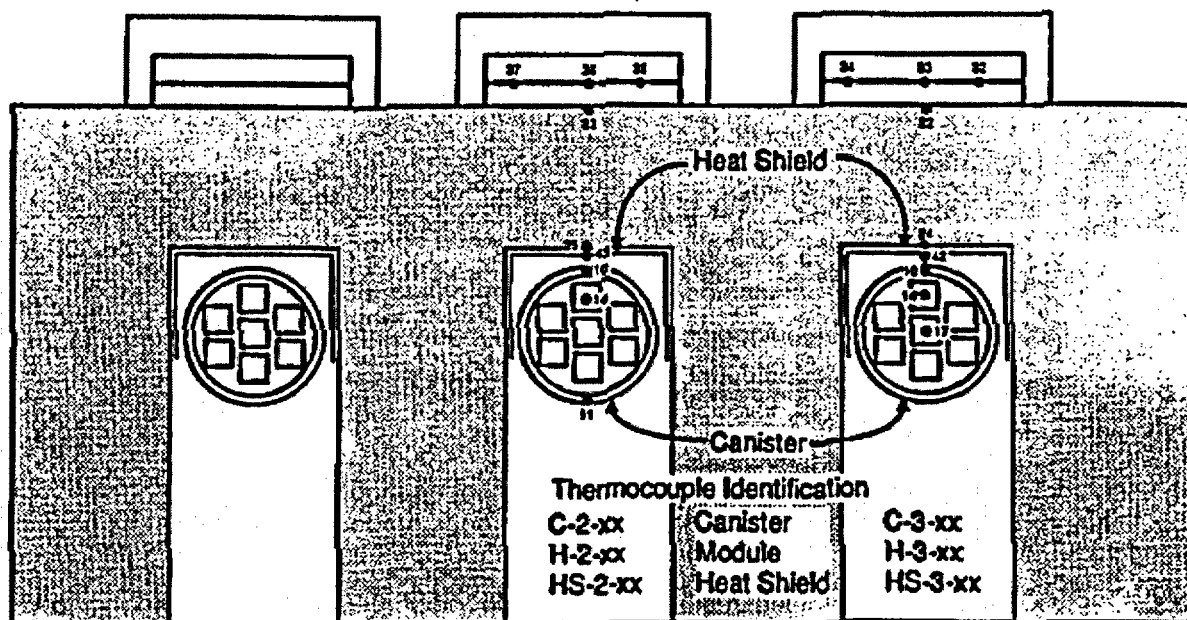


Figure A.4.10-4
Thermocouple Locations 5'-2" from Front of Modules

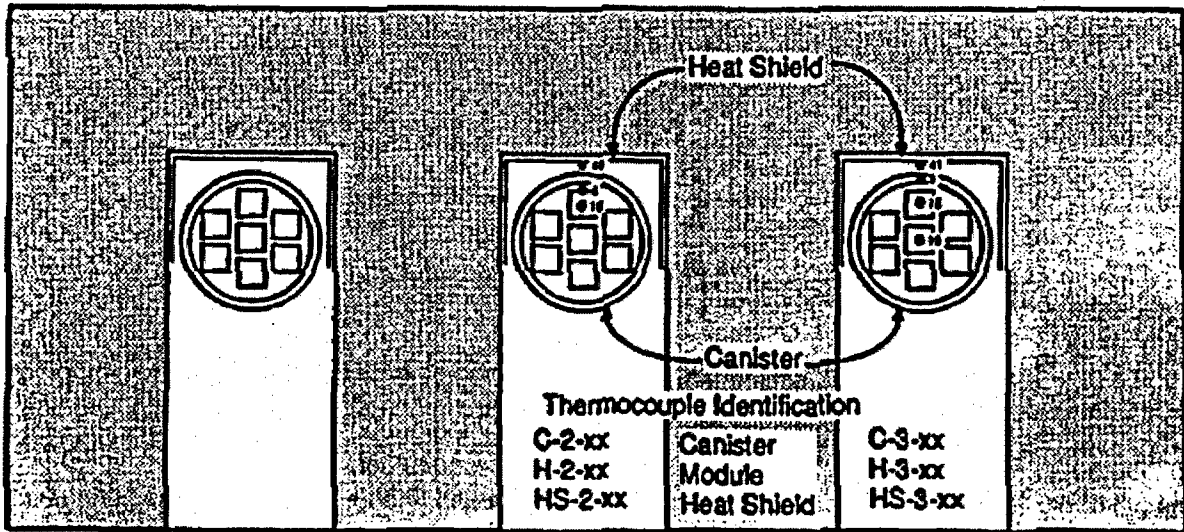


Figure A.4.10-5
Thermocouple Locations 7'-2" from Front of Modules

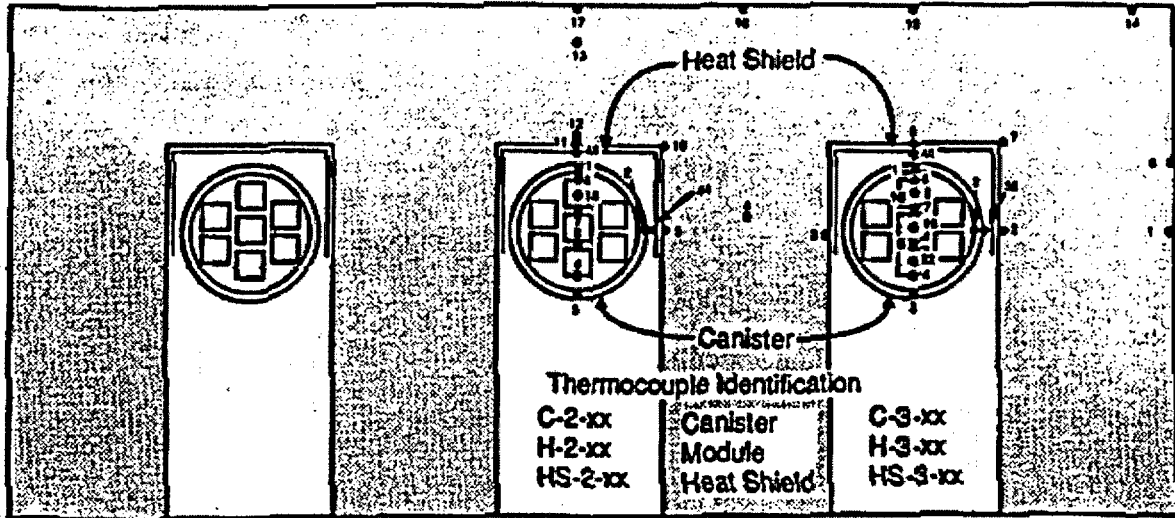


Figure A.4.10-6
Thermocouple Locations 9'-3" from Front of Modules (Center)

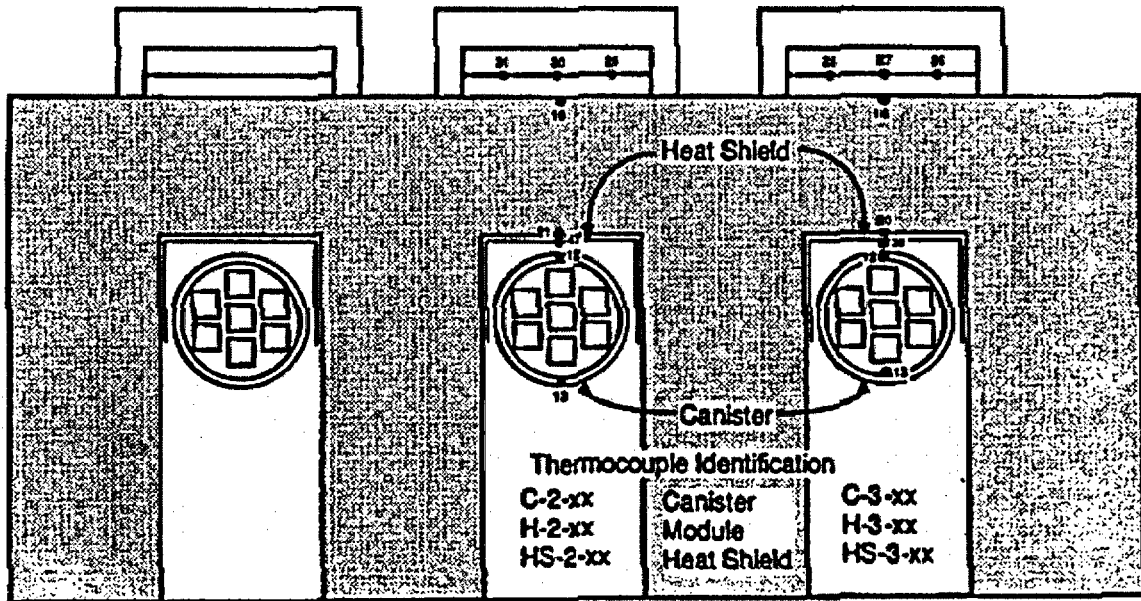


Figure A.4.10-7
Thermocouple Locations 15'-6" from Front of Modules

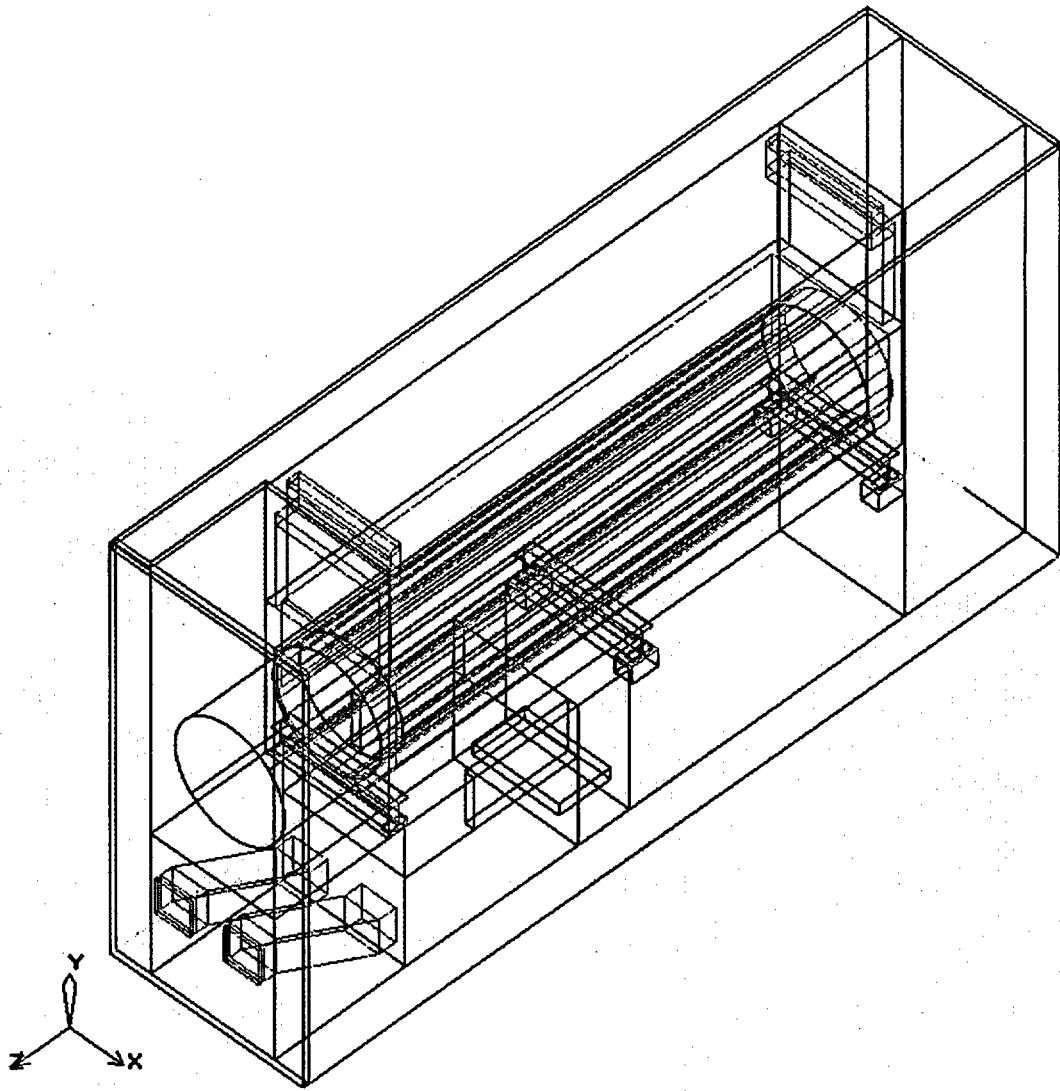


Figure A.4.10-8
Isometric, Wireframe View of NUHOMS®-7P HSM Model Layout

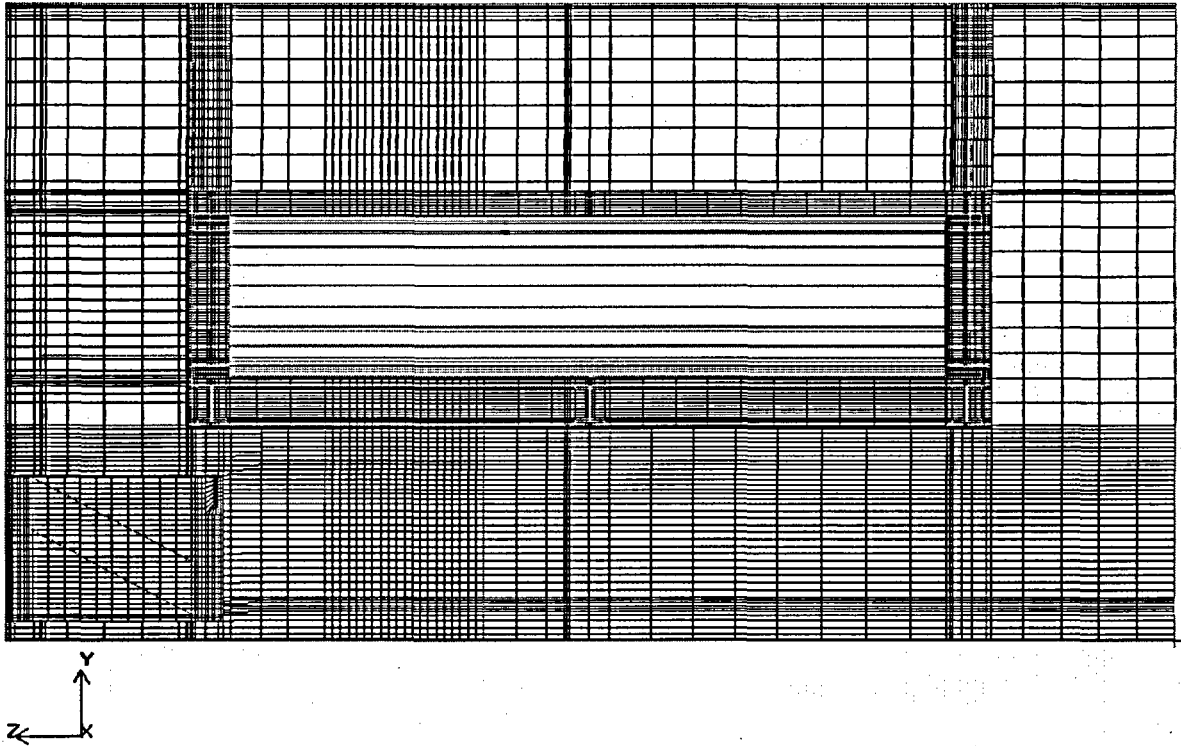


Figure A.4.10-9
Elevation View of Meshing along Axial Center Plane of 7P HSM

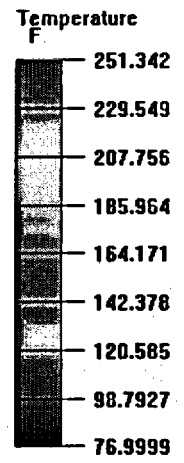
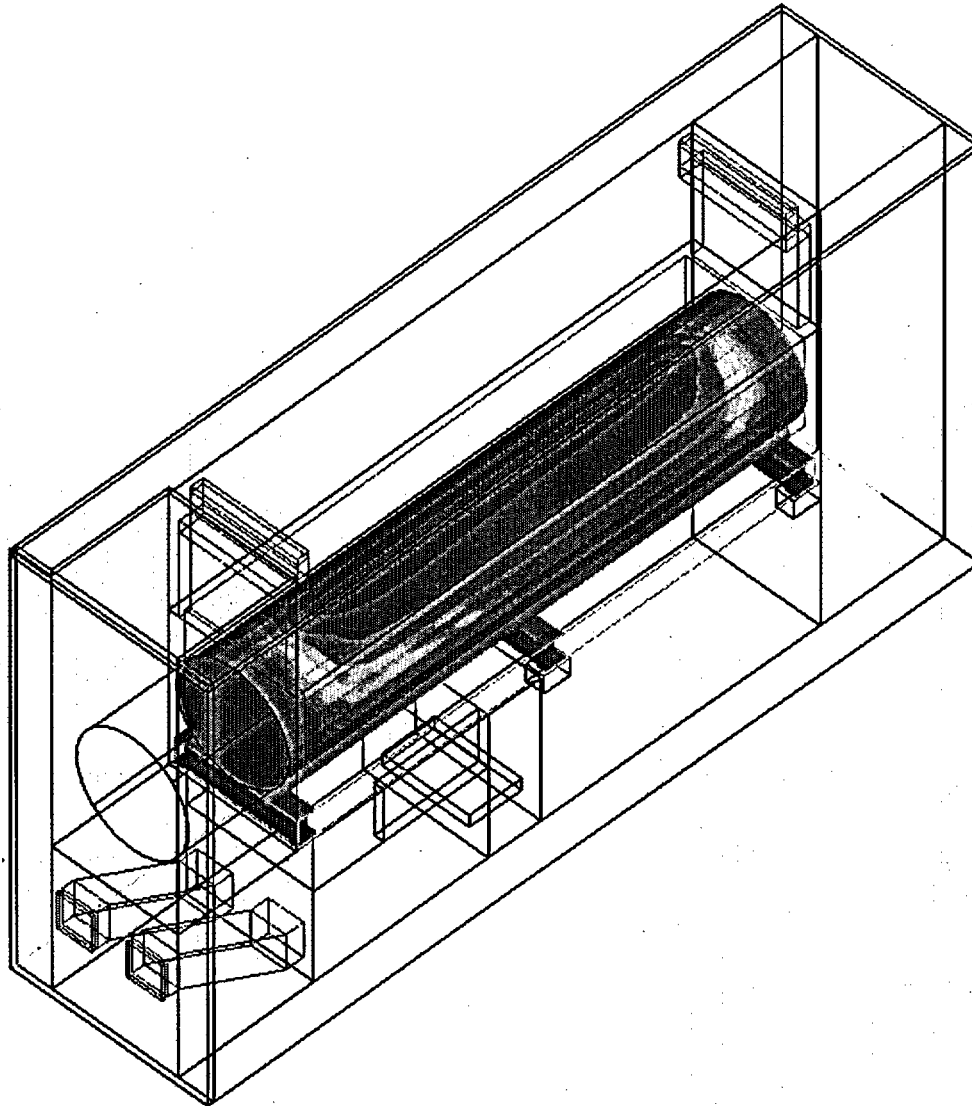


Figure A.4.10-10
Temperature Distribution on 7P DSC Surface

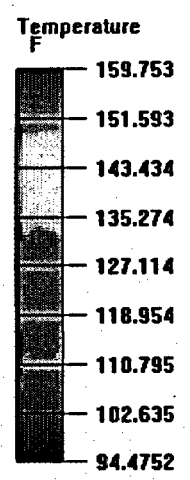
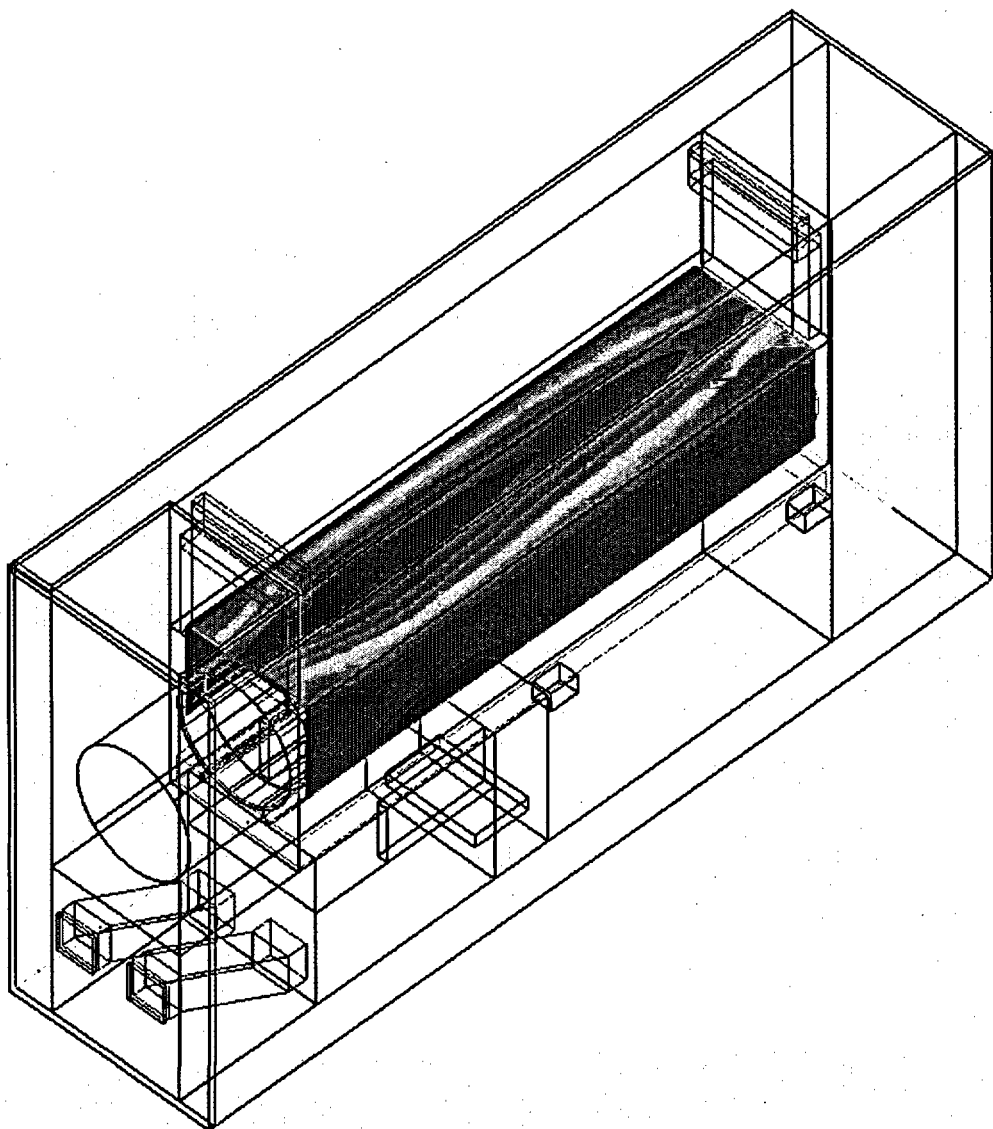


Figure A.4.10-11
Temperature Distribution on Heat Shield Surfaces

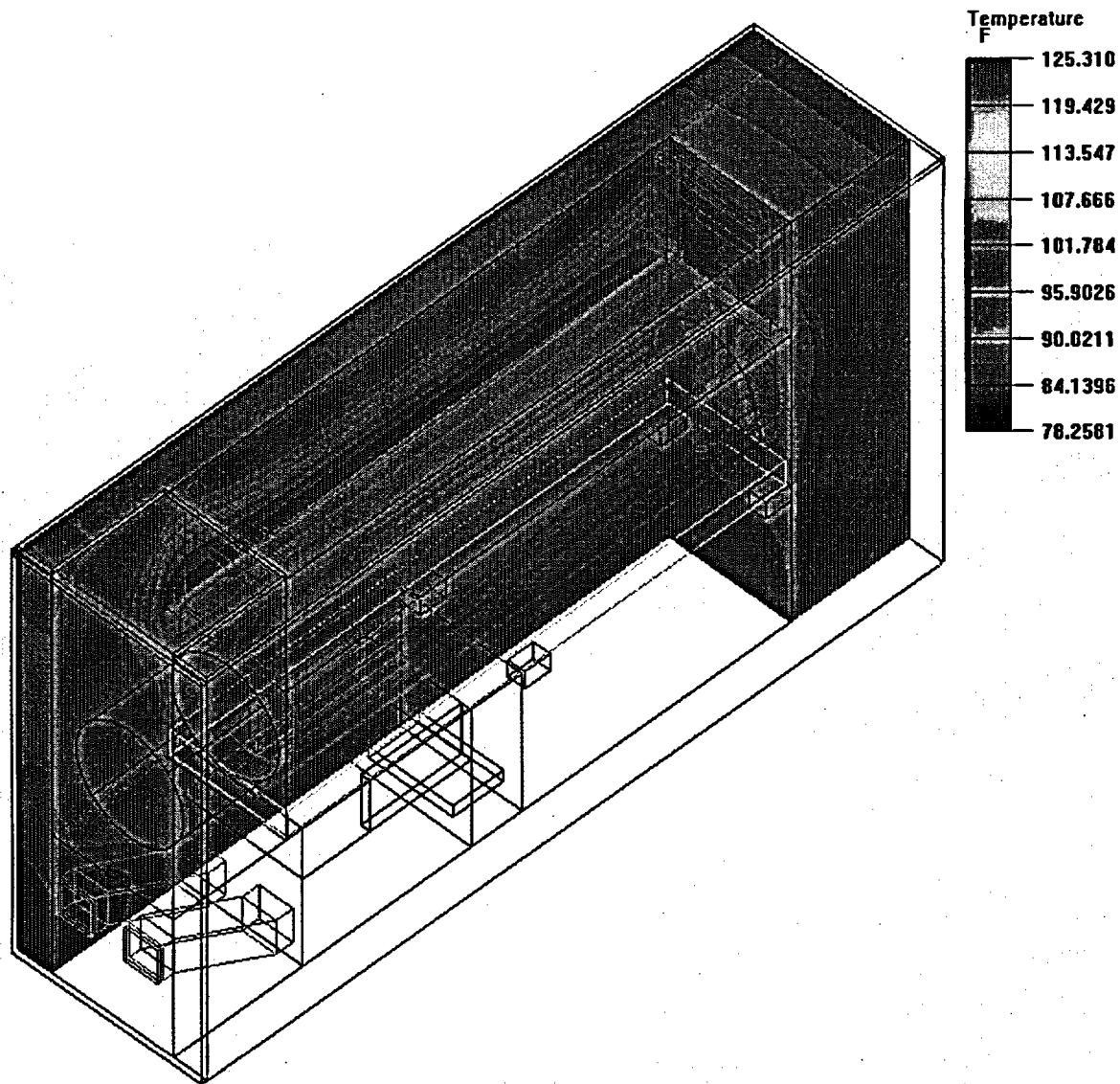


Figure A.4.10-12
Temperature Distribution on Side & Rear Concrete Surfaces

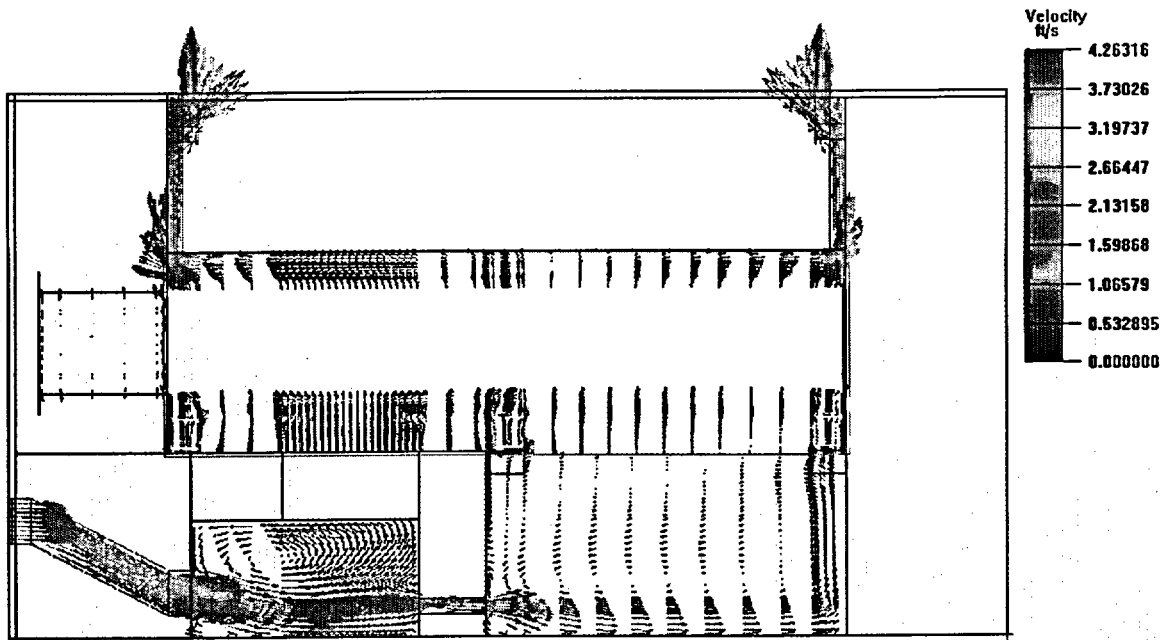


Figure A.4.10-13
Axial Velocity Profile

(Note: Profile is taken through center of right inlet. Front face of HSM module is to the left)

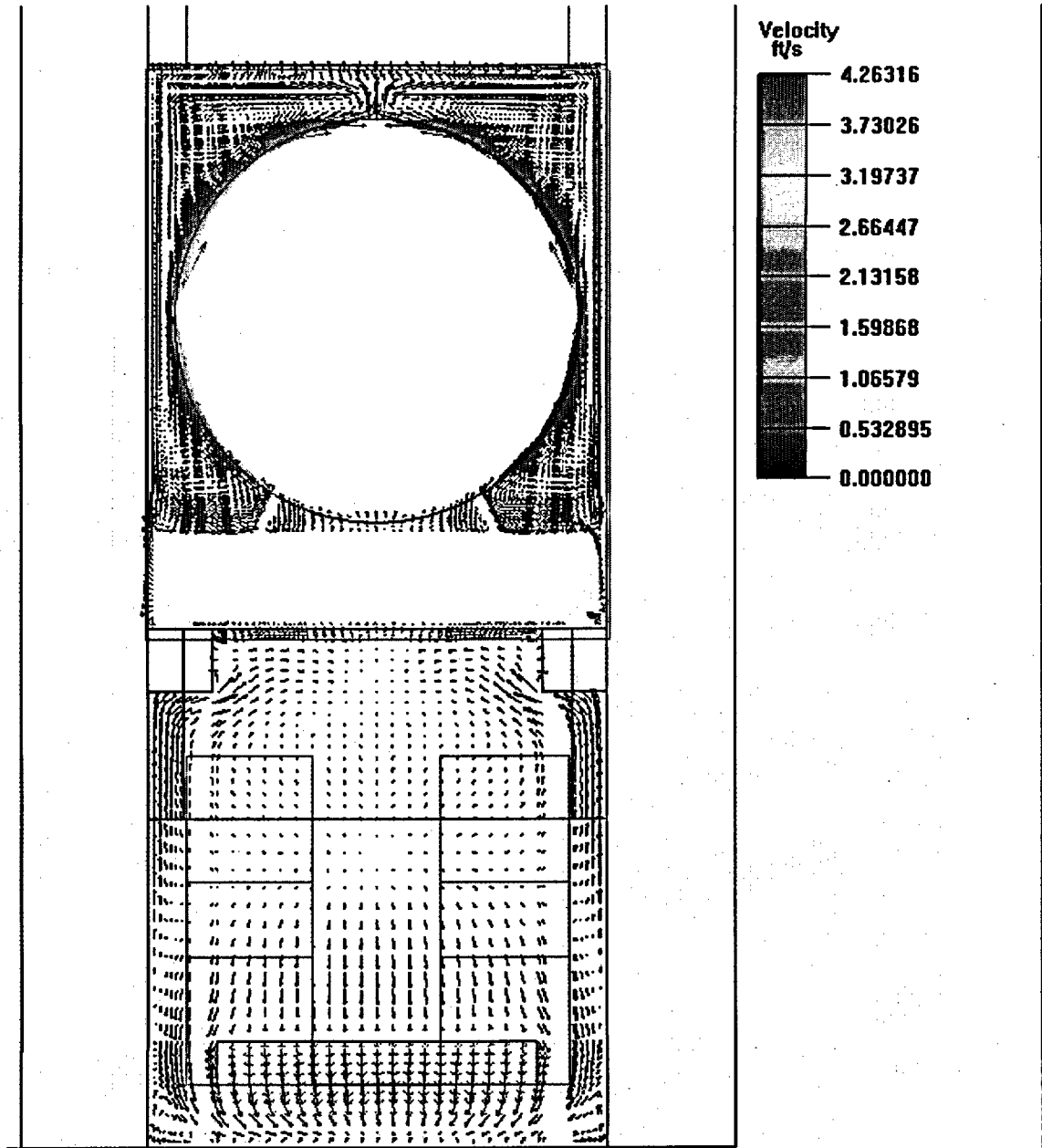


Figure A.4.10-14
Velocity Profile along X-Y Plane at Center of Module

A.4.11 Supplemental Information

A.4.11.1 References

- [A4.1] "Topical Report on Actinide-Only Burnup Credit for PWR Spent Nuclear Fuel Packages," Office of Civilian Radioactive Waste Management, DOE/RW-0472, Revision 2, September 1998.
- [A4.2] NRC NUREG-1536, Standard Review Plan for Dry Cask Storage Systems, January 1997.
- [A4.3] Bolz, R. E., G. L. Tuve, CRC Handbook of Tables for Applied Engineering Science, 2nd Edition, 1973.
- [A4.4] American Society of Mechanical Engineers, Boiler & Pressure Vessel Code, Section III, 1992 Edition with Addenda through 1994 with Code Cases N-595-1 and N-499-1.
- [A4.5] "Standard Specification for BORAL[®] Composite Sheet," Specification Number BPS-9000-04, AR Advanced Structures, Livonia, Michigan. PROPRIETARY.
- [A4.6] E. A. Brandes (Editor), Smithells Metals Reference Book, 6th Ed., Butterworths, London, UK, 1983.
- [A4.7] Roshenow, W. M., J. P. Hartnett, and Y. I. Cho, Handbook of Heat Transfer, 3rd Edition, 1998.
- [A4.8] Incropera, F. P., D. P. DeWitt, Fundamentals of Heat and Mass Transfer, 4th Edition, Wiley, 1996.
- [A4.9] Bucholz, J. A., Scoping Design Analysis for Optimized Shipping Casks Containing 1-, 2-, 3-, 5-, 7-, or 10-Year old PWR Spent Fuel, Oak Ridge National Laboratory, January 1983, ORNL/CSD/TM-149.
- [A4.10] Siegel, R. and J. R. Howell, Thermal Radiation Heat Transfer, 2nd Edition, Hemisphere, 1981.
- [A4.11] MATPRO – Version 11: A Handbook of Materials Properties for Use in the Analysis of Light Water Reactor Fuel Rod Behavior, EG&G Idaho, Idaho Falls, February 1979, NUREG-CR/0497.
- [A4.12] *Transnuclear, Inc.*, Final Safety Analysis Report for the Standardized NUHOMS[®] Horizontal Modular Storage System for Irradiated Nuclear Fuel, Revision 8, June 2004, NRC Docket No. 72-1004.
- [A4.13] Title 10, Code of Federal Regulations, Part 71 (10CFR71), Packaging and Transportation of Radioactive Materials, U.S. Nuclear Regulatory Commission, 1997.

- [A4.14] Frank Kreith, Principles of Heat Transfer, Third Edition, Harper and Row Publishers.
- [A4.15] ANSYS User's Manual for ANSYS Revision 5.6.2.
- [A4.16] Hottel, H. C. and A. F. Sarofim, Radiative Transfer, Chapter 4, p. 164, McGraw-Hill, New York, 1967.
- [A4.17] Fax From DAV-Tech Plating, Emissivity of Electroless Nickel on Carbon Steel, March 30, 2000, Transnuclear Project File SCE-01.0100.
- [A4.18] 10CFR 72, Rules and Regulations, Title 10, Code of Federal Regulations - Energy, U.S. Nuclear Regulatory Commission, Washington, D.C., "Licensing Requirements for the Independent Storage of Spent Nuclear Fuel and High-Level Radioactive Waste."
- [A4.19] *Deleted.*
- [A4.20] "NUHOMS® Modular Spent-Fuel Storage System: Performance Testing", Report PNL-7327/UC-812/EPRI NP-6941, Pacific Northwest Laboratory & Carolina Power and Light Company, September 1990.
- [A4.21] Interim Staff Guidance No. 11, ISG-11, Rev. 3, Cladding Considerations for the Transportation and Storage of Spent Fuel, US NRC, November 2003.
- [A4.22] *Deleted.*
- [A4.23] Lide, David R., CRC Handbook of Chemistry and Physics, 83rd Edition, 2002-2003, CRC Press.
- [A4.24] SINDA/FLUINT™, Systems Improved Numerical Differencing Analyzer and Fluid Integrator, Version Cullimore and Ring Technologies, Inc., Littleton, CO, 2001.
- [A4.25] Thermal Desktop™, Version 4.4., Cullimore and Ring Technologies, Inc., Littleton, CO, 2001.
- [A4.26] Manual of Steel Construction, 8th Edition, 1980.
- [A4.27] Archie, W. Culp, Jr., Principles of Energy Conversion, McGraw-Hill, New York, NY, 1979.
- [A4.28] Incropera, F. P., D. P. DeWitt, Fundamentals of Heat and Mass Transfer, 3rd Edition, Wiley, 1990.
- [A4.29] McKinnon, M.A. et. al, Testing and Analysis of the TN-24P PWR Spent Fuel Dry Storage Cask Loaded With Consolidated Fuel, February, 1989, Electric Power Research Institute, EPRI Document NP-6191.
- [A4.30] I.E. Idelchik, Handbook of Hydraulic Resistance, 3rd Edition, 1994.

- [A4.31] *FLUENT™, Version 6.1, FLUENT, Inc., Lebanon, NH, 2003.*
- [A4.32] *ICEPAK™, Version 4.1, FLUENT, Inc., Lebanon, NH, 2003.*
- [A4.33] *"Characteristics of Spent Fuel, High Level Waste, And Other Radioactive Wastes Which May Require Long-Term Isolation," DOE/RW-0184, Volume 3 of 6, dated December 1987.*
- [A4.34] *"Domestic Light Water Reactor Fuel Design Evolution, Volume III," Nuclear Assurance Corporation, September 1981, DOE/ET/47912-3.*
- [A4.35] *NUREG/CR-0497, A Handbook of Materials Properties for Use in the Analysis of Light Water Reactor Fuel Rod Behavior, MATPRO - Version 11 (Revision 2), EG&G Idaho, Inc., TREE-1280, August 1981.*
- [A4.36] *SAND90-2406, Sanders, T. L., et al., A Method for Determining the Spent-Fuel Contribution to Transport Cask Containment Requirements, TTC-1019, UC-820, November 1992.*
- [A4.37] *"Spent Nuclear Fuel Effective Thermal Conductivity Report", prepared TRW Environmental Safety Systems, Inc. for DOE Civilian Radioactive Waste Management System (CRWMS), Report BBA000000-01717-5705-00010, Rev. 0, July 1996*
- [A4.38] *"SONGS Unit 2/3 Fuel Assembly Materials and Masses" SCE No. N-1020-162. Transnuclear, Inc. No. SCE-23.0100-11*

14. Perform dye penetrant weld examination of the top shield plug assembly weld.
15. Prior to start of blowdown with air, refill the DSC with water to ensure that all fuel is submerged in a water boundary condition. The Tech Spec 3.1.1.b vacuum drying time applies for blowdown. Connect the VDS to the siphon and vent ports. This step is not required if helium is used for blowdown.
16. Install temporary shielding to minimize personnel exposure throughout the subsequent draining/drying and welding operations as required.

NOTE: Do not use strongback during blowdown with 24PT4-DSC.

17. Engage the helium or air supply and open the valve on the vent port and allow compressed gas to force the water from the 24PT4-DSC cavity through the siphon port.
18. Once the water stops flowing from the 24PT4-DSC, close the siphon port and disengage the gas source.
19. Connect the hose from the vent port and the siphon port to the intake of the vacuum pump. Connect a hose from the discharge side of the VDS to the plant's radioactive waste system or spent fuel pool or other appropriate filtration system. Connect the VDS to a helium source.
20. Open the valve on the suction side of the pump, start the VDS and draw a vacuum on the 24PT4-DSC cavity. The cavity pressure should be reduced in steps to approximately 100 torr, 50 torr, 25 torr, 15 torr, 10 torr, 5 torr, and 3 torr. This staged drawdown will verify no ice blockage of the evacuation path. After pumping down to each level, the pump is valved off and the cavity pressure monitored. The cavity pressure will rise as water and other volatiles in the cavity evaporate. When the cavity pressure stabilizes, the pump is valved in to complete the vacuum drying process. It may be necessary to repeat some steps, depending on the rate and extent of the pressure increase. Vacuum drying is complete when the pressure stabilizes for a minimum of 30 minutes at 3 torr or less as specified in the Technical Specifications.

NOTE: If air is used as the medium for blowdown in Step 17, the Technical Specifications contain limitations on the duration of vacuum drying as a function of the specific heat load configuration for the DSC. The duration of vacuum drying shall be monitored and appropriate corrective actions taken if required vacuum levels are not reached within the time limits. No time limits apply for vacuum drying of the 24PT4-DSC, if helium is used for blowdown in Step 17 of this section.

21. Open the valve to the vent port and fill the 24PT4-DSC cavity with helium.

NOTE: Helium gas introduced into the 24PT4-DSC shall be welding grade (>99% purity) and Important to Safety.

22. Pressurize the 24PT4-DSC with helium in accordance with Technical Specifications requirements.